UNIVERSITY OF NAIROBI

CLAY DERIVED ZEOLITES FOR REMOVAL OF NITRATES, PHOSPHATES AND HEAVY METALS FROM WATER

BY
MAKANI BUNGISHABAKU RACHEL
I56/11841/2018

A Thesis Submitted in Fulfillment of the Requirements for the Award of the Degree of Master of Science in Industrial Chemistry of the University of Nairobi.

2023

DECLARATION

"I declare that this thesis is my original work and has not been submitted elsewhere for examination, the award of a degree, or publication. Where other people's work or my work has been used, this has properly been acknowledged and referenced in accordance with the University of Nairobi's requirements".

Signature:  Date: 04-09-2023

Makani Bungishabaku Rachel
I56/11841/2018
Department of Chemistry
Faculty of Science and Technology
University of Nairobi

"This thesis is submitted with our approval as research supervisors".

Dr. Njagi B. Njomo
Department of Chemistry
Faculty of Science and Technology
University of Nairobi
Nairobi, Kenya

Signature:  Date: 05-09-2023

Dr. Patrick K. Tum
Department of Chemistry
Faculty of Science and Technology
University of Nairobi
Nairobi, Kenya.

Signature:  Date: 05-09-2023

DEDICATION

“I dedicate this thesis to my family, in appreciation of their steadfast love and encouragement”.

ACKNOWLEDGEMENTS

I wish to express my gratitude to those who have played a part in the successful culmination of this thesis. First, I express my gratitude to Dr. Njagi Njomo and Dr. Patrick K. Tum, my supervisors, for their guidance and understanding during the whole process.

Secondly, I am thankful to Dr. Benard K. Rop for his enormous assistance and guidance during the research experiment in the analytical laboratory of the University of Nairobi, I extend my gratitude to all the staff in the analytical laboratory.

Thirdly, a special thanks to Jersfrey Omwega, for his assistance with the Brunauer Emmett Teller (BET). In a very special way, I want to acknowledge my parents for their moral, spiritual and financial assistance.

Lastly, I want to convey my appreciation to all those who played a role, whether directly or indirectly, in the accomplishment of this thesis.

ABSTRACT

Access to clean and safe water for domestic and industrial use remains a significant challenge in developing countries of the Third World. In Kenya, safe drinking water is accessible to only 59% of the population. Multiple factors, including droughts, forest degradation, population growth, and inadequate water supply management, contribute to water scarcity in Kenya. Freshwater resources are unevenly distributed across the country and face heavy pollution from raw sewage, domestic and industrial waste, agricultural waste, and emerging pollutants like plastic, significantly limiting clean water accessibility. The main freshwater sources in Kenya encompass groundwater, water basins, dams, rivers, lakes, swamps, and springs. To address these water crises, cost-effective water treatment methods are essential. This study's focus was on water pollutants, specifically nitrates (NO^{-}_{3}), phosphates (PO_4^{3-}), and heavy metals including copper (Cu^{2+}), lead (Pb^{2+}), and cadmium (Cd^{2+}), originating primarily from agrochemicals like fertilizers and pesticides. This research investigated the potential application of clay-derived zeolites, produced from kaolinite clay material sourced from Mukurweini in Nyeri County, Kenya, for treating water contaminated with agricultural waste. The study employed wastewater containing each salt at a 1000 ppm stock solution, serially diluted to the desired concentration for evaluating zeolite efficacy in pollutant removal. Raw clay mineral samples weighing 3 kg each were subjected to thermal activation in a kiln, undergoing calcination at 600 °C and 700 °C for 2 hours. Following this, 50 g of the calcined clay mineral was mixed with NaOH (6 M, 7 M, and 8 M) using a mechanical shaker at 60 °C for 30 minutes to form a homogenous paste. The paste was then autoclaved, dried at 120 °C for 3 hours, and subsequently heated at 650 °C for 2 hours to fully activate the raw clay into zeolites. The synthesized clay-derived zeolites underwent comprehensive characterization using diverse analytical techniques: energy dispersive X-ray fluorescence (EDXRF), Fourier transform infrared spectroscopy (FTIR), scanning electron microscopy (SEM), X-ray fluorescence (XRF), and Brunauer Emmett Teller (BET). These techniques provided insights not only into the zeolite morphology but also their structural composition, physical attributes, and chemical properties. FT-IR spectrum analysis revealed O-H stretching between 3732 and 3400 cm-1, Si-O stretching at 418 cm-1, and varied peak intensities. SEM displayed an irregular heterogeneous surface with pores smaller than 0.5 µm, and surface area ranged from 3.911 to 54.311 m/g. Batch adsorption studies determined optimal conditions for pollutant removal in wastewater: calcination temperature (550–900 °C), equilibrium contact time (30 minutes), pH (7), and temperature (25 °C). Under these conditions, a remarkable 99.2% removal of NO_3^{-}, PO_4^{3-}, $Cu^{2+,}$ $Pb^{2+,}$ and Cd^{2+} was achieved for solutions with a concentration of 100 ppm for all ions. pH notably influenced adsorption capacities of the five substances. Kinetic studies demonstrated pseudo-second-order reaction models, and data aligned with the Freundlich isotherm. Reactions were exothermic and spontaneous. These findings highlight the potential of activated clay-derived zeolites in remediating agricultural waste-contaminated wastewater, offering promise for sustainable water treatment solutions.

TABLE OF CONTENTS

LIST OF FIGURES

LIST OF TABLES

LIST OF APPENDICES

LIST OF ABBREVIATIONS, ACRONYMS AND SYMBOLS

AAS	Atomic Absorption Spectroscopy
BET	Brunauer Emmett Teller
EDX	Energy-dispersive X-ray spectroscopy
FTIR	Fourier-Transform Infrared Spectroscopy
SEM	Scanning Electron Microscopy
TEM	Transmission Electron Microscopy
WHO	World Health Organization
XRD	X-Ray Diffraction
XRF	X-Ray Fluorescence
AOPs	Advanced Oxidation Processes
EC	Electrical conductivity
UV	Ultraviolet
UV-Vis	Ultra-violet visible
UON	University of Nairobi

CHAPTER ONE: INTRODUCTION

1.1 Background

Water is a valuable resource on our planet, essential for the well-being of all living organisms. Given that two-thirds of the human body comprises water, its continuous supply is essential for optimal organ function. In addition to bodily processes, water is integral to daily tasks like cooking, cleaning, and irrigation. The significance of water lies not only in its necessity but also in its quality and quantity. Excessive water can lead to destructive flooding, impacting plants, animals, and causing diseases such as cholera and hepatitis A. Conversely, water scarcity results in drought, leading to famine and exacerbating fungal and bacterial infections.

The availability of freshwater has become a notable concern in the 21st century (Saeijs & Van Berkel, 1995). Achieving a balance in freshwater distribution has become increasingly difficult as certain regions experience flooding while others face water scarcity. Numerous factors contribute to the shortage of freshwater, including the global population growth from 6.3 billion in 2000 to 7.3 billion in 2015 (United Nations, 2015). This growth has heightened the demand for clean water, particularly in industries such as food and beverage manufacturing, as well as in urban areas (Pathak *et al.*, 2015). Moreover, global warming has disrupted freshwater availability through perturbed water cycles and elevated temperatures leading to increased evaporation, heavier rainstorms, and elevated rates of drought and flooding (Jarraud, 2008)

Africa, with its arid climate exacerbated by global warming and lack of affordable water purification technologies, suffers notably from freshwater scarcity, resulting in increased shortages. This scarcity contributes to water pollution by impeding natural wastewater treatment and recycling processes. Water pollution occurs when undesired substances infiltrate water sources. Water's solvency properties make it capable of dissolving various substances, including harmful toxins detrimental to human health (Haseena *et al*., 2017)

Water pollution occurs through direct contact, such as the discharge of industrial wastewater directly into water bodies, pipe leaks, and indirect contact like the seepage of agrochemicals (fertilizers, pesticides) into groundwater and septic tank malfunctioning (Pathak *et al.*, 2015).

1.1.1 Pollution of water resources

Sources of water pollution are classified into domestic, industrial and agricultural origin.

1.1.1.1 Domestic Sources of Water Pollution

Domestic activities significantly contribute to water pollution through various means. Toxic substances, including household cleaning agents, pharmaceuticals, and personal care products, can leak from poorly maintained wastewater pipes, ultimately contaminating water bodies and posing risks to aquatic life and human health. Excessive use of fertilizers in home gardening can lead to nutrient leaching, where nitrogen and phosphorus from these fertilizers enter water sources,

fuelling algal blooms and disrupting aquatic ecosystems. Inadequate functioning of septic tanks in areas without centralized sewage treatment can result in untreated sewage entering groundwater and surface water, carrying pathogens and pollutants with it. Moreover, improper disposal of household waste, such as chemicals and oils, can introduce hazardous pollutants into water systems. Even seemingly innocent activities like car washing can release oils, grease, and chemicals that end up in storm drains and flow directly into rivers and streams, exacerbating water pollution issues.

1.1.1.2 Industrial Sources of Water Pollution

Industrial operations are another major contributor to water pollution, with a range of adverse impacts. The leakage of toxic substances from industrial sites, often containing hazardous chemicals and heavy metals, can result in water contamination, affecting both aquatic life and human populations. Ineffective treatment of industrial wastewater, which harbours contaminants such as heavy metals and organic compounds, can lead to the release of harmful substances into water bodies. Industries that discharge untreated or poorly treated waste directly into water sources contribute to the deterioration of water quality. Agricultural runoff, which is sometimes considered an industrial activity due to its scale, introduces fertilizers, pesticides, and sediment into water bodies, causing nutrient pollution and ecological harm. Moreover, mining activities can release heavy metals and sediments into water sources, causing detrimental effects on aquatic ecosystems (Jaiswal *et al.,* 2018). Addressing these industrial sources of water pollution requires stringent regulations, responsible waste management practices, technological advancements in wastewater treatment, and collaborative efforts between industries and regulatory bodies.

1.1.1.3 Agricultural Contaminants

Contaminants arising from agricultural activities stem from the necessity to enhance crop yields in response to the increasing demands of the population. This has led to the utilization of agrochemicals such as fertilizers, pesticides, and herbicides. The ongoing use of chemical fertilizers leads to the build-up of harmful substances in the soil, which subsequently leach into groundwater, causing underground water pollution (Pathak *et al.,* 2015). Agricultural practices contribute to water pollution through sedimentation, fertilizer application, irrigation, drainage, and more. The utilization of chemical fertilizers, herbicides, and pesticides stands out as a primary source of pollution. Chemical fertilizers introduce pollutants like nitrates, phosphates, potassium, copper, cadmium, and lead into water systems. Nitrate contamination, primarily originating from fertilizers, as well as sewage and industrial waste, poses health risks. Nitrate consumption can be particularly harmful to pregnant women, potentially causing foetal oxygen deficiency and leading to complications such as abortions. It can also induce methemoglobinemia (blue baby syndrome) in infants, affecting oxygen distribution in the body. Prolonged consumption of nitrate-

contaminated drinking water is associated with gastrointestinal issues and, at times, prostate cancer. Increased phosphate concentrations, surpassing the threshold of 0.5 mg/L, in water bodies lead to eutrophication, characterized by excessive algal growth that reduces oxygen levels, causing fish and other aquatic life to perish. Additionally, this phenomenon diminishes water quality due to toxins produced by algal blooms (Singh, 2013). Copper, essential in small amounts for human health, becomes detrimental when present at elevated levels, surpassing 1.3 mg/L, causing harm to the kidneys and liver. It enters the human body through food and drinking water, often originating from herbicides, accumulating in soil and finding its way into water bodies through leaching and runoff. Lead, a toxic metal present in many fertilizers, accumulates within the body, primarily targeting organs such as the brain, liver, and bones. For children, lead accumulation can lead to irreversible neurological damage (Jaishankar *et al*., 2014). Cadmium is predominantly found in phosphate-based chemical fertilizers. Even minimal cadmium concentrations within the body can lead to considerable harm. Regular cadmium consumption is linked to bone abnormalities and various health issues, including high blood pressure, lung disorders, kidney dysfunction, and chest discomfort (Singh, 2013).

1.1.2 Clay-Derived Zeolites as Potential Wastewater Adsorbent

Clay and zeolites have played roles in water treatment processes as effective adsorbents, known for their cost-effectiveness and efficiency (Caponi *et al*., 2017). Clay and zeolite, both aluminosilicates, occur naturally. Zeolites, with their robust structures resistant to easy disruption, can be synthesized from clay through heat treatment (Kianfar, 2019). Clay exhibits diverse properties depending on conditions—plasticity when wet, acquiring permanent physical and chemical traits upon firing, which can be controlled (Fernandes *et al.*, 2010). Zeolites, microporous aluminosilicates, are widely used as adsorbents and catalysts (Mastropietro *et al*., 2016).

1.2 Problem Statement

Water is indispensable for human life, crucial for various purposes like drinking, cooking, farming, and hygiene. However, access to clean water remains problematic, particularly in developing nations like Kenya. Often, women and children must journey long distances to access water, often of subpar quality. The critical importance of providing cost-effective means to enhance water quality becomes evident when considering that approximately 340,000 children under five die annually due to insufficient water quality (Connor, 2015). Agriculture is pivotal in Africa's economy, leading to extensive use of fertilizers, herbicides, and pesticides. Their components, such as nitrates, phosphates, and heavy metals like lead, copper, and cadmium, can be hazardous when not used judiciously, finding their way into water bodies via runoff and leaching. Clay minerals and microporous zeolites are effective adsorbents utilized in water treatment primarily for their affordability and widespread accessibility (Pranoto *et al*., 2018). In light of these factors, this study

aims to synthesize microporous zeolites from natural clay and evaluate their capacity to adsorb agricultural pollutants from water.

1.3 Objectives

1.3.1 General Objective

To synthesize microporous zeolites from natural clay and determining its adsorptive capacities for the removal of agricultural pollutants from water.

1.3.2 Specific Objectives

i) To characterize the natural clay samples.
ii) To synthesize and characterize microporous zeolites from the clay.
iii) To determine and compare the adsorptive capacities of both the clay and Zeolites in the removal of nitrates, phosphates, lead, copper and cadmium from water.

1.4 Justification and Significance

Though clay samples from Mukurweini, Nyeri County, were once exported, little research has been done to understand their properties and composition. However, locals have utilized this clay for domestic purposes, particularly in making clay briquettes. This study intends to capitalize on this clay to create zeolites for water treatment. Access to clean water remains a challenge in many developing nations, necessitating effective, low-cost water treatment technologies. Given the proven potential of zeolites and clay in water treatment, evaluating the adsorption properties of this specific clay from Nyeri County, as well as the synthesized zeolites, holds significant promise.

CHAPTER TWO: LITERATURE REVIEW

2.1 Water pollution

Water is not only an important substance, but it is also an indispensable natural resource that is relied upon by plants and animals, either as their habitat or for their development. Water contains neither energy nor nutrients, but it is necessary for the survival of every living being. The chances of human survival without water are very slim compared to their survival without food. Approximately two-thirds of the human body consists of water, and vital organs such as the brain consist of approximately 85% water (Sammel & McMartin, 2014). Water possesses several properties, some of which are unique and indispensable for the operations of plants, animals, and the human body. Water is a universal solvent and can therefore dissolve compounds that could be harmful to the environment or detrimental to human health. Consequently, there is a pressing need to monitor the quality of water discharged into the surroundings, and most importantly, the water that is consumed. Water quality has significantly deteriorated, a phenomenon attributed to two primary factors: i) environmental degradation, which has resulted in global warming and subsequent climate change, and ii) human careless actions, such as the indiscriminate release of untreated wastewater and toxic chemicals into aquatic environments, among other factors (Khan, 2011).

Water pollution has several repercussions, which can be summarized into two groups: environmental degradation and the deterioration of life. Polluted water affects the environment by either disrupting or destroying ecosystems. The major environmental effect of water pollution is the reduction of biodiversity on Earth, especially in aquatic life, where a hostile habitat is created, leading to the destruction of aquatic ecosystems. This destruction creates an imbalance in the ecosystem, which has dangerous long-term effects, such as climate change and global warming (Adejumoke *et al.,* 2018).

On the other hand, water pollution can severely impact human health, depending on the pollutants found in the water. This means that water pollution can be the source of various diseases, ranging from waterborne diseases like vomiting and diarrhea to more severe conditions such as cardiovascular diseases, kidney failure, and different types of cancer, among others (Ur Rehman, 2019).

2.2 Pollutants

Water becomes contaminated by various forms of pollutants due to its ability to serve as a sink for a variety of substances. The different types of substances stored within a water body can either be beneficial or detrimental to human well-being. Consequently, it is crucial to monitor water quality to identify the types of pollutants present and their sources in order to control them.

Water pollutants have various origins, including sewage effluent, industrial waste, pesticides, chemical fertilizers, microplastics, among others (Pathak *et al*., 2015). Generally, the sources of water pollution can be categorized into three: domestic, commercial, and agricultural. i) The domestic source primarily includes household pollutants such as bathwater and cleaning water, which often contain detergents with toxic chemicals. When these pollutants are released untreated into water bodies, they lead to water pollution. ii) Commercial sources of pollution originate from various businesses, each contributing to water pollution differently depending on its nature. For example, chemical industries tend to contribute more significantly to water pollution compared to other types of businesses due to the hazardous nature of their wastes. They deal with toxic chemicals and radioactive substances that are highly detrimental to human health and therefore require more stringent handling procedures. iii) Agricultural activities make a substantial contribution to water pollution and are considered a major non-point source of water pollution. They contribute to underground water pollution through the leaching of chemical fertilizers and pesticides. Rainwater also pollutes surface water by dissolving and carrying chemical fertilizers from agricultural activities into water bodies (Sagasta *et al*., 2017).

2.3 Agricultural pollutants

Population growth has significantly contributed to the widespread usage of chemical fertilizers, indirectly leading to water pollution (Sagasta *et al*., 2017). While chemical fertilizers do contribute to both water and air pollution, their use remains a crucial aspect of agricultural activity. To ensure the maximum productivity of land, it is essential to maintain sufficient nutrients in the soil. However, the continuous extraction of nutrients from the soil by crops necessitates the application of fertilizers to achieve desired yields (Selim, 2020). The substantial population growth in recent decades has heightened the demand for agricultural production, leading to an excessive use of chemical fertilizers.

The fertilizer industry stands prominently among the key culprits responsible for the introduction of heavy metals and radionuclides into the environment. This is largely attributed to the extensive and often unregulated application of agrochemicals, with fertilizers at the forefront. The consequence of this indiscriminate use is the gradual build-up of heavy metals within the soil, creating a concerning environmental challenge (Alengebawy *et al*., 2021). Over time, these accumulated heavy metals, alongside nitrates and phosphates, become susceptible to being washed away through surface runoff. This runoff, containing a cocktail of pollutants, subsequently finds its way into water reservoirs, rivers, and lakes. Here, it triggers a series of ecological disturbances, primarily contributing to eutrophication—an overabundance of nutrients that leads to excessive algal growth. The repercussions of this process extend beyond environmental concerns, as it also raises apprehensions about various health issues affecting both humans and aquatic ecosystems (Savci, 2012).

2.3.1 Nitrates

Nitrates supply nitrogen, a crucial element for plant development and a significant contributor to the production of amino acids used in synthesizing proteins. Proteins have a pivotal function in the overall growth and development of plants. They are involved in regulating phototropism, which is the plant's response to light and darkness. Additionally, proteins participate in chemical reactions that generate energy, enabling membrane transport and the formation of intracellular structures (Leghari *et al*., 2016). Consequently, a deficiency in nitrates significantly hampers plant growth.

It's important to note that nitrates are not typically found in fertilizers in their simple form; they are usually combined with other elements such as ammonium nitrate or sometimes with essential metals for plant development, like calcium (as in calcium ammonium nitrate). Often, ammonium nitrate undergoes oxidation, resulting in the separation of ammonia and nitrate. Nitrate can enter the human body directly through unwashed vegetables or via drinking water (Bryan & van Grinsven, 2013).

The nitrate that accumulates in the soil due to leaching can contaminate both underground and surface water through runoff. Nitrate consumption has significant implications for human health, including the development of methemoglobinemia (blue baby syndrome), a hemoglobin disorder resulting from the oxidation of hemoglobin. Oxidized hemoglobin becomes methemoglobin, interfering with the efficient distribution of oxygen in the blood to other body tissues (Majumdar, 2003). Methemoglobinemia predominantly affects infants and can be fatal. In pregnant women, it may lead to miscarriage (Singh, 2013). Nitrate intake has also been linked to gastrointestinal cancer, prostate cancer in some cases, as well as thyroid and reproductive system diseases. Children with a history of early nitrate intake are at a higher risk of developing diabetes mellitus (Huang, 2013).

2.3.2 Phosphate

Phosphate plays a vital role in plant biomass production through photosynthesis, a process that converts solar energy into chemical energy, fueling plant growth and development (Thuynsma *et al*., 2016). Additionally, phosphate serves as a crucial source of phosphorus, the second macronutrient essential for plant growth. However, it becomes harmful to both the environment and humans when used excessively. When phosphate levels exceed 0.5mg/L in a water body, it becomes evident through a phenomenon called eutrophication, characterized by an excessive nutrient enrichment, especially phosphate (Ansari *et al*., 2011).

Factors such as population growth, climate change, and economic development contribute to an increased demand for freshwater, necessitating measures to combat eutrophication, which poses a significant threat to water quality (Ansari *et al*., 2011). Eutrophication not only restricts economic activities like fishing and recreational water use but also hampers access to safe drinking water, among other adverse effects. As dead algae decay, organic matter accumulates in the water body,

depleting dissolved oxygen levels and ultimately leading to the death of aquatic life (Ansari & Gill, 2013). Algae can also produce toxins that are harmful to both animals and humans, potentially causing various health issues such as neurotoxicity, liver damage, and eye and skin irritation, among others (Hofbauer, 2021).

2.3.3 Copper

Copper is a crucial micronutrient required for the growth of plants, playing a crucial role in photosynthesis. Its absence can be detected through changes in leaf coloration, ultimately leading to a substantial decrease in crop production (Yamasaki *et al*., 2008). Copper is primarily found in herbicides and occasionally in fertilizers. Additionally, it is an essential element for human health, contributing to the formation of red blood cells. However, excessive copper intake can be highly detrimental to the human body, potentially causing severe diseases.

Copper toxicity primarily impacts specific body systems, including the cardiovascular system, where it disrupts red blood cells, leading to the release of hemoglobin into the bloodstream, a condition known as hemolysis. The accumulation of copper also manifests in the gastrointestinal system, resulting in symptoms such as nausea and vomiting. Furthermore, copper's toxicity is most pronounced in the hepatic system, where elevated concentrations can damage the liver. High copper intake also affects the central nervous system and renal system, potentially leading to kidney failure (Council *et al*., 2000).

2.3.4 Lead

Lead is typically found in chemical fertilizers in trace amounts and does not have any essential value for plant growth (Gupta *et al*., 2014). However, unregulated usage of chemical fertilizers leads to the buildup of lead in the soil. This accumulation, when taken up by plant roots, disrupts nearly all aspects of plant function, causing dysfunction in each part of the plant. This disruption can lead to delays or a complete halt in plant growth. Lead also affects the biochemical functioning of the plant, resulting in the disruption of chlorophyll production and influencing protein content, among other effects (Shahid *et al*., 2011).

Lead readily contaminates underground water through leaching, a phenomenon observed in many Sub-Saharan African countries. Lead exposure primarily impacts the neurological system of children, often leading to a decrease in a child's IQ (Intelligence Quotient) or attention span, with some of these harmful effects being permanent and irreversible. Lead can also affect an unborn child through the mother's blood, potentially damaging the neurological system or causing a miscarriage (Manna *et al*., 2019). Additionally, it has an impact on the cardiovascular, renal, and reproductive systems, leading to infertility in both males and females (Assi *et al*., 2016).

2.3.5 Cadmium

Cadmium is considered a non-essential element for plant growth (Cannata *et al*., 2013). It is often present in fertilizers, especially phosphate fertilizers, due to the high cadmium content in phosphate rock (Roberts, 2014). The accumulation of cadmium in the soil and groundwater is linked to overuse of chemical fertilizers, resulting in adverse effects on plant development, environmental pollution, and human health.

Cadmium negatively impacts human health by damaging or impeding the proper functioning of various body organs. Similar to arsenic, cadmium affects the renal system, leading to nephropathy, which damages kidney blood vessels and hinders kidney function, potentially resulting in kidney failure (Nordberg *et al*., 2014). It also affects the skeletal system, interacting with bone cells, reducing bone mineralization, and inhibiting collagen production. This can lead to osteoporosis, a condition characterized by weakened bones prone to fractures (Rahimzadeh *et al*., 2017).

Furthermore, cadmium affects the cardiovascular system, contributing to several diseases such as hypertension, diabetes, vascular endothelium dysfunction, peripheral arterial disease, and an increased risk of cardiovascular-related deaths (Bernhoft, 2013). In the mammalian male reproductive system, it diminishes libido and increases the production of immature sperm (Pizent *et al*., 2012). In the female reproductive system, it interferes with the proper functioning of the ovarian system, impairs oocyte development, and raises the risk of spontaneous abortions (Thompson & Bannigan, 2008). Additionally, cadmium is carcinogenic, causing various types of cancer, including renal, lung, liver, and bladder cancer (Filipič, 2013).

2.4 Methods of water treatment

Water treatment methods are chosen based on their efficiency, cost-effectiveness, and availability. Additionally, the selection of methods may be influenced by the specific quality of the water that needs treatment. There are several methods of water treatment, though they can be summarized into four as follows;

i) Flocculation and coagulation,
ii) Disinfection and
iii) Filtration
iv) Advanced oxidation processes

2.4.1 Flocculation and coagulation

Flocculation and coagulation are used in the treatment of both wastewater and potable water. These treatment methods are most often used together in water treatment plants and are usually followed by filtration and/or sedimentation. They consume less energy, and their operation is based on the removal of turbidity, implying that the removal of suspended particles might also lead to the reduction or even destruction of the microorganism support structure (Pooi & Ng, 2018).

Coagulation is a chemical process in water treatment where small particles are destabilized and then agglomerated. The coagulants, which are positively charged substances, are used to neutralize the negative charge of suspended particles, preventing them from repelling each other. The most common coagulants used are metallic salts (such as aluminum salts) and polymers (polyelectrolytes). Flocculation, on the other hand, is a physical process that facilitates the agglomeration of destabilized small particles into larger particles called floccules. This process uses flocculants such as ferric chloride and aluminum sulfate, which are gradually added to the water while agitating it, allowing the floccules to gradually increase in size and form larger aggregates. The larger particles tend to settle at the bottom due to gravitational forces (Tzoupanos & Zouboulis, 2008).

Electro-coagulation (EC) is a wastewater treatment technique widely used for stubborn pollutants such as organic waste and emulsified oil. This technique incorporates several mechanisms at once, including coagulation, adsorption, electro-oxidation, electro-reduction, and more (Bener *et al*., 2019).

2.4.2 Disinfection

Disinfection is a water treatment process that focuses on the destruction or inactivation of microorganisms. There are different disinfectants based on the type of microorganism suspected to be present in the water being treated (Pooi & Ng, 2018). Disinfectants are effective when used in the correct dosage; however, an overdose of disinfectant can lead to the accumulation of its by-products, such as trihalomethanes and halo nitromethanes, among others, which can sometimes be harmful to human health, aquatic life, and the environment (Sun *et al*., 2019).

There are several methods used in the water disinfection process. One of the oldest methods is chlorination, which is a process of using chlorine to destroy or inhibit harmful microorganisms. Chlorine has been proven to be more effective in the destruction of bacteria. It is, however, a corrosive substance. If used in the correct dosage, it will kill most microorganisms, after which it reacts with the air and volatilizes. Chlorine disinfectants exist in three states: liquid, solid, and gas. In the gaseous state, chlorine is highly poisonous and very lethal to humans, even in small quantities. Liquid chlorine is highly corrosive and should be handled with great care, while solid chlorine, which is the most commonly used and less dangerous, is normally combined with calcium (Calcium hypochlorite), making it a stable compound (O'Connor, 2011). Other methods that can also be used in the disinfection of water treatment processes include UV irradiation and the use of ozone gas (O_3) to kill microorganisms (Pooi & Ng, 2018).

2.4.3 Filtration

Filtration is one of the methods commonly used in water treatment. The principle behind filtration is based on particle size, where the water to be treated is passed through a medium that traps solids and only allows water to pass through (Patel, 2010). The filter medium (membrane) determines the effectiveness of filtration. The filtration medium can be classified into five groups, as illustrated in Figure 2.1 below.

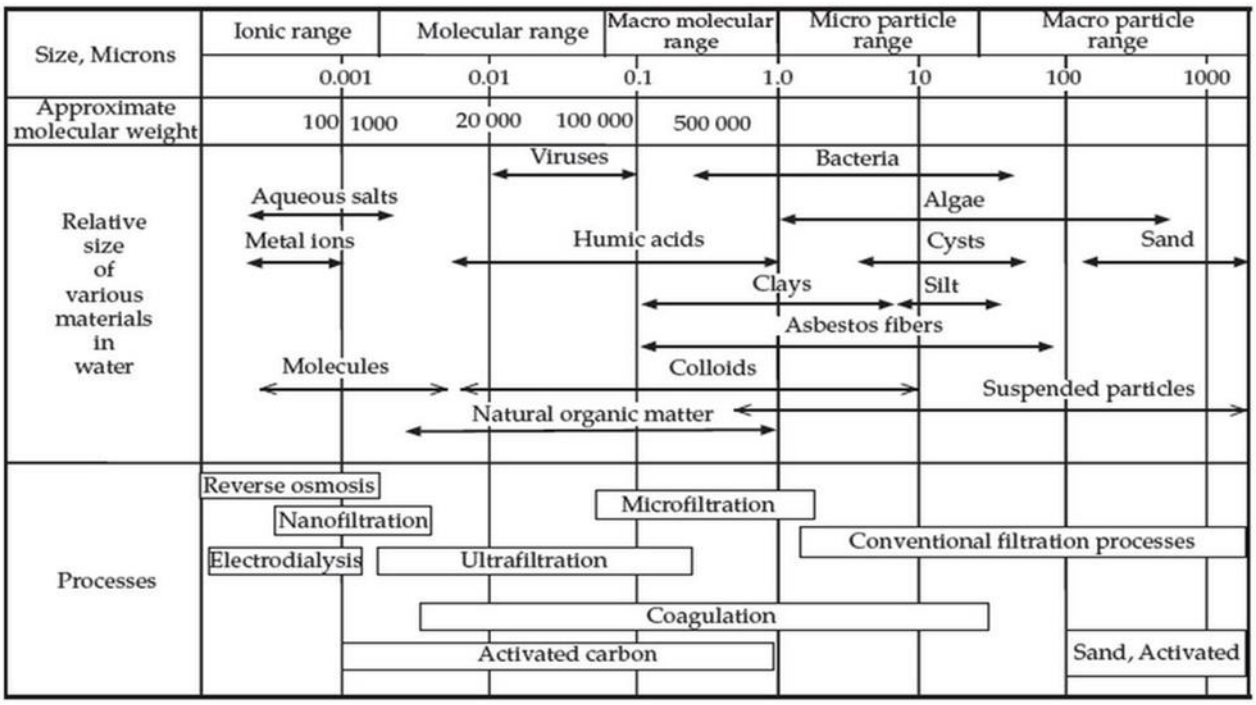

Figure 2. 1 Classification of filtration media approximate by MWCO

2.4.4 Advanced Oxidation Processes (AOP)

AOP is a series of chemical water treatment techniques that utilize oxidation to eliminate organic contaminants. This represents one of the more expensive methods for treating wastewater, primarily employed for stable pollutants that cannot be easily removed. The hydroxyl free radical, being a potent oxidant, is predominantly used in AOP for the destabilization and mineralization of pollutants (Mahdi *et al*., 2021). There are several AOP methods, including UV/hydrogen peroxide, ozonation, sonolysis, gamma radiation, among others.

2.4.4.1 Ozonation

Ozonation is an AOP chemical water treatment technique that utilizes ozone to treat wastewater. This method can be used for both water treatment and disinfection. I) For water treatment, ozone is introduced into wastewater, where it decomposes into hydroxyl groups, which are highly potent oxidants that destabilize and mineralize pollutants (Ahmaruzzaman & Laxmi Gayatri, 2010). II) Ozone, when used as a disinfection method, can eliminate various harmful microorganisms by breaking down their cell walls. This action creates a toxic environment within the cell due to the combination of ozone by-products and the cell's contents, ultimately causing harm to the pathogenic organisms (Nghi *et al*., 2018).

2.4.4.2 Sonolysis

This technique employs ultrasonic irradiation for water treatment. The production of hydroxyl free radicals occurs after the dissociation of protons and hydroxyl radicals from water using ultrasound irradiation. Similar to Ozonation, sonolysis can also be employed for water disinfection. Furthermore, the combination of these two techniques can result in more effective wastewater disinfection (Naddeo *et al*., 2015).

2.4.4.3 Gamma-radiolysis

This is an expensive wastewater treatment technique primarily used for nuclear waste. Gamma radiolysis involves the use of gamma irradiation to dissociate molecules. The water molecule is decomposed into both oxidizing agents (hydroxyl radicals and hydrogen peroxide) and reducing agents. The oxidizing agents are then used to dissociate and mineralize pollutants (Nawaz & Sengupta, 2019).

2.5 Adsorption Isotherms

The adsorption isotherm is one of the most effective ways to study adsorption while representing the relationship between the adsorbent, the adsorbate, and various external factors (Bleam, 2017). Adsorption isotherms depict these relationships through graphs. By examining the adsorption isotherm graph, one can determine the conditions under which adsorption capacity is greatest and how to enhance it. Various models of adsorption isotherms exist, including Langmuir, Freundlich, Temkin, Dubinin-Radushkevick, Harkins–Jura, Halsey, Redlich–Peterson, and Brunauer, Emmett, and Teller (BET) isotherm models (Bushra & Ahmad, 2016).

2.5.1 Langmuir isotherm model

This isotherm model posits that adsorption takes place at a precise location on the adsorbent's homogeneous surface. This method is effective in adsorption processes that involve a molecular monolayer. This model assumes the following factors:

i) The adsorbent has an active site, and only one adsorbate can interact with each adsorbent active site.
ii) All adsorbed molecules have the same energy; therefore, there is no interaction between neighboring molecules.
iii) The adsorption frequency is proportional to the solution concentration.
iv) The adsorbate completely occupies the active sites on the adsorbent (Sahu & Singh, 2019).

The linear Langmuir isotherm is given by the following equation:

$$\frac{C_e}{q_e} = \frac{1}{bK_L} + \frac{C_e}{b}$$ Equation 0:1

Where;

C_e is the equilibrium concentration in mg/L,

q_e the amount adsorbed per unit mass of adsorbent mg/g and

K_L the Langmuir equilibrium constant

A plot of $\frac{C_e}{q_e}$ versus C_e gives a straight line having a slope as $\frac{1}{b}$ and an intercept as $\frac{1}{bK_L}$

2.5.2 Freundlich isotherm model

The Freundlich isotherm model deals with adsorption processes on heterogeneous sites of the adsorbent with molecular multilayers. This model offers several advantages: i) It provides an adequate description of non-linear adsorption in a clear and well-defined manner regarding the adsorbate concentration. ii) It offers a simplified mathematical equation that is easy to use and describes adsorption sites with different energy levels, unlike the Langmuir isotherm model (Proctor & Toro-Vazquez, 2009). However, the Freundlich isotherm model cannot predict the maximum adsorption occurrence (Sparks, 2013).

The Freundlich isotherm is given by the following model equation.

$q_e = k_f (C_e^{1/n})$ Equation 0:2

$$lnq_e = lnK_f + \frac{1}{n} lnC_e$$ Equation 0:3

Where;

K_f the Freundlich isotherm is constant expressed in (mg/g),

C_e the equilibrium concentration in mg/L,

q_e the amount adsorbed per unit mass of adsorbent mg/g.

The graph will have a straight line from the plot of q_e versusC_e with a slope of 1/n and an intercept of$\ln K_f$.

2.5.3 Temkin isotherm model

Temkin isotherm model focuses on the adsorbate-adsorbent interaction regardless of external factors. Therefore, it is often used in adsorption processes with non-uniform distribution of heat. This model assumes that the decrease in temperature affects adsorption linearly, rather than following the logarithmic trend suggested by the Freundlich model (Erhayeml *et al*., 2015). Temkin isotherm model has the following model equation

$$q_e = \left(\frac{RT}{b}\right) (\ln A + \ln Ce)$$ Equation 2:4

where,

C_e is the equilibrium concentration in mg/L,

q_e is the amount adsorbed per unit mass of adsorbent mg/ g,

A and B are Temkin constant,

R is the universal gas constant and T is absolute temperature.

2.6 Adsorption thermodynamics and Kinetics

Adsorption thermodynamics is a crucial parameter in the adsorption process as it offers insights into the spontaneity of the adsorption process. This information is determined from Gibbs's free energy(ΔG°), which is calculated based on the change in both the entropy (ΔS°) and enthalpy (ΔH°) of the system (Das & Chowdhury, 2011).

$\Delta G^{\circ} = -RT\ln K_{\circ}$ Equation 2:5

$\Delta G^{\circ} = \Delta H - T\Delta S$ Equation 2:6

$-RT\ln K_{\circ} = \Delta H - T\Delta S$ Equation 2:7

$\ln K_{\circ} = \frac{\Delta S^{\circ}}{R} - \frac{\Delta H^{\circ}}{RT}$ Equation 2:8

Where,

ΔG° is Change in Gibb's free energy,

ΔS° change in entropy,

ΔH° change in enthalpy,

R the universal gas constant,

K the equilibrium constant and

T absolute temperature.

Adsorption kinetics involve measuring the speed of adsorption over time. It describes the adsorption mechanism and assists in assessing the adsorbent. Numerous kinetic models have been created to assess the rates of adsorption. The most frequently applied adsorption kinetic models in the removal of water pollutants are the Pseudo-first-order and Pseudo-second-order kinetic models.

2.6.1 Pseudo-first- order kinetic model

The Pseudo-first-order kinetic model is the first kinetic model ever used to determine adsorption rates. This model utilizes the adsorption capacity to calculate the adsorption rate (Vijayakumar *et al*., 2012).

The linear form of the model is given in Equation 2:9.

$\ln(q_e - q_t) = \ln q_e - K_1 t$ Equation 2:9

Where:

q_e is the amount of adsorbate consumed at equilibrium,

q_t the amount of adsorbate consumed at time t and

K_1 the first order rate constant

2.6.2 Pseudo-second-second kinetic model

The pseudo-second-order kinetic model, unlike the pseudo-first-order kinetic model, is based on the adsorbent concentration for determining the adsorption rate. (Vijayakumar *et al*., 2012). Equ 2.10 gives the linear equation from of this model

$$\frac{t}{q_t} = \frac{1}{K_2\ q_e{}^2} + \frac{1}{q_e}t \qquad \text{Equation 2:10}$$

$$h = K_2\ q_e{}^2 \qquad \text{Equation 2:11}$$

Where;

h is the initial adsorption rate and

$K_2$is the second order rate constant.

2.7 Adsorbents

The adsorbent, which serves as the surface where adsorbates gather and attach during the adsorption process, has a significant role in the adsorption study. The structural and chemical composition of the adsorbent, including ruptures, pores, and extremities, has a profound influence on the adsorption study (Tien, 2018). In the present study, the focus was directed toward clay minerals and zeolites among several available adsorbents because their effectiveness, efficiency, and affordability for water treatment involving various types of pollutants (adsorbates) such as heavy metals and inorganic pollutants have been demonstrated on multiple occasions (Caponi *et al*., 2017).

Battas *et al*. conducted a study in 2019 using local clay as an adsorbent to remove nitrate in a batch experiment. The experiment's findings showed that nitrate was efficiently removed from the aqueous solution, and as the adsorbent concentration increased, so did the adsorption efficiency.

Cho *et al*. (2010) conducted a similar experiment in which they used clay minerals as adsorbents to remove nitrate and ammonia from underground water. According to the study's findings, clay minerals are highly efficient. In a different study, El Ouardi *et al*. (2015) used Moroccan clay minerals in their search for an inexpensive adsorbent to remove nitrate from water. Moroccan clay minerals were found to be affordable and effective adsorbents for eliminating nitrate from water. Different types of clay minerals were used during the experiment, such as Smectite and kaolinite; these adsorbents effectively removed nitrate and phosphate ions from the water. The findings of the experiment conducted by Hamdi & Srasra (2012) demonstrated that phosphate ion removal is more efficient at a lower aqueous pH. In another experiment, Zamparas *et al*. (2012) found that 80% of the phosphate was eliminated in just one hour when using modified clay minerals for lake restoration. Saki *et al*. (2019) studied the usage of halloysite clay minerals for the successful removal of phosphate from agricultural runoff water. Additionally, studies have demonstrated the effectiveness of clay minerals in removing heavy metals from water. (Yadav *et al*., 2019). They

have been successfully used to remove copper and cadmium from water using a mixture of clay as an adsorbent (Mnasri-Ghnimi & Frini-Srasra, 2019).

2.7.1 Clay

Clay is a natural material formed from fine-grained minerals that belong to the crystalline hydrous silicate group. It exhibits some plasticity when wet and shows different properties when heated under controlled conditions. Clay minerals are composed of various finely grained minerals, which are responsible for different types of clay minerals. Clay minerals mostly belong to the phyllosilicate family, meaning they are primarily formed from several silicate layers. However, it is essential to note that not all clay minerals are from the phyllosilicate family (Hillier, 1978).

2.7.2 Mineral structure of clay

Clay minerals are composed of hydrous silicate layers that consist of an arrangement of planes of atoms, forming layers. These layers are reflected through their crystal morphologies and behavior (Hillier, 1978). They are mostly composed of silicate layers (phyllosilicates) that have essentially two different components: tetrahedral and octahedral sheets, depending on their structures.

2.7.2.1 Tetrahedral and Octahedral sheet

The tetrahedral sheets are usually composed of silicon ion surrounded by four oxygen atoms, and they are described as corner-linked tetrahedral. The principal atom in this tetrahedral sheet is silicon ion (Si^{4+}cation), but aluminium ion (Al^{3+}) is sometimes present in some tetrahedral sheet substituting the silicon ion, leading to some charge deficiency due to the difference in charge between Si^{4+} and Al^{3+} which has to be balanced. The tetrahedral sheet is usually formed by linking several tetrahedrons; each tetrahedron shares three out of their four oxygen atoms surrounding their silicon ion. Only one oxygen atom is shared between two tetrahedrons, implying two tetrahedrons are only linked by one oxygen atom, leading to the formation of a continuous tetrahedral sheet (Ani & Sarapää, 2008). The octahedral sheet also referred to as edge sharing octahedral. It has different cations from those of tetrahedral sheet as the main cations that include aluminium (Al^{3+}), iron (Fe^{2+},Fe^{3+}) and magnesium (Mg^{2+}) ions surrounded by oxygen and/or hydroxide (Gibbons *et al.*, 2020). Octahedral sheets occur between two planes of closely packed anions, which can be oxygen and/or hydroxide surrounding a cation. The cations positioned in the middle of the sheet and adjacent to each anion occupy three positions within these two planes of densely packed anions (Huggett, 2020). The octahedral sheet is divided into two groups; di- and tri-octahedral sheets, depending on the ratio between the cation and the anion that enable the charge balance. The di-octahedral sheet has one vacant site, meaning that, for every two octahedral sheets containing a trivalent cation there is a vacant site. The tri-octahedral sheet on the other hand has no vacant site,

and the cation is divalent (Bergaya *et al*., 2006) the tetrahedral and octahedral structures are illustrated in figure 2.2.

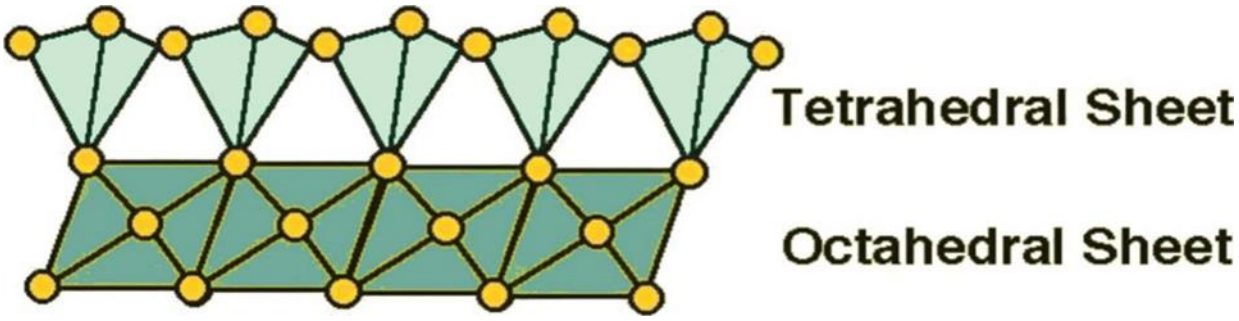

Figure 2. 2: Tetrahedral sheet structure is represented in the upper section and octahedral sheet structure is represented in the lower section

2.7.2.2 Layers

The main components of a phyllosilicate are tetrahedral and octahedral sheets. The combination of these sheets forms a layer, which is considered the basic unit of a clay mineral. This combination is quite feasible because their lateral dimensions are nearly equivalent. Therefore, two types of layers are formed: i) 1:1 layer, also referred to as T-O layer, is formed by replacing the octahedral anions with oxygen from the tetrahedral sheet. Every two octahedral anions out of three are replaced by oxygen (Hillier, 1978). ii) 2:1 layer, also referred to as T-O-T layer, in this configuration, two tetrahedral sheets are situated between an octahedral sheet, and oxygen from the tetrahedral sheet substitutes for approximately two-thirds of the hydroxide ions. (Ani & Sarapää, 2008). Figure 2.3 illustrates a layer formed from the combination of both tetrahedral and octahedral sheets.

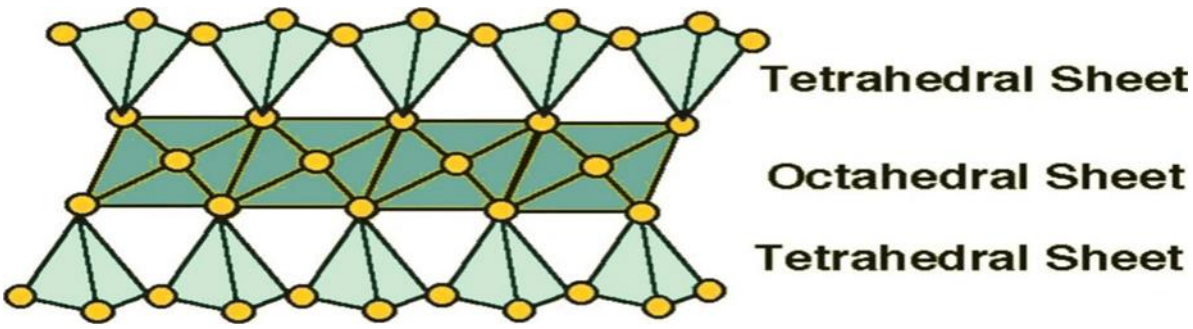

Figure 2. 3: Phyllosilicate layer

2.7.3 Classification of clay minerals

Clay mineral classification is generally based on the type of layer, the charge present, and the different compartments of each species. Therefore, classification is rooted in the differences in their structures and chemical components. Phyllosilicates comprise two types of layers: i) A 1:1 layer, which constitutes a group of serpentine-kaolin. ii) A 2:1 layer, composed of six groups that include talc-Pyrophyllite, Smectite, vermiculite, mica, illite, chlorite, and sepiolite-palygorskite. Figure 2.4 provides a detailed classification of clay minerals according to (El-Shater *et al*., 2021).

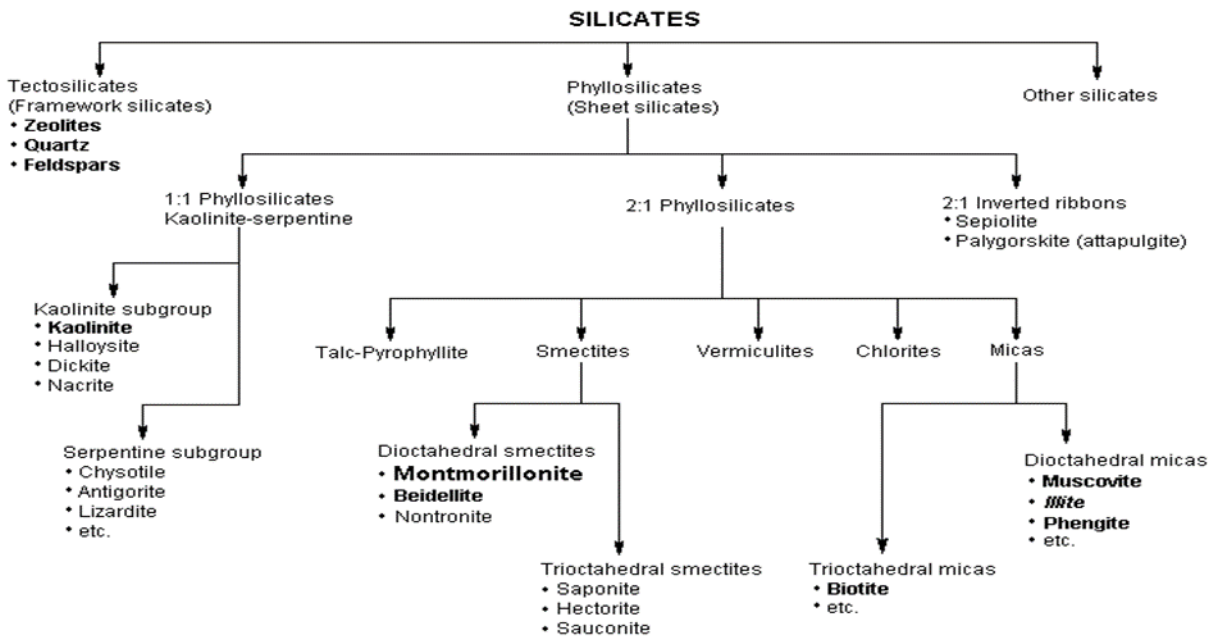

Figure 2. 4: Detailed classification of clay minerals

2.7.4 Zeolite

Zeolites are microporous minerals used primarily as adsorbents to control environmental pollution and as catalysts in chemical reactions. The zeolite structure consists of aluminosilicates carrying a negative charge, which is balanced by either positive ions or external cations surrounding the zeolites (Rhodes, 2010). Zeolites exhibit distinct properties compared to other aluminosilicates due to their aluminium-to-silicon ion ratio and complex structure. The aluminosilicates structure of zeolites is formed by linking tetrahedral sheets composed of either silicon or aluminium ions as their cations, resulting in a polyhedral structure. This polyhedral structure takes on three different forms: cubic, hexagonal prism, and truncated octahedral. These forms are organized in a way that creates pores and supercages within their structures. These supercage structures are responsible for the sieving effect of zeolites. Notably, the supercage has a well-defined hole, allowing only specific-sized molecules to pass through it. The pores in their structure have different orientations, leading to various structures, including 1D, 2D, and 3D (Wright & Lozinska, 2011).

2.7.5 Conversion of clay mineral to zeolite

Synthetic zeolites are prepared from aluminosilicate precursor gel under steam at elevated temperatures in an autoclave. The aluminosilicate precursor gel is prepared from pure solutions of sodium silicates, which introduce silicon cations into the tetrahedral sheet, and sodium aluminate, which introduces alumina cations into the tetrahedral sheet (Johnson *et al.*, 2014). The raw materials used to produce aluminosilicate precursor gel are more expensive compared to naturally occurring clay. Therefore, the usage of clay for zeolite production offers the best option considering its low cost and availability. Clay has been utilized in the synthesis of zeolites in

numerous experiments. Kaolin is a type of clay mineral commonly used in zeolite production. The conversion of clay minerals to zeolite is based on two methods: i) Heating at a specific temperature to thermally activate the clay. ii) Hydrothermal treatment of clay with specific solutions such as alkali, depending on the type of zeolite needed (Cundy & Cox, 2003).

Olaremu *et al*. (2018) activated kaolin clay by isothermally heating it to 600°C for 2 hours to form metakaolin, which was then subjected to hydrothermal treatment using sulfuric acid to regulate the ratio between aluminium and silicon cations. Characterization of the material obtained through X-Ray diffraction (XRD), infrared spectral analysis, and Transmission Electron Microscopy confirmed its identity as zeolite.

CHAPTER THREE: MATERIALS AND METHODS

3.1 Sample Collection

The excavation of the clay material was conducted using an assortment of manual tools, which included shovels, spades, a hoe, and trowels. The excavation procedure adhered to the grid method and reached a depth of one meter (1m) below the surface.

Following the excavation, the gathered clay material underwent meticulous handling. It was placed in sealed plastic bags to preserve its structural integrity. Subsequently, these sealed bags containing the clay samples were transported to the University of Nairobi (UON) Chiromo campus. Importantly, this transportation occurred without any additional purification of the clay material and transpired under standard temperature and atmospheric conditions.

3.1.1 Sampling Site

The location was a defunct mining facility in Nyeri County, and its altitude and geographic coordinates are listed in Table 3.1 below.

Table 3. 1: Location of sampling sites

Sampling site	Longitude	Latitude
Mukurweini	37^{e} 9’ 43.8’’	0^{e} 37’ 55.9’’

The clay samples were obtained from Mukurweini in Nyeri County, Kenya

3.1.2 Sampling period and average temperature

Table 3.2 below lists the sample period and the average atmospheric temperature in Nyeri County.

Table 3. 2: Sampling duration

Sampling sites	sampling duration	Mean wastewater temperature
Mukurweini	August 2019	25℃

The average atmospheric temperature in Nyeri County during the research, as indicated in Table 3.2, was 25.1°C. The samples were obtained only once in August, 2019.

3.1.3 Map – Nyeri County

Figure 3.1 below shows a map of the study area (sampling location) in Mukurweini in Nyeri County.

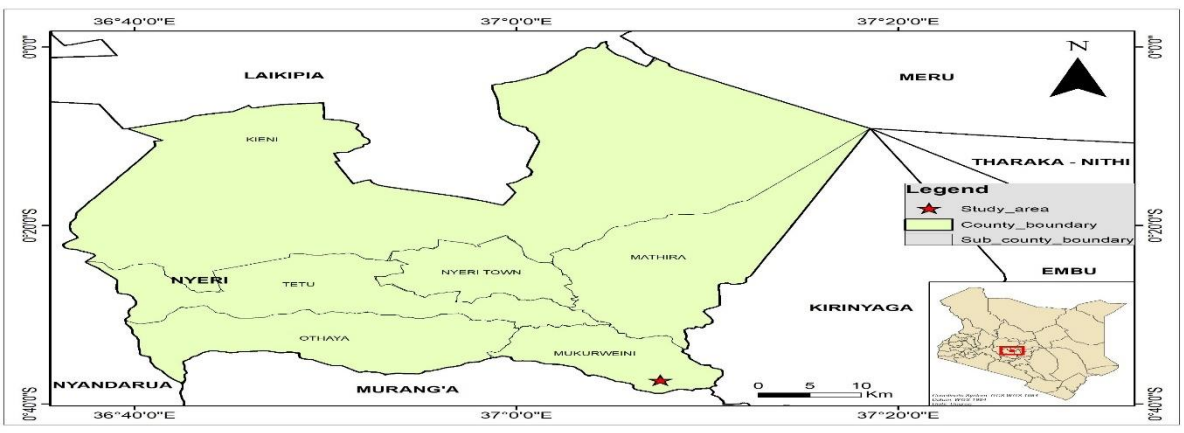

Figure 3. 1: Map of sampling area (Mukurweini. Nyeri County)

Nyeri County, situated in the Eastern Kenya highlands, experiences a cold, humid, and damp climate with an average annual rainfall of 2000 mm.

3.2 Chemicals and Reagents

The chemicals and reagents used in the study are listed in Table 3.3 below.

Table 3. 3: Chemicals and reagents

Item No.	Chemical	Quantity	Manufacturer
1	Sodium hydroxide	2000g	ACME chemicals Ltd
2	Ethanol	2.5l	ACME chemicals Ltd
3	Potassium Bromide	1000g	ACME chemicals Ltd
4	Sodium Chloride	500g	Kobian Kenya Ltd
5	Sulfuric acid	2.5l	Kobian Kenya Ltd
6	Copper Nitrate	500g	Kobian Kenya Ltd
7	Cadmium Nitrate	100g	Kobian Kenya Ltd
8	Lead Nitrate	500g	Kobian Kenya Ltd
9	Sulphanic acid	100 ml	ACME chemicals Ltd
10	Ammonium molybdate	100g	Sigma-Aldrich Ltd
11	Brucine Sulphate	25 g	Kobian Kenya Ltd
12	Hydrochloric acid	2.5l	Kobian Kenya Ltd
13	Hydrazine sulphate	500g	Kobian Kenya Ltd

3.3 Instruments

Table 3.4 below shows the list of equipment used in the study.

Table 3. 4: Equipment

Item No.	Equipment	Model
1	X- Ray Diffractometer	A Panalytical Empyrean
2	Energy Dispersive X-Ray Fluorescence	Malvern Panalytical Epsilon4
3	UV/Vis Spectrophotometer	Shimadzu UV-1700
4	Brunauer Emmett Teller	Quantachrome Novawin Version 11.02
5	Atomic Absorption Spectrophotometer	Shimadzu AA-6300
6	Environmental Incubator Shaker	Brunswick Scientific Co. Inc Edison
7	Micrometric Trista	3000 V4.02
8	Scanning Electron Microscope	Fei Nova Nanosem (WSLR S044).
9	Fourier-Transform Infrared Spectrometer	Biotech Engineering Management CO.LTD FT-IR 600.
10	Muffle Furnace	400 Fischer Scientific A-160
11	Oven	Mammert Um
12	pH- meter	Japan Ltd
13	Pelletizer	NSP 001
14	Weight balance.TY	Memmert UM 400
15	Heating mantle	Labtech Ltd
16	Mortar and pestle	

3.4 Preparation of the Adsorbents

3.4.1 Sample Preparation

The dried clay samples were left overnight in an oven set at 110°C. Subsequently, they were finely ground into particles using a pestle and mortar and then passed through a 90-micron sieve. A portion of the sample was placed in a sealed polythene bag and stored in a desiccator for characterization and adsorption studies. The other portion was utilized in the synthesis of zeolites.

3.4.2 Hydrothermal Synthesis of Zeolites from Clay Mineral

The hydrothermal synthesis process comprised three distinct steps: the thermal activation of the clay mineral, the reaction of the thermally activated clay mineral with an alkali solution, and the purification of the formed zeolites (Georgieva *et al*., 2011).

3.4.2.1 Thermal Activation of the Clay Mineral

The clay mineral underwent isothermal heating in separate batches of 500g each, lasting for 2 hours, at two distinct temperatures: 600°C and 700°C. This choice of temperature range was made because it is conducive to initiating the process of dehydroxylation, a pivotal step in activating the clay mineral and an essential prerequisite in the synthesis of zeolites (Acevedo *et al*., 2017).

3.4.2.2 Hydrothermal Treatment of the Activated Clay Mineral Using Sodium Hydroxide

The activated clay was divided into three portions, with each portion treated using 50mL solutions of 6, 7, and 8 M NaOH while being agitated using a mechanical shaker for 30 minutes at 60°C to achieve a homogenous paste. Subsequently, these mixtures were placed in a pressurized cooker, heated for 3 hours, washed with ethanol, oven-dried at 110°C for 1 hour, and finally activated in a muffle furnace at 650°C for 2 hours (Georgieva *et al.*, 2011).

3.4.3 Adsorbate preparation

A range of adsorbate concentrations containing nitrate, phosphate, lead, copper, and cadmium ions, spanning from 1000-ppm to 0.1-ppm, were meticulously prepared. To facilitate the daily preparation of 1000-ppm stock solutions, the following formula was employed, dividing the salt's molecular weight by the molecular weight of the ions dissolved in 1000 mL of distilled water. Subsequently, these stock solutions underwent dilution to achieve various concentrations required for the adsorption studies, utilizing the well-established dilution formula:

$$C_1V_1 = C_2V_2 \qquad \text{Equation 3.1}$$

Therefore, to prepare 10 ppm solutions derived from a 1000-ppm stock solution, 10 mL of the 1000-ppm stock solution was transferred into a 1000 mL conical flask. The flask was then carefully filled to the mark with distilled water to achieve the desired concentration.

3.5 Characterisation of Materials

3.5.1 Energy Dispersive X-ray Fluorescence (EDXRF)

The EDXRF analysis used a Malvern Panalytical Epsilon4 X-ray fluorescence spectrometer. The instrument was equipped with a 15 W silver anode X-ray tube, a ten-sample changer, and a helium gas flush option. An energy-dispersive silicon drift detector was utilized for the analysis. Sample preparation involved the fine grinding of samples using a motor and pestle. Subsequently, the finely ground samples were carefully packed into polypropylene XRF cups and positioned within the X-ray beam. Data collection was carried out using Epsilon Software, ensuring the acquisition of precise and comprehensive analysis results.

3.5.2 X-Ray Diffraction (XRD)

The XRD measurements were conducted at room temperature, with the angle fixed within the range of 4 to 90 degrees in 2θ. The diffractometer was equipped with a sealed copper tube X-ray radiation source (λ=1.5406). Soller apertures were positioned on both sides of the incident receiving optics. Finely ground particles were packed into a metal sample cup, which was subsequently positioned in a monochromatic X-ray beam.

The XRD doors were opened, and the samples were loaded into the instrument. After closing the doors, the following parameters were configured: a step size of 0.5 - 0.1 - 2θ and a set time of 1 second. The samples underwent scanning, and the resulting data were recorded for subsequent analysis.

3.5.3 Fourier-transform Infrared Spectroscopy (FTIR)

The samples underwent an initial drying process in an oven at 90°C for a duration of 3 hours. Subsequently, pellets were prepared using KBr in a 1:100 ratio, with 100 mg of KBr accurately weighed and combined with 1 mg of the sample. The mixture was meticulously ground in a mortar using a pestle until thorough homogenization was achieved. Following this, the prepared samples were inserted into the sample holder, which was then subjected to pressing using a hydraulic press at a pressure of 15 psi for a duration of 90 seconds.

Upon the release of pressure, the resulting sample was gently positioned within the FT-IR beam. Before recording the spectrum, the beam was purged with nitrogen gas. Ultimately, the spectrum data were recorded using a computer connected to the FT-IR instrument and were subsequently plotted using Excel for further analysis.

3.5.4 Scanning Electron Microscopy (SEM)

A FEI Nova NanoSEM (WSLR S044) scanning electron microscope was utilized. Prior to the analysis, the samples underwent preparation steps. They were initially sprinkled onto a double-sided carbon substrate and subsequently polished with epoxy to ensure a suitable surface for

examination. Following this preparation, the samples were subjected to drying in an oven for a duration of 3 hours at 65°C to remove any residual moisture.

Once dried, the prepared samples were loaded into the SEM (Scanning Electron Microscope) holder, and the chamber doors were securely closed. The SEM instrument was configured with specific parameters, including an acceleration voltage of 20 kV and the lowest magnification setting of 30X. During the scanning process, the images of the samples were meticulously reviewed to ensure quality and accuracy before being saved for further analysis and documentation.

3.5.5 Brunauer Emmett Teller (BET)

This technique was utilized to determine the surface area of the samples through multipoint adsorption data. For the BET analysis, the Quantachrome NovaWin Version 11.02 instrument was employed. Nitrogen adsorbate was used for data analysis to determine the surface area of the adsorbents. The nitrogen gas was operated under specific conditions, including a temperature of 77.350 K, a cross-sectional area of 16.200 $Å^2$, and a liquid density of 0.808 g/cc.

The analysis method was adopted from Olaremu *et al*. (2018) and included the following steps: an empty BET glass tube was initially weighed, and subsequently, 0.3 g of the sample was loaded into it, with the total weight recorded. To remove any physically adsorbed water molecules, the sample underwent degassing using nitrogen gas at 200°C for a duration of 3 hours. After degassing, the sample was re-weighed using a micrometric Trista 3000 V4.02.

Subsequently, the system was connected to a computer operating under liquid nitrogen temperature, and a nitrogen isotherm was executed. This allowed for the automatic calculation of BET surface area and porosity, providing valuable data for analysis.

3.6 Batch adsorption study

Batch adsorption studies facilitate the evaluation of adsorption capacity, adsorption isotherms, kinetics, and thermodynamics. Furthermore, they allow for the examination of the adsorbent's absorption capability under various external conditions, such as temperature, pH, adsorbate concentration, and adsorbent dosage adjustments.

3.6.1 Nitrate

In the nitrate batch adsorption study, a UV-VIS Spectrophotometer was utilized, following the Brucine method as outlined by Bain *et al*. (2009). The process involved precise dilution of the 1000-ppm nitrate stock solution to create various nitrate concentrations. These distinct nitrate solutions were then mixed with specified quantities of either clay mineral or zeolite. To ensure thorough blending, mechanical agitation was employed at a speed of 60 rpm, with the agitation duration tailored for each specific study. Subsequent to agitation, the mixtures were subjected to filtration using Whatman filter paper, and the resulting sample solutions were stored as needed.

Before reagent preparation, a series of nitrate standard solutions were meticulously prepared, spanning concentrations from 0-ppm to 10-ppm, derived from the 1000-ppm nitrate stock solution. To prepare a 30% NaCl solution, 30 grams of sodium chloride were dissolved in 100 mL of distilled water as part of the reagent preparation process. Additionally, a mixture was created by combining 50 mL of concentrated sulfuric acid with 12.5 mL of distilled water, maintaining a 4:1 ratio of sulfuric acid to distilled water, and sealing the resulting solution. Subsequently, a carefully measured blend of 1 gram of brucine sulfate, 0.1 gram of sulfanilic acid, and 3 mL of concentrated hydrochloric acid was employed to create a brucine-sulfanilic acid solution in a 100 mL conical flask.

In the experiment, both sample solutions and nitrate reference solutions were accurately measured using a 10 mL pipette within the range of 1 to 5 mL. Subsequently, while stirring and cooling the solutions in tap water, 10 mL of distilled water and 10 mL of sulfuric acid were added to each solution. The procedure was completed by slowly adding 0.5 mL of the Brucine-Sulfanilic acid solution while gently swirling the conical flask. The resulting mixture was then heated for 25 minutes at 100°C in a water bath. Following this, the solution was transferred to a cuvette for cooling and subsequently analyzed using the UV-VIS Spectrophotometer SHIMADZU UV1700.

3.6.2 Phosphate

The phosphate batch adsorption study followed the methodology outlined by Ganesh *et al*. (2012). The process involved dilution of the 1000-ppm stock phosphate solution to create various phosphate concentrations. These phosphate solutions were then mixed with distinct quantities of zeolite or clay mineral. To ensure thorough blending, mechanical agitation at a speed of 60 rpm was utilized, with the agitation duration customized for each specific study. Subsequent to agitation, the mixtures underwent filtration using Whatman filter paper, and the resulting sample solutions were stored as needed.

Before reagent preparation, a series of phosphate standard solutions were prepared from the 1000-ppm phosphate stock solution. For analysis, a 10 mL conical flask was placed in a water bath, and 1 mL of ammonium molybdate and 0.4 mL of hydrazine sulfate were added. Subsequently, the solution was diluted with distilled water. A blue-colored solution was then formed by combining 5 mL of this solution with 5 mL of either the standard solution or the sample solution, followed by heating for 30 minutes in a water bath at 60°C. After cooling, the absorbance was determined using a SHIMADZU UV1700 UV-VIS Spectrophotometer.

3.6.3 Heavy Metals

In the heavy metals batch adsorption study, sample solutions were analyzed alongside standard solutions using an AA-6300 SHIMADZU Atomic Absorption Spectrophotometer. The following procedure was adhered to:

Initially, different concentrations of heavy metals were prepared by diluting a 1000-ppm heavy metal stock solution. These heavy metal solutions were then mixed with varying quantities of clay mineral or zeolite. Mechanical agitation at 60 rpm was employed to ensure thorough mixing, with the agitation duration customized for each study. Subsequent to agitation, the mixtures were subjected to filtration using filter paper, and the resulting sample solutions were stored as required. Before reagent preparation, a series of standard solutions with known concentrations of heavy metals, ranging from 0-ppm to 10-ppm, were generated from the 1000-ppm stock solution of heavy metals.

To initiate the analysis, the computer connected to the AAS was powered on, and specific parameters were configured. The AAS lamp was adjusted based on the metal being analyzed. Subsequently, the compressed air and acetylene cylinder valves were opened, and the flame was ignited. Calibration curves were established using different prepared standards. Different prepared samples were then injected into the flame, and their absorbance values were recorded.

CHAPTER FOUR: RESULTS AND DISCUSSION

4.1 Adsorbent preparation

The adsorbents were synthesized in triplicate under two distinct temperature conditions, specifically at 600°C and 700°C. In the preparation process, three different NaOH concentrations, namely 6 M, 7 M, and 8 M, were utilized. The samples calcined at 600°C were labelled as S1, S2, and S3, corresponding to the use of 6 M, 7 M, and 8 M NaOH solutions. The same NaOH concentration variations were applied to those subjected to calcination at 700°C, denoted as S4, S5, and S6. Additionally, three more samples, S7, S8, and S9, were included in the study, representing the raw clay mineral, clay calcined at 600°C, and clay calcined at 700°C, respectively (Table 4.1).

Table 4. 1: Adsorbent identification

The table 4.1 presents the identification of adsorbents used in the study.

Name	Temperature in ◦C	NaOH concentration in Molar
S1	600	6
S2	600	7
S3	600	8
S4	700	6
S5	700	7
S6	700	8
S7	0	0
S8	600	0
S9	700	0

Figure 4.1 depicts the untreated clay mineral, exhibiting a grey color. Subsequent to calcination at two distinct temperatures (600°C and 700°C), a significant color transformation is evident in Figure 4.2 during the adsorbent preparation process. The shift from grey to pale red can be attributed to several factors, including the removal of water molecules, structural alterations, and the oxidation of iron impurities within the mineral during thermal treatment (Mulinta & Thiansem, 2019). Additionally, changes in mineral structure, composition, and the presence of new mineral phases can influence how the clay interacts with light. Some minerals or mineral phases may absorb and scatter light differently, resulting in a shift in color perception (Ibrahim *et al*., 2014). Figure 4.3 further demonstrates a pronounced color change, this time transitioning from pale red to light blue following NaOH hydrothermal treatment.

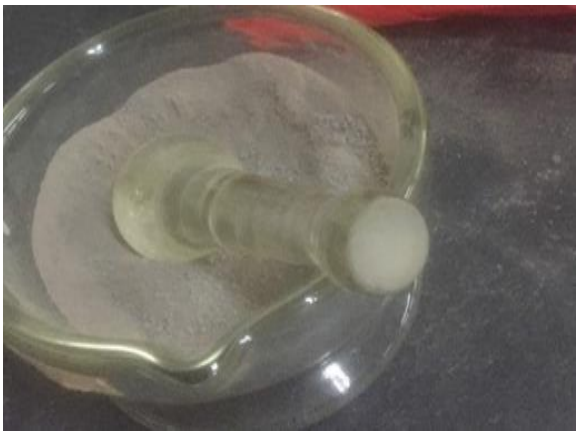

Figure 4. 1: Raw clay mineral

Figure 4. 2: Calcined clay mineral

Figure 4. 3: Zeolites

In Figure 4.1, the untreated clay mineral is depicted with its characteristic grey color. However, upon subjecting the clay to calcination at 600°C and 700°C, Figure 4.2 reveals a significant color shift from grey to a pale red hue. This transformation is attributed to several factors, including the removal of water molecules, structural adjustments, and the oxidation of iron impurities—an expected outcome of thermal treatment (Mulinta & Thiansem, 2019). Moreover, the alterations in mineral structure, composition, and the presence of new mineral phases can influence light interaction. As elucidated by Ibrahim *et al*. (2014), such variations can lead to differing light absorption and scattering properties, resulting in perceptible color changes.

Figure 4.3 demonstrates another compelling transformation, with the color transitioning from pale red to light green following NaOH hydrothermal treatment. This observation underscores the clay mineral's dynamic response to interaction with NaOH at varying concentrations. These changes, driven by the presence of new mineral phases and compositional adjustments, significantly impact the mineral's suitability as an adsorbent material.

These color shifts, coupled with the concurrent alterations in mineral properties, lay the foundation for comprehending the clay mineral's behaviour as an adsorbent. They provide valuable insights into how its structure and composition evolve under different treatment conditions, a pivotal aspect of our study.

4.2 Characterization of the adsorbent

4.2.1 Energy dispersive X-ray fluorescence (EDXRF)

EDXRF was employed to analyze the elemental composition, and the findings are presented in Tables 4.1, 4.2, and 4.3. After calcination of clay mineral (metakaolinite) samples S8 and S9 at two distinct temperatures (600°C and 700°C), it was observed that they exhibited similar elemental compositions (Table 4.2). This similarity is attributed to the typical dehydroxylation phase of clay minerals occurring within the temperature range of 400-800°C (Acevedo *et al*., 2017). Given the use of temperatures at 600°C and 700°C in this study, it is evident that hydroxide groups were lost in both S8 and S9.

Following hydrothermal treatment with NaOH solutions at three different concentrations (6 M, 7 M, and 8 M) using metakaolinite derived from two different temperatures (600°C and 700°C), the six different adsorbents (S1, S2, S3, S4, S5, and S6) exhibited similar elemental compositions.

Table 4. 2: Percentage composition of the Raw Clay mineral

Raw clay mineral kaolinite 1A (S7)												
Si	**Al**	**Fe**	**Ti**	**K**	**Ca**	**Mg**	**V**	**Mn**	**Sn**	**Cr**	**Ba**	**Nb**
48.37	28.892	12.539	6.815	1.256	0.633	0.412	0.111	0.108	0.082	0.069	0.085	0.052
Zn	**Na**	**Cu**	**Ni**	**Sr**	**Zr**	**Y**	**Ga**	**Te**	**Pb**	**Rb**	**Sb**	**As**
0.051	0.05	0.048	0.035	0.035	0.27	0.021	0.017	0.015	0.013	0.012	0.006	0.002

Table 4. 3: Percentage composition of the Clay mineral after calcination

After Calcination (similar for S8 and S9)												
Si	**Al**	**Fe**	**Ti**	**K**	**Ca**	**Mg**	**V**	**Mn**	**Cr**	**Sn**	**Na**	**Ba**
46.125	30.719	12.749	6.961	1.331	0.625	0.442	0.112	0.11	0.07	0.056	0.065	0.072
Nb	**Zn**	**Cu**	**Ni**	**Sr**	**Zr**	**Y**	**Ga**	**Rb**	**Te**	**Pb**	**Sb**	**As**
0.051	0.051	0.048	0.035	0.035	0.267	0.021	0.017	0.012	0.012	0.011	0.005	0.001

Table 4. 4: Percentage composition of Zeolites

After hydrothermal treatment of calcined clay mineral with NaOH(similar for S1,S2,S3,S4,S5 and S6)												
Na	**Si**	**Al**	**Fe**	**Ti**	**K**	**Ca**	**Zr**	**Mn**	**V**	**Sn**	**Ba**	**Cr**
36.102	26.625	19.426	10.233	4.893	1.433	0.449	0.237	0.088	0.078	0.075	0.058	0.054
Zn	**Nb**	**Ni**	**Sr**	**Cu**	**Y**	**Ga**	**Te**	**Rb**	**Pb**	**Th**	**Sb**	**As**
0.047	0.042	0.03	0.03	0.023	0.018	0.014	0.015	0.011	0.008	0.006	0.006	0.001

In the raw clay mineral, identified as kaolinite 1A, Si and Al accounted for 77.26% of the total elemental composition, suggesting a high degree of kaolinite purity in this clay mineral (Dewi *et al*., 2018). Other elements such as Fe, Ti, K, and Ca were also present. The Si/Al ratio in raw clay mineral (kaolinite 1A) measured at 1.6, slightly lower than the typical Si/Al ratio for kaolinite, which is typically 1.8. However, after calcination of the clay mineral at 600°C and 700°C (Table 4.2), the Si/Al ratio decreased to 1.5. This reduction was accompanied by a color change from pale grey to red, attributed to the presence of Fe impurities (Mulinta & Thiansem, 2019).

It's worth noting that various studies have reported the average silicate content in clay minerals typically falls between 47-48% (Shaaibu *et al*., 2020). A substantial shift in elemental composition was observed during hydrothermal treatment with sodium hydroxide, where Si content was significantly reduced from 48.37% to 26.625% (Table 4.3). This reduction was attributed to SiO2 precipitation, with sodium (Na) becoming the predominant element at 36.1% and forming hydrosodalite.

4.2.2 X-Ray diffraction (XRD)

This is a crucial technique employed for the characterization of clay minerals, facilitating the determination of their structural composition. This characterization relies on precise measurements of cell unit, size, peak position, intensity, and atomic arrangements, which are derived from X-ray powder patterns (Ismadji *et al*., 2015). Utilizing the Panalytical Data Collector Software, we were able to identify various types of clay minerals and non-clay minerals

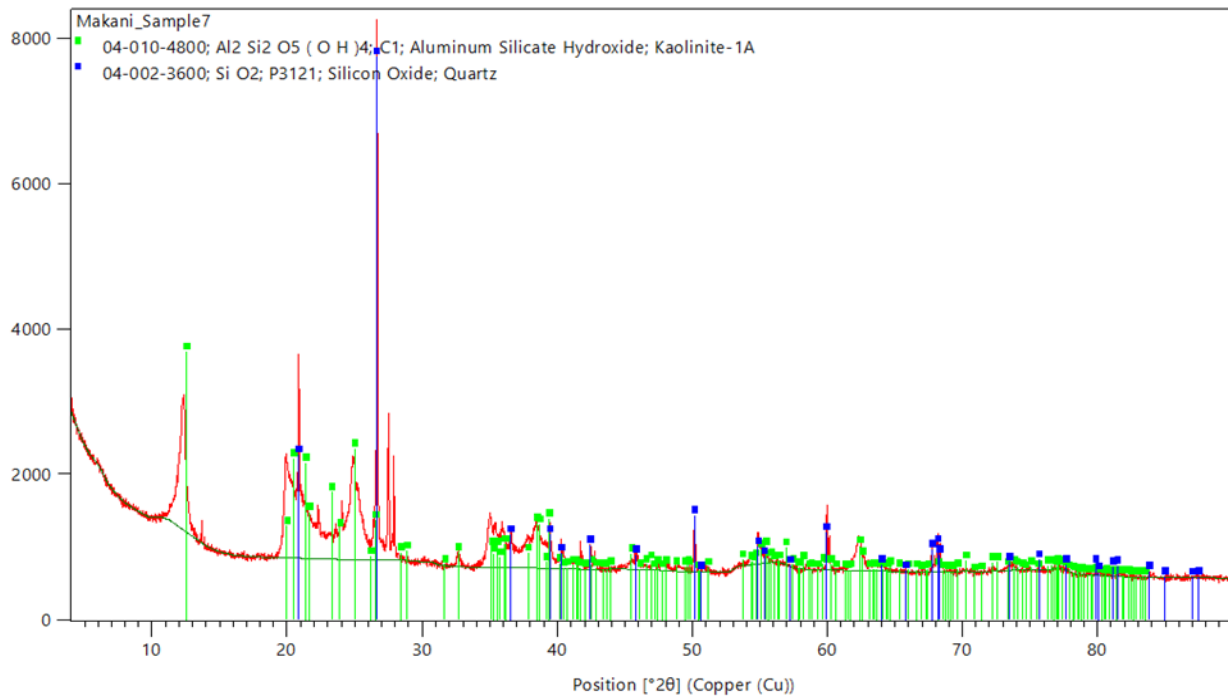

Figure 4. 4: XRD Adsorbent S7

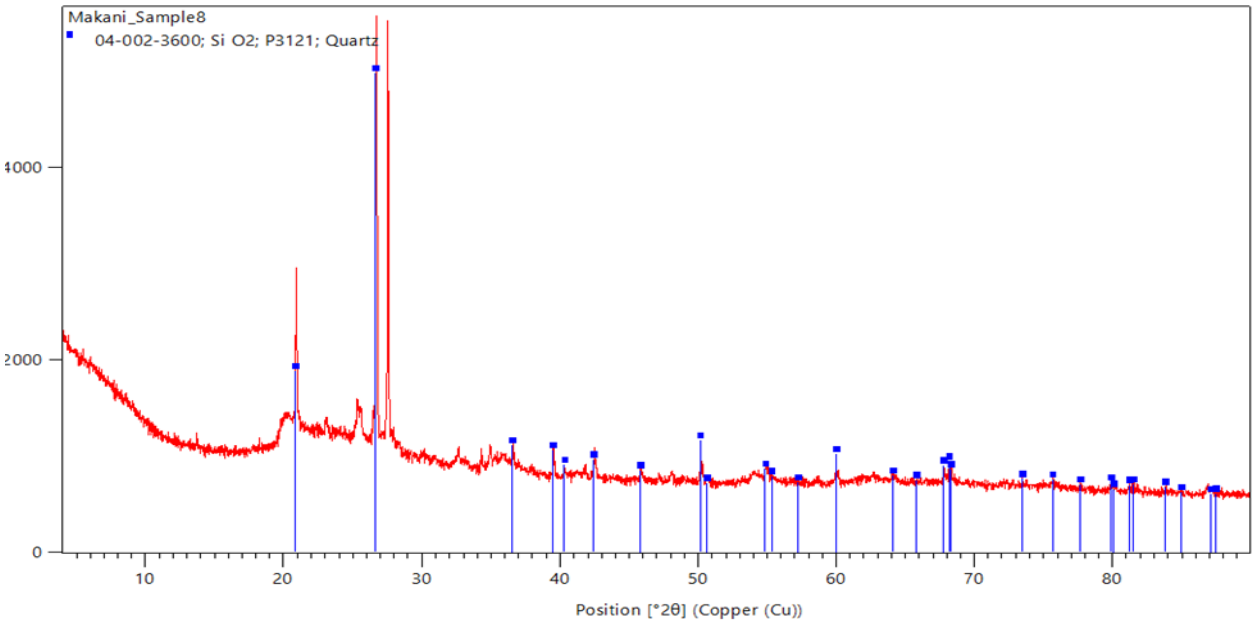

Figure 4. 5: XRD Adsorbent S8/S9

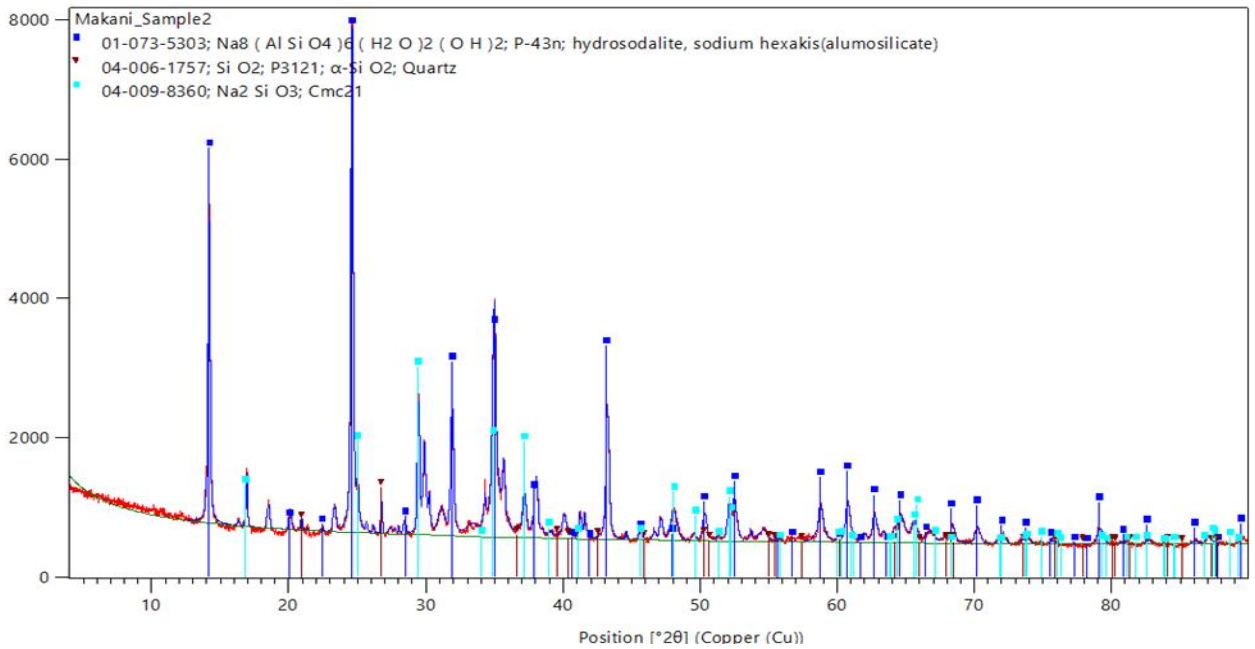

Figure 4. 6: XRD Adsorbent S1/S2/S3/S4/S5/&S6

The predominant crystalline phase in the raw clay mineral (S7) was identified as kaolinite 1A, with quartz also present (Figure 4.4). Ombaka conducted a similar study in the neighboring area, Rugi ward, in 2016, identifying kaolinite as one of the main clay minerals. After calcination at 600°C and 700°C (S8 and S9), the X-ray powder patterns for kaolinite disappeared in both samples due to the removal of hydroxide groups as water molecules, resulting in the formation of metakaolinite, known as low quartz (Figure 4.5) (Romero-Guerrero *et al*., 2018). Notably, S8 and S9 exhibited similar peak patterns.

Subsequently, following hydrothermal treatment of metakaolinite using different NaOH concentrations, SiO2 precipitated, leading to the formation of hydrosodalite, specifically sodium hexakis (Na8(AlSiO4)6(H2O)2(OH)2) (Figure 4.6). All six adsorbents (S1, S2, S3, S4, S5, and

S6) exhibited similar major peaks. These findings align with the results obtained by Heller-kallai and Lapides (2007) and Zhang *et al*. (2012).

4.2.3 Fourier- transformed infrared spectroscopy (FTIR)

The FT-IR spectrum analysis revealed a consistent spectral profile across all adsorbents, characterized by distinct features. Notably, these features included O-H stretching bands within the range of 3732-3400 cm^{-1} and Si-O stretching at 418 cm^{-1}.

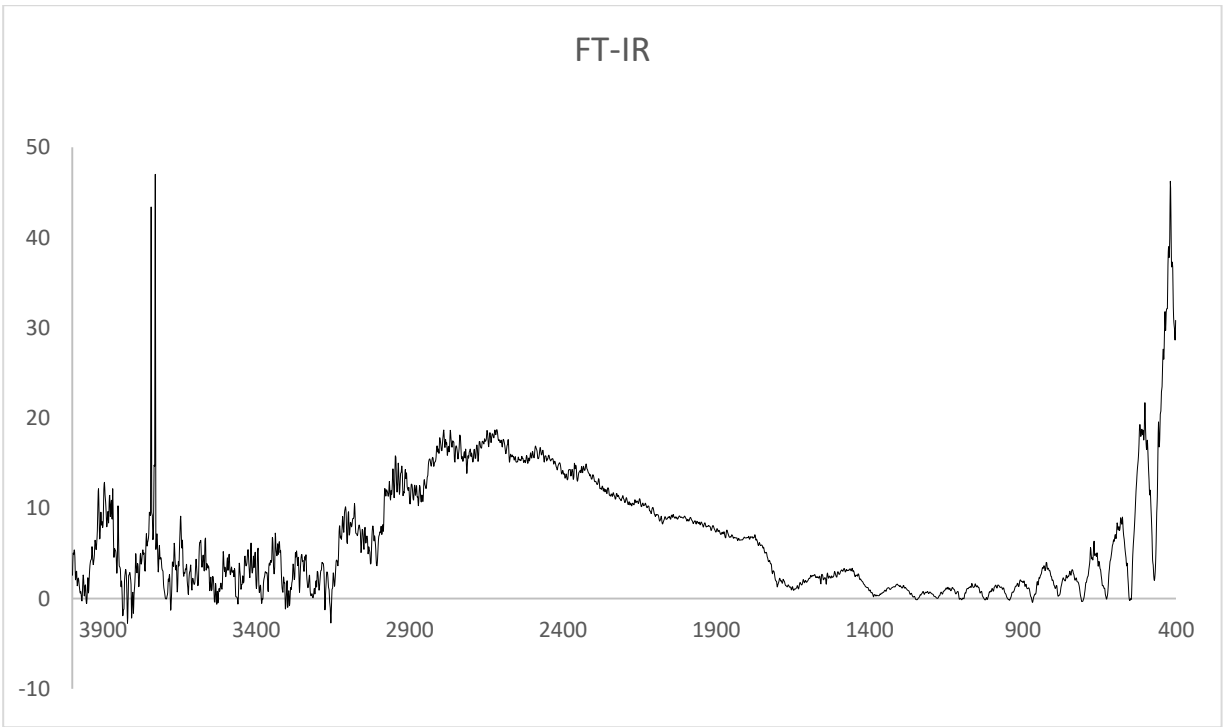

Figure 4. 7: FT-IR for Adsorbent S7

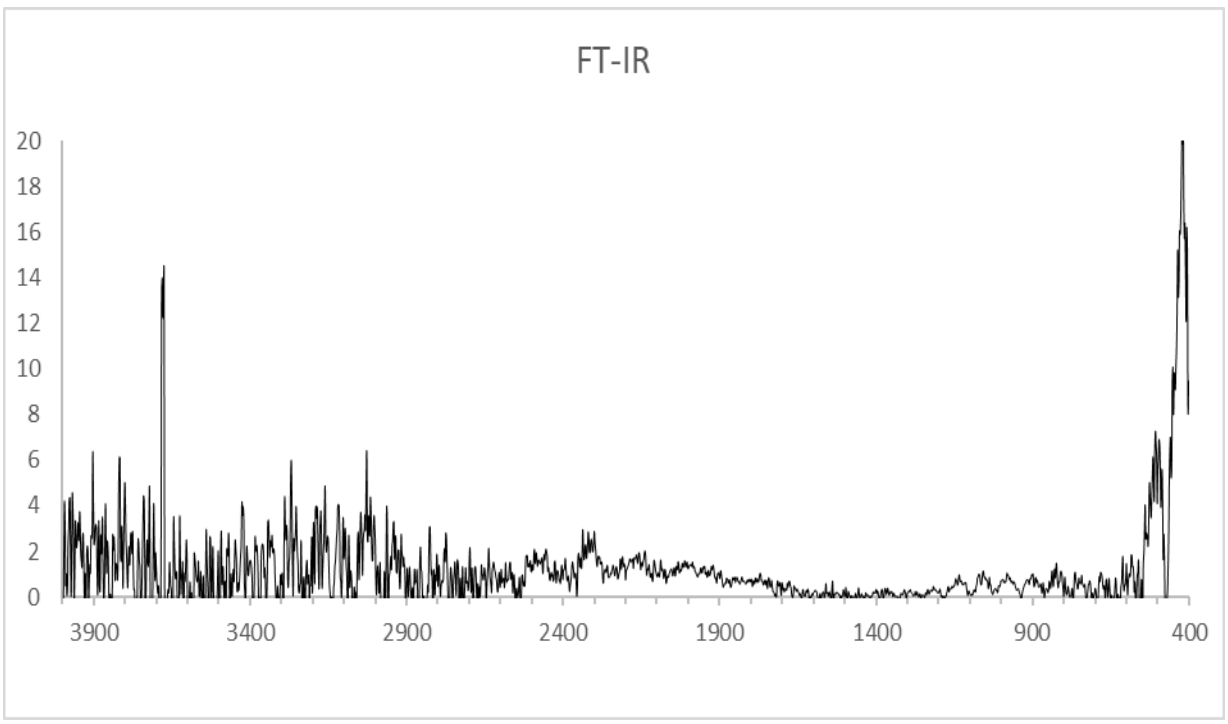

Figure 4. 8: FT-IR for Adsorbent S8/S9

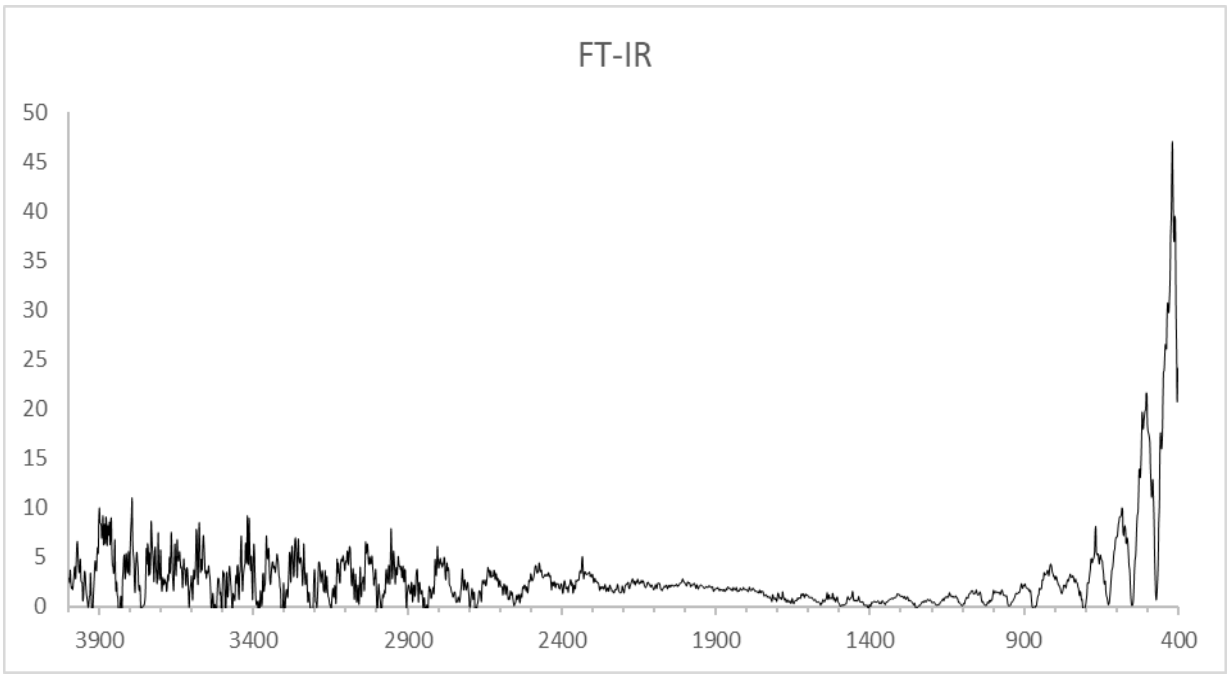

Figure 4. 9: FT-IR for Adsorbent S1, S2, S3, S4, S5 &S6

The primary variation among the adsorbents was observed in the O-H stretching region. Specifically, in the case of the kaolinite-based adsorbent S7 (Figure 4.7), the O-H stretching peaks were identified at 3743 and 3729 cm^{-1}, exhibiting considerable intensity, indicative of the presence of free O-H stretching vibrations. This O-H stretching behavior aligns with previous studies on kaolinite, corroborating findings reported by Roudouanead *et al*. (2020) and Dewi *et al*. (2018).

In contrast, the calcined adsorbents, namely S8 and S9, displayed weaker peaks at 3644 and 3646 cm^{-1}, respectively (Figure 4.8). These weaker peaks suggest that the O-H bonds in these materials were not free but rather engaged in hydrogen bonding. This change in O-H stretching characteristics can be attributed to the loss of water molecules during the calcination process.

Furthermore, the FT-IR spectra of the hydrothermally treated clay minerals (S1, S2, S3, S4, S5, and S6) exhibited a consistent profile, featuring weak peaks around 3400 cm^{-1} (Figure 4.9). These observations suggest that the O-H stretching vibrations in these materials were associated with hydrogen bonding.

Following adsorption experiments involving five different adsorbates (nitrates, phosphate, lead, copper, and cadmium), no discernible changes were observed in the IR spectra. This absence of spectral alterations indicates that the adsorption processes were primarily of a physical nature, leaving the chemical bonds within the materials intact. Such physical adsorption mechanisms are commonly governed by intermolecular forces, including van der Waals forces between the adsorbents and adsorbates (Hu & Xu, 2020). This phenomenon is well-documented and frequently encountered in adsorption studies, particularly in the context of activated carbon (Yahia & Wjihi, 2020).

4.2.4 Scanning electron microscopy (SEM)

Particle size and distribution significantly influence the applicability of clay minerals, particularly in adsorption processes where smaller particle sizes generally result in higher adsorption capacities. The SEM analysis revealed distinct characteristics among the various adsorbents.

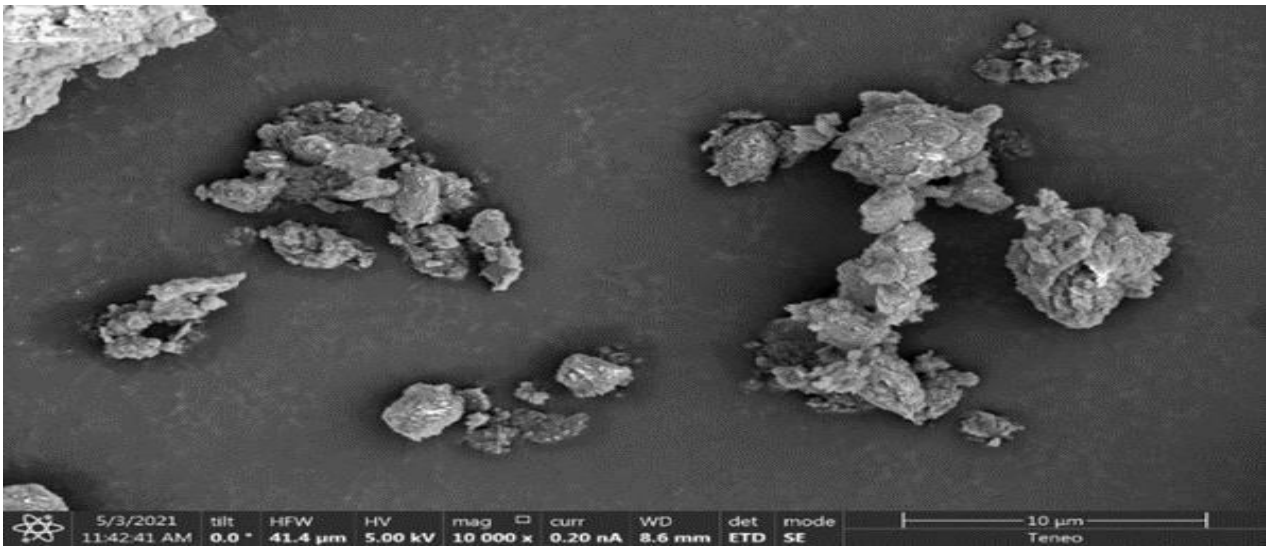

Figure 4. 10: SEM for Adsorbent S1

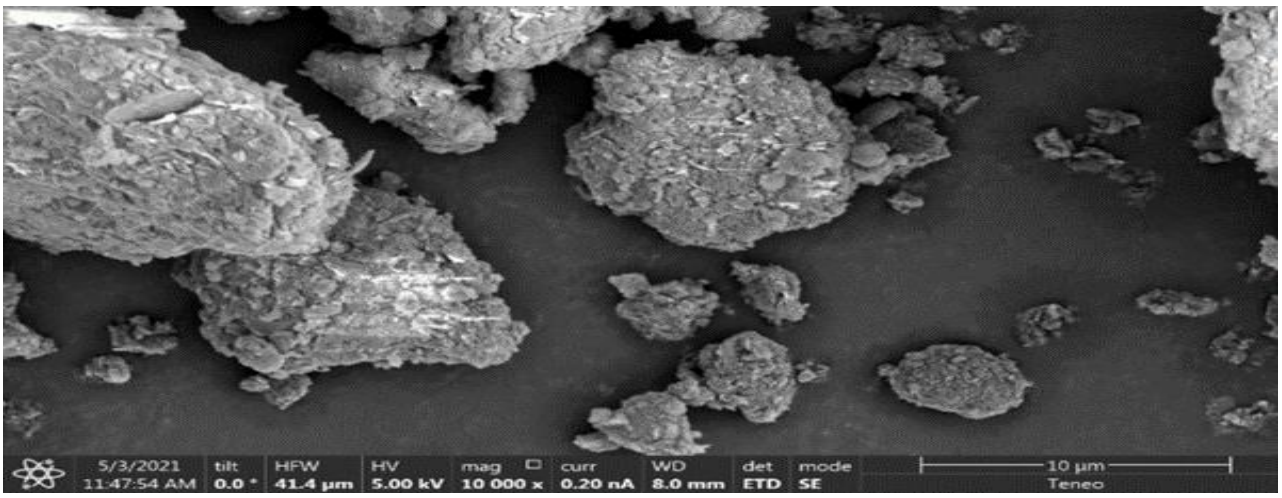

Figure 4. 11: SEM for Adsorbent S8/S9

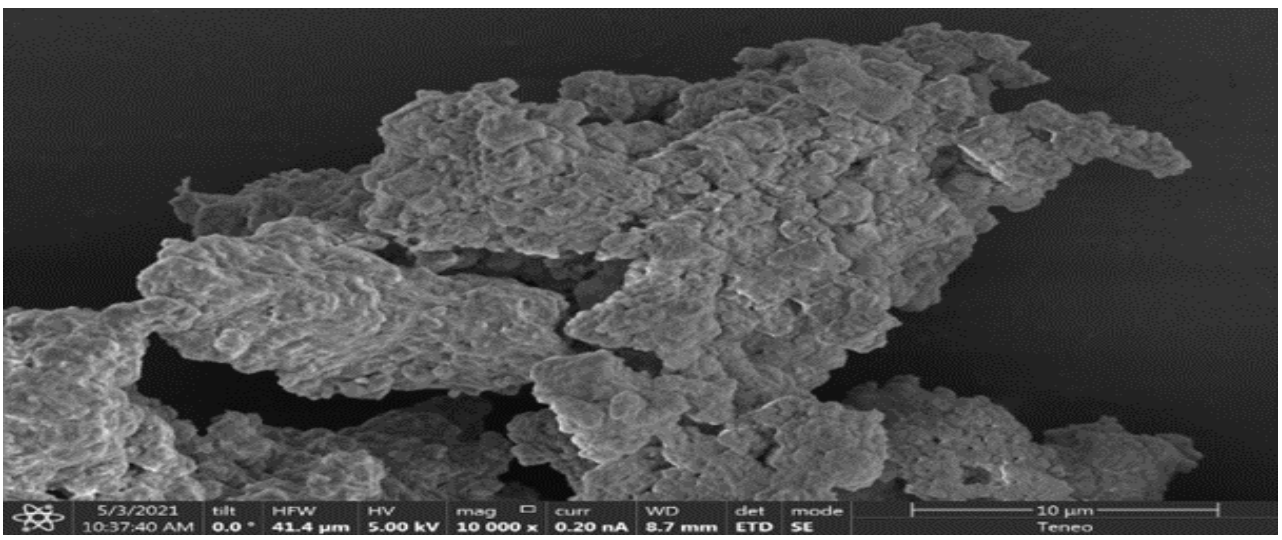

Figure 4. 12: SEM for Adsorbent S1/S2/S3/S4/S5 & S6

In the case of adsorbent S7 (Figure 4.10), particle sizes were observed to be consistently below 2 µm, accompanied by irregular and disordered surface areas, aligning with previous studies on kaolinite (cf. Astuti *et al*., 2020). Notably, particle aggregation in S7 was limited.

Similarly, adsorbents S8 and S9 (Figure 4.11) displayed particle sizes below 2 µm with irregular and disordered surface areas akin to S7. However, the key differentiation lay in the extent of particle agglomeration. S8 and S9 exhibited more pronounced particle aggregation compared to S7. Conversely, adsorbents S1, S2, S3, S4, S5, and S6 (Figure 4.12) exhibited uniform characteristics. They featured irregular heterogeneous surfaces, closely agglomerated particles, and very small pores, each measuring less than 0.5 µm. These attributes play a pivotal role in enhancing adsorption capacities. Furthermore, all these adsorbents maintained particle sizes below 2 µm, albeit the aggregation of small particles into larger structures. The SEM analysis offers valuable insights into the particle size and surface characteristics of the adsorbents, highlighting their potential for efficient adsorption processes.

4.2.5 Brunauer Emmett Teller (BET)

The BET multiple point analysis holds pivotal significance in delving into the complexities of adsorbent porosity within adsorption studies. This analytical technique serves as an indispensable means of unraveling the nuanced interactions occurring between adsorbate and adsorbent molecules. At the heart of this analytical approach lies the essential parameter, the BET constant C. Derived from the BET adsorption isotherm equation, this parameter plays a fundamental role in quantitatively characterizing the depth and strength of molecular interactions taking place at the adsorbent's surface.

The BET constant C, as a cornerstone of this analytical framework, assumes profound importance in elucidating the essence of adsorption phenomena. Its numerical value encapsulates the intensity of adsorption forces, providing us with a quantitative measure of the underlying interactions' strength. A higher C value signifies a more robust molecular engagement, implying the potential for enhanced adsorption capabilities.

In practical applications, the BET constant C assumes a defining role, typically falling within a specified range, often spanning from 100 to 200 for most adsorbents. While this range is not absolute, it serves as a practical reference point for assessing an adsorbent's adsorption propensity. Importantly, when the C value drops below 20, it raises doubts about the applicability of the BET method for determining surface area, rendering it ineffective in such cases. Conversely, C values exceeding 200 suggest that the adsorbent possesses a significant degree of porosity, inherently linked to heightened adsorption capabilities (Lowell *et al*., 2012).

Additionally, the adsorbent's surface area emerges as another crucial parameter in BET multiple point analysis. This area, intimately tied to adsorption capacity, assumes prominence as adsorption predominantly occurs at the material's surface. Increasing the surface area results in a

corresponding rise in available adsorption sites, consequently enhancing adsorption capacity. Thus, the surface area plays a pivotal role in evaluating a material's adsorption potential (Hu & Xu, 2020).

Table 4. 5: BET multipoint parameters

Adsorbent	**S1**	**S2**	**S3**	**S4**	**S5**
Slope	8.81E+02	1071.776	35508.11	11820.53	6915.928
Intercept	9.11E+00	2.21E+03	-3.44E+03	-6.82E+02	-6.59E+03
Correlation Coefficient	0.997	0.068	0.919641	0.97812	0.038566
C Constant	97.74	1.49	-9.328	-16.345	-0.05
Surface Area	3.911 m^2/g	1.061 m^2/g	0.109 m^2/g	0.313m^2/g	10.530m^2/g
Adsorbent	**S6**	**S7**	**S8**	**S9**	
Slope	-3021922	64.048	75.562	112.407	
Intercept	4.53E+05	7.43E+02	4.10E-01	-1.72E+00	
Correlation Coefficient	0.329075	0.999838	0.999996	0.99885	
C Constant	-5.673	862.818	185.29	-64.526	
Surface Area	0.000m^2/g	54.311 m^2/g	45.839 m^2/g	31.462 m^2/g	

In light of this discussion, the empirical data presented in Table 4:4 merits contemplation. Six adsorbents, specifically S2, S3, S4, S5, S6, and S9, exhibit diminished BET constant C values, rendering the BET method unsuitable for estimating their surface areas. In contrast, the trio of adsorbents, S1, S7, and S8, provides valuable insights. Particularly, S7 stands out with the highest BET constant, an impressive 862.818, indicative of a remarkably robust interaction between the adsorbent and adsorbate components. Similarly, S8 displays a respectable BET constant of 185.29, while S1 exhibits the most modest BET constant at 97.774. Concerning surface areas, S7 boasts the highest surface area at 54.311 m2/g, followed by S8 with a commendable 45.839 m2/g, while S1 records the lowest surface area at 3.911 m2/g.

4.3 Adsorption study

The adsorption study involved seven distinct adsorbents (S1, S2, S3, S4, S5, S6, and S7) and five different adsorbates (nitrate, phosphate, lead, cadmium, and copper). Nitrate and phosphate adsorption investigations utilized a UV-VIS Spectrometer, while lead, copper, and cadmium adsorption studies employed AAS. The analysis encompassed several parameters, including dosage, contact time, concentration, pH, temperature, adsorption isotherms, kinetics, and thermodynamics. Notably, adsorbents S1, S2, S3, S4, S5, and S6 exhibited consistent behavior throughout the entirety of the adsorption study.

4.3.1 Effect of dosage

The influence of dosage on the adsorption process was systematically investigated under controlled conditions, including an initial concentration of 10 ppm, a temperature of 298 K, and a pH of 7. Dosage variations were applied to the adsorbents, ranging from 0.1 g to 0.020 g for nitrate and phosphate, and from 0.5 g to 0.05 g for copper, lead, and cadmium.

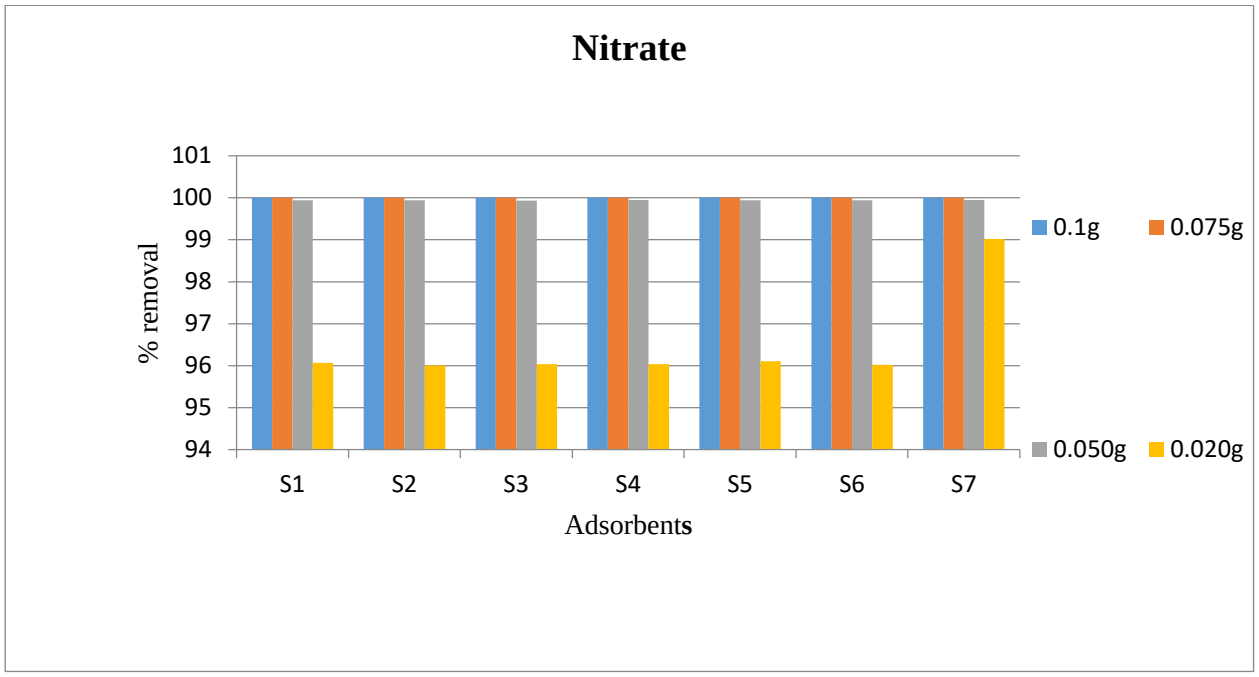

Figure 4. 13: Effect of adsorbents dosage on the percentage removal of NO_3^-

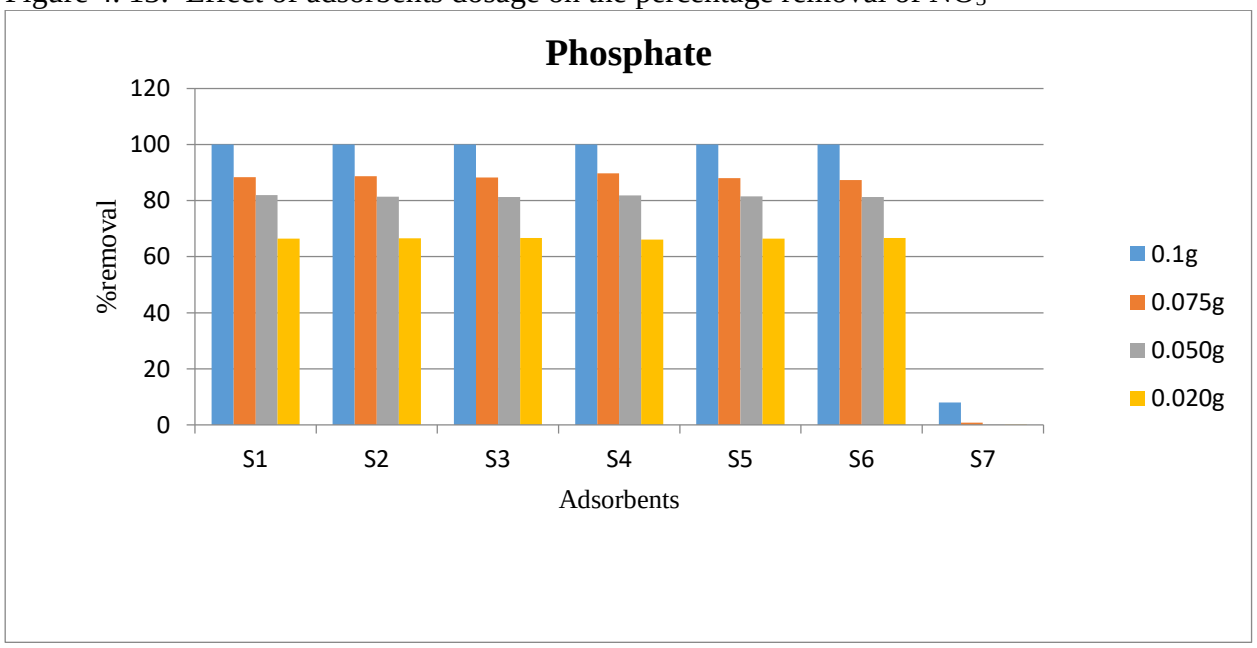

Figure 4. 14: Effect of adsorbents dosage on the percentage removal of PO_4^{3-}

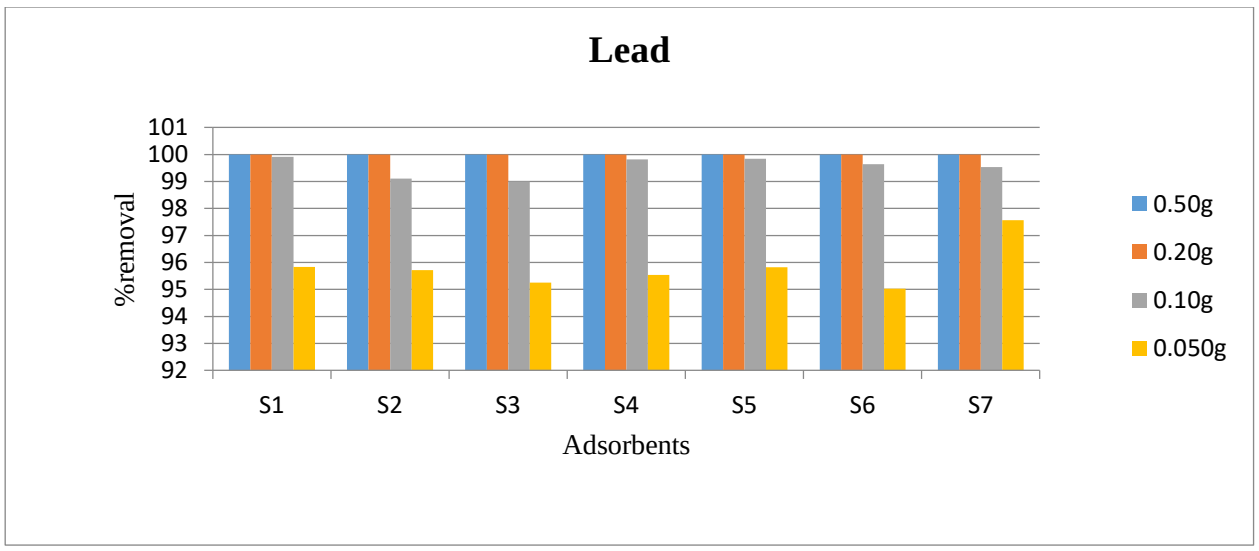

Figure 4. 15: Effect of adsorbents dosage on the percentage removal of Pb^{2+}

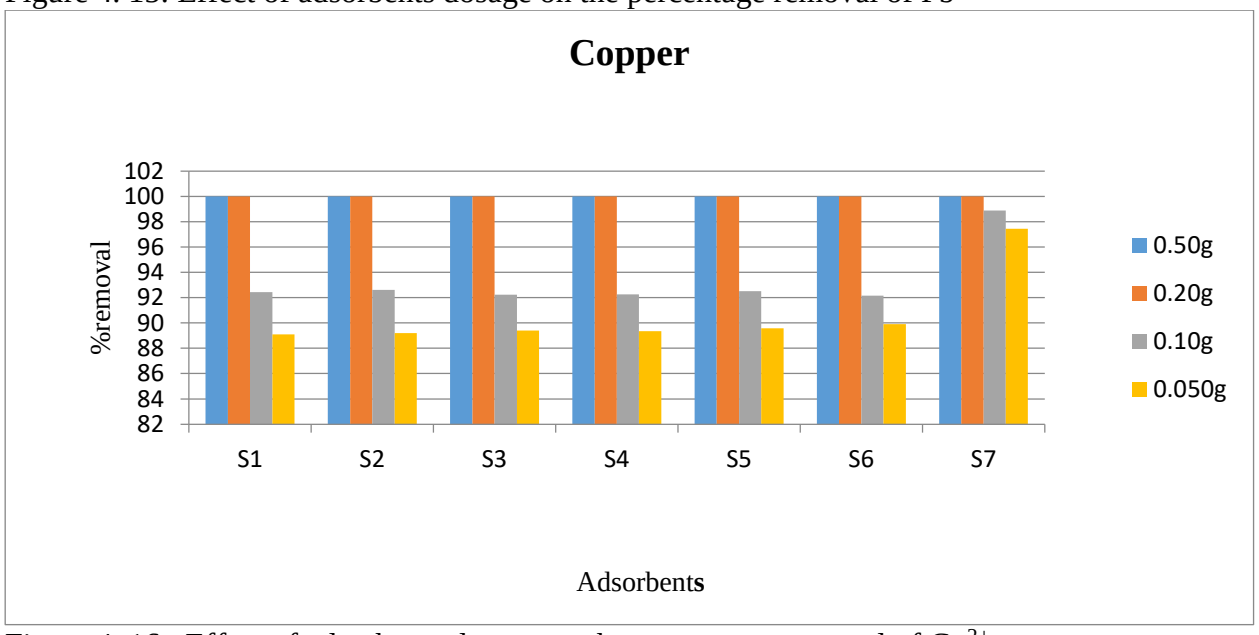

Figure 4. 16: Effect of adsorbents dosage on the percentage removal of Cu^{2+}

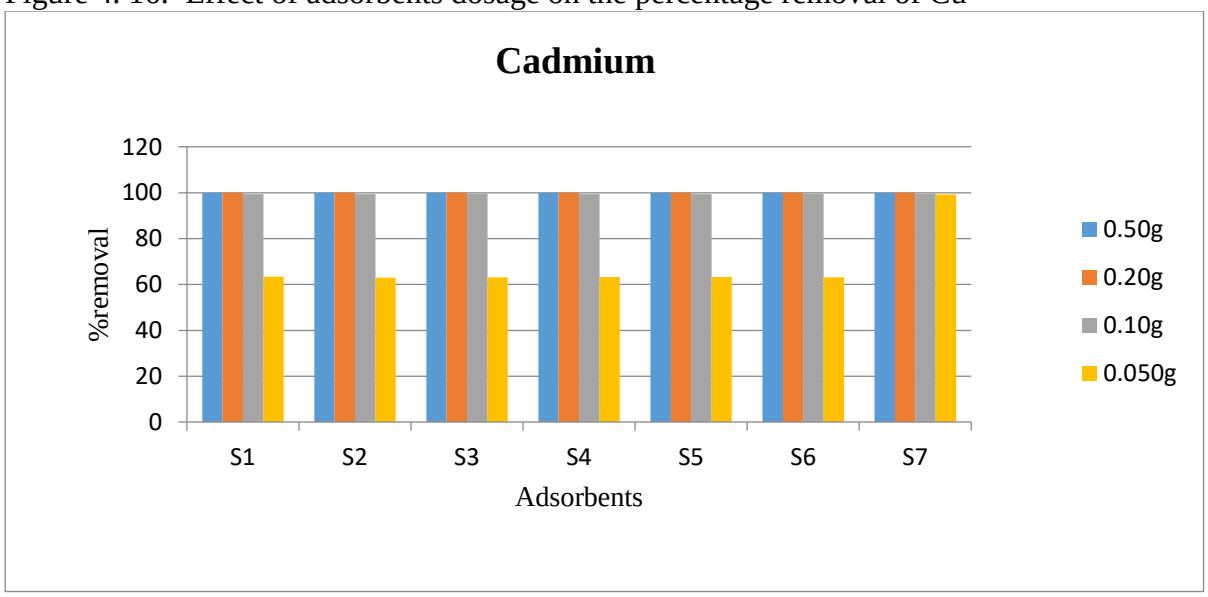

Figure 4. 17: Effect of adsorbents dosage on the percentage removal of Cd^{2+}

Figures 4.13 to 4.17 provide a visual representation of the impact of adsorbent dosage on the percentage removal of different ions (NO^{-}_{3}, PO_4^{3-}, Cu^{2+}, Pb^{2+} and Cd^{2+}).

The dosage factor plays a crucial role in determining the number of available sorption sites. A clear trend emerged from Figure 4.13 to Figure 4.17, illustrating that an increase in adsorbent dosage corresponded to a higher percentage of adsorbate removal, while a decrease in adsorbent dosage resulted in reduced removal efficiency. This trend aligns with findings in numerous other adsorption studies (Gupta & Babu, 2006; Wang *et al*., 2010; Padmavathy *et al.*, 2016). Essentially, higher dosage leads to an increased availability of sorption sites, indicating the presence of elevated unbalanced surface energies favorable for intermolecular interactions (Hu and Xu, 2020).

However, it is noteworthy that an exception was observed in this study regarding the removal of phosphate using kaolinite (S7). Remarkably, adsorbent S7 demonstrated limited efficacy in phosphate removal. This finding is consistent with the research conducted by Carbinatti *et al.*

(2021), who similarly observed that commercial kaolinite struggled to adsorb phosphate. Furthermore, Adeyi *et al*. (2019) reached a similar conclusion, stating that phosphate adsorption by kaolinite proved challenging unless within an acidic medium. Kaolinite's preference for adsorbing phosphate in an acidic medium is primarily attributed to changes in its surface charge characteristics and the electrostatic interactions that occur under these conditions. In neutral or basic media, the electrostatic repulsion between negatively charged kaolinite and phosphate ions limits adsorption.

4.3.2 Effect of contact time

The impact of contact time on the adsorption process was systematically investigated under controlled conditions, including room temperature, a neutral pH, and an initial concentration of 10 ppm. The contact time varied from 1 minute to 60 minutes for the different adsorbates (50 mL), with 0.10g of adsorbent used for nitrate and phosphate and 0.20g for copper, lead, and cadmium.

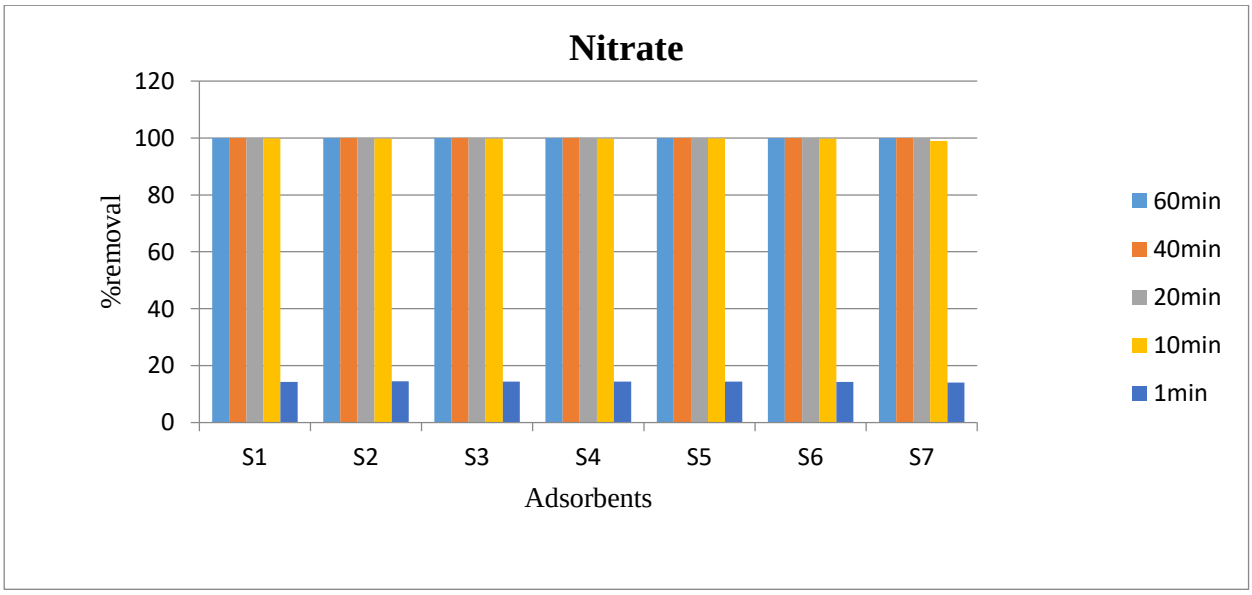

Figure 4. 18: Effect of contact time on the percentage removal of NO_3^-

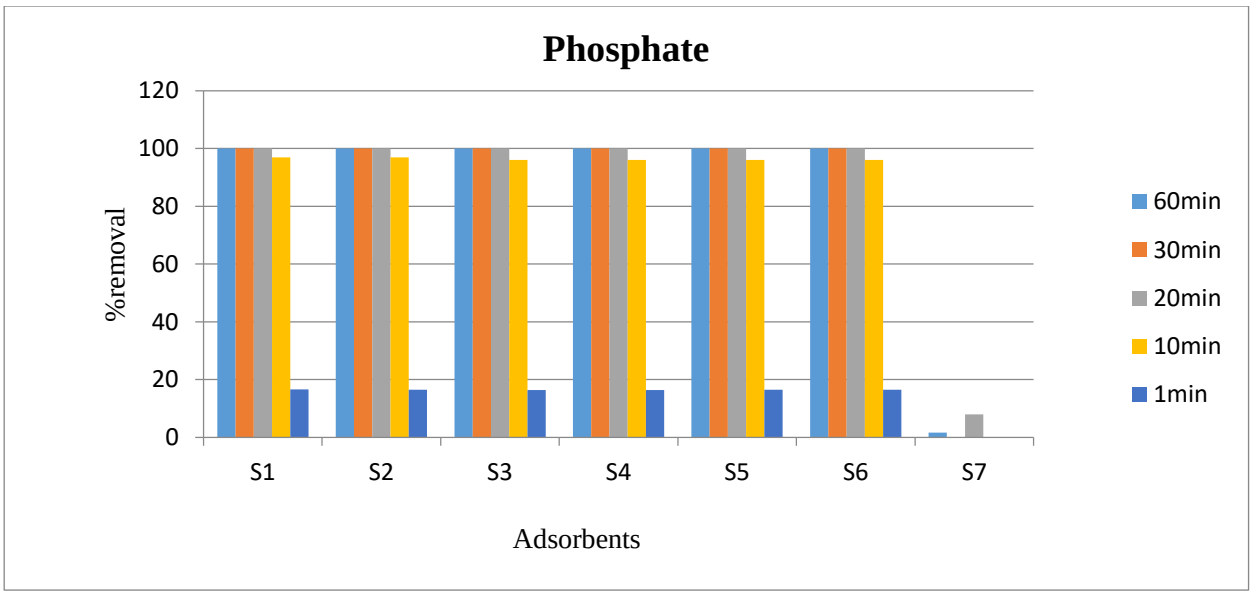

Figure 4. 19: Effect of contact time on the percentage removal of PO_4^{3-}

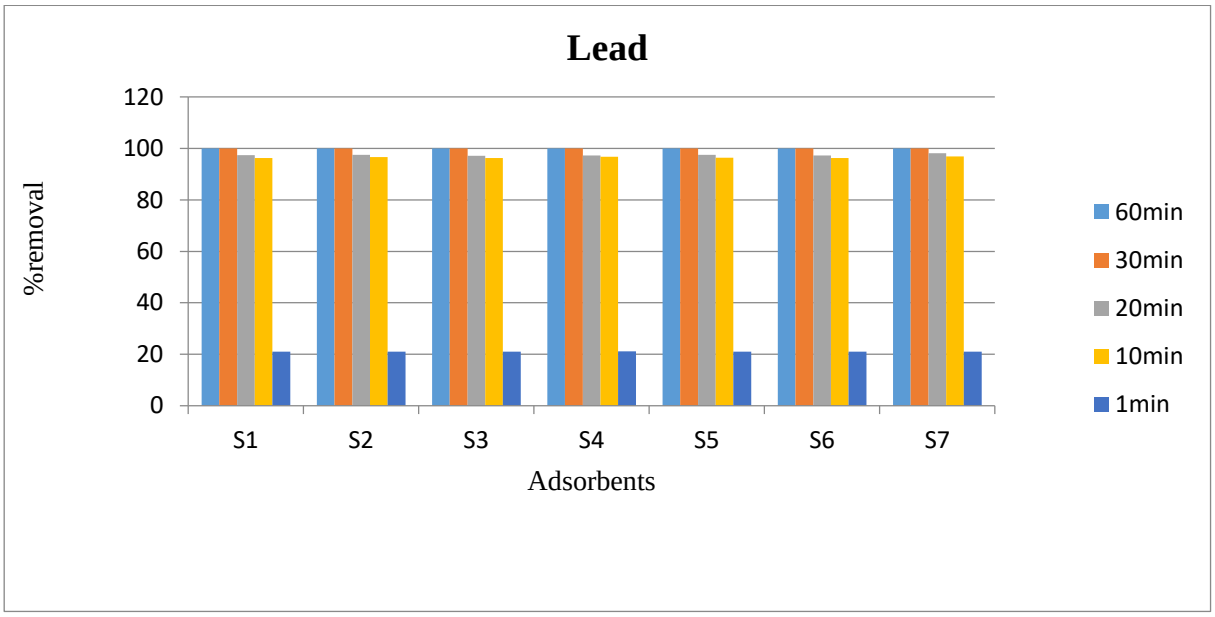

Figure 4. 20: Effect of contact time on the percentage removal of Pb^{2+}

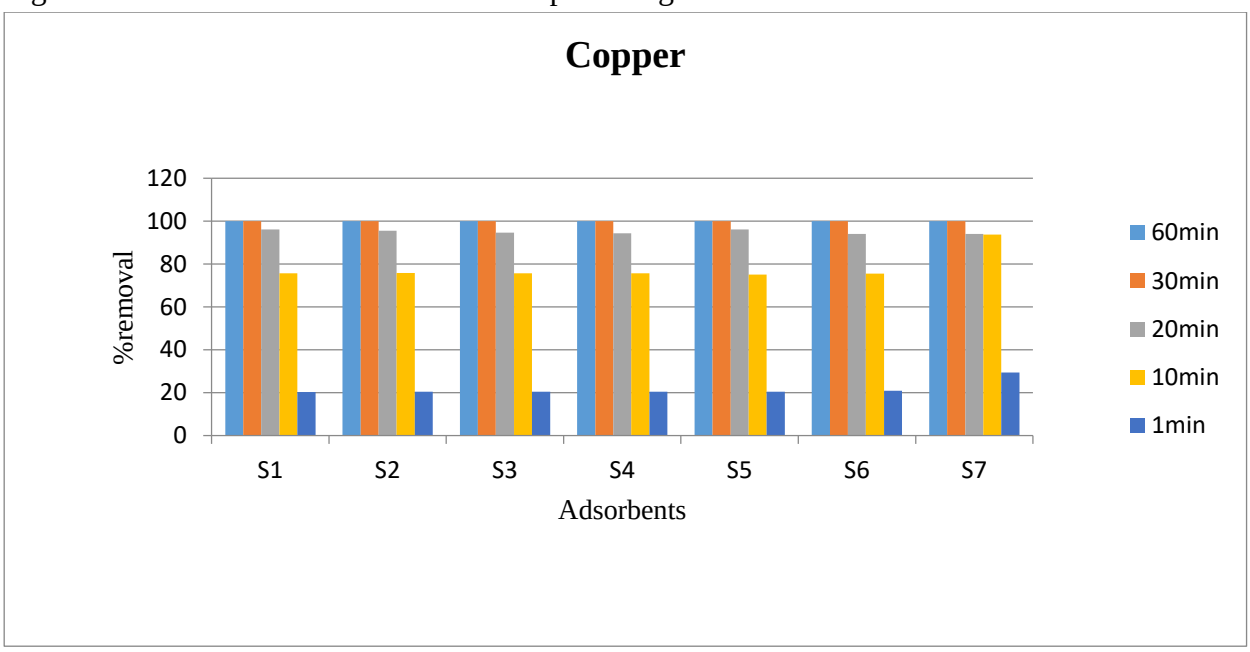

Figure 4. 21: Effect of contact time on the percentage removal of Cu^{2+}

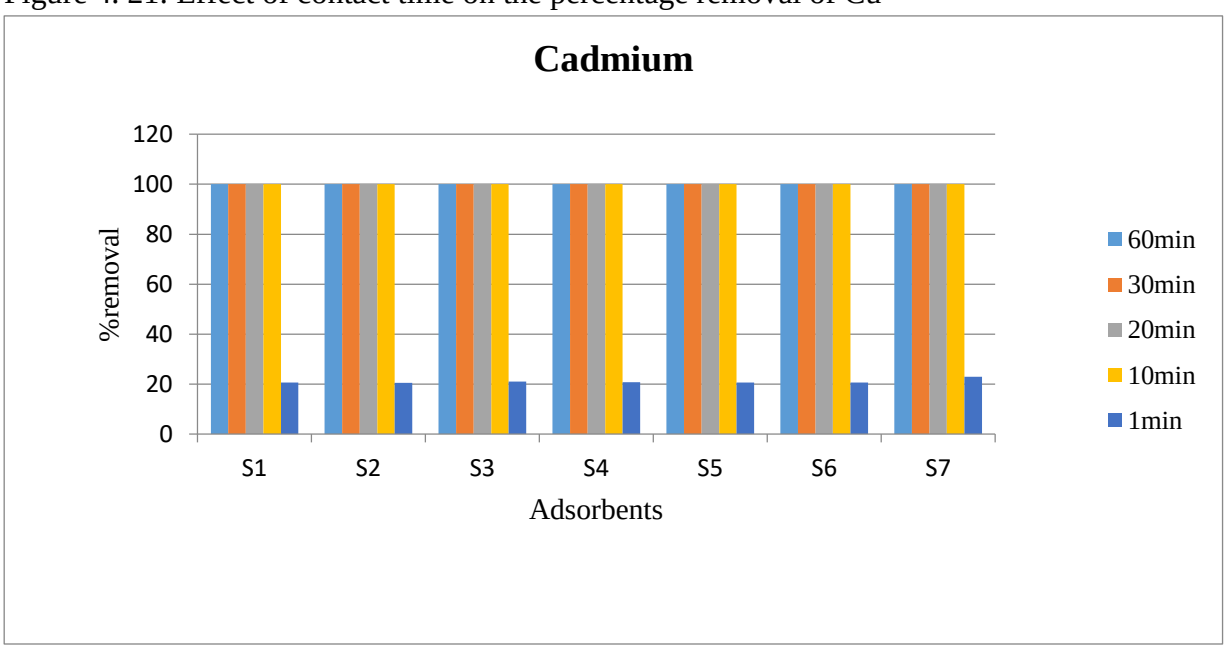

Figure 4. 22: Effect of contact time on the percentage removal of Cd^{2+}

The analysis of contact time revealed an interesting trend. As documented in prior studies (Dali Youcef *et al*., 2019 and Gamoudi & Srasraa, 2019), the impact of contact time typically involves a rapid increase in the percentage removal of adsorbate during the initial 10 to 20 minutes. In line with these findings, the present study observed that for nitrate, phosphate, lead, copper, and cadmium (Figure 4.18 to Figure 4.22), 99%, 96%, 96%, 75%, and 100% removal efficiency were achieved, respectively, within the first 10 minutes. Subsequently, there was only a marginal change in removal efficiency between 10 and 20 minutes, followed by negligible variations from 20 to 60 minutes.

This rapid removal of contaminants during the initial 10 to 20 minutes can be attributed to two key factors. First, a substantial concentration gradient exists during this period, driving the rapid uptake of contaminants. Second, the active adsorption sites on the adsorbent surface are readily accessible for adsorption processes during this timeframe (Ajala *et al*., 2023). As a result, it can be inferred that adsorption equilibrium was reached at approximately 30 minutes of contact time. This finding underscores the importance of optimizing contact times to achieve efficient contaminant removal.

4.3.3 Effect of initial ion concentration

The influence of the initial ion concentration on the adsorption process was systematically investigated under controlled conditions. The experiments utilized an initial dosage of 0.10g for nitrate and phosphate and 0.20g for lead, copper, and cadmium, with a working pH of 7, a contact time of 30 minutes, 50mL adsorbates and a temperature of 298K. The concentration range spanned from 10 ppm to 100 ppm.

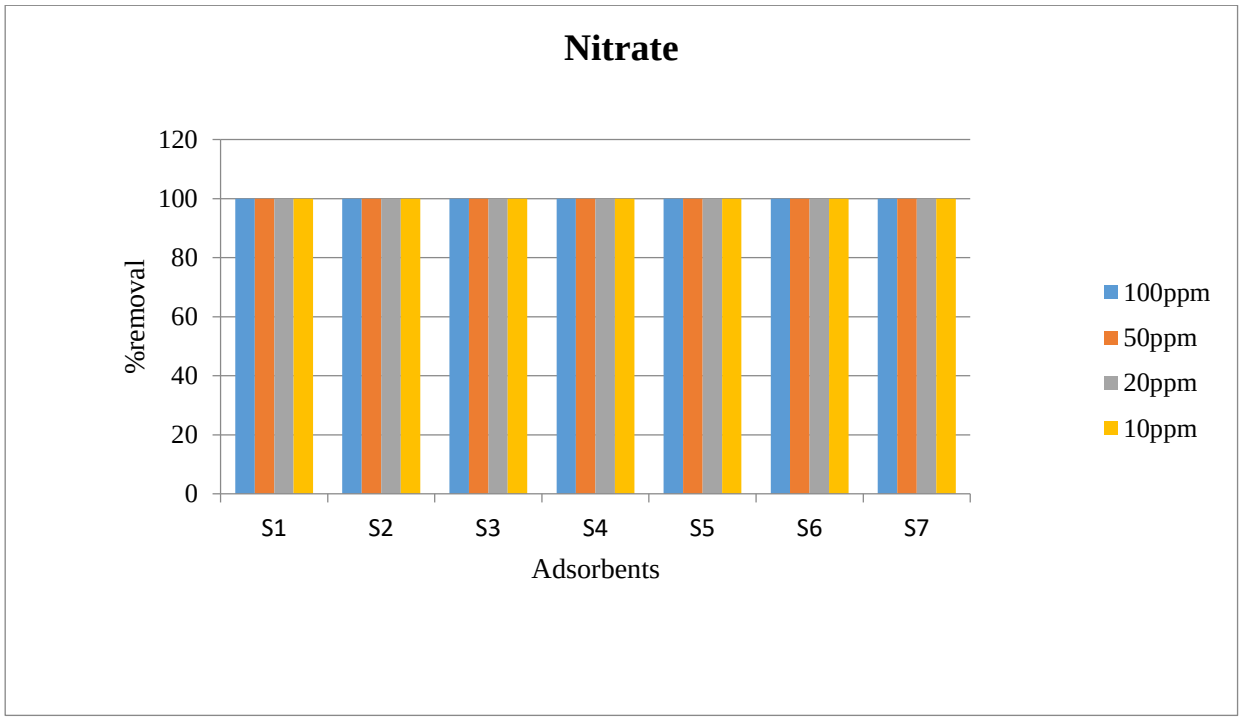

Figure 4. 23: Effect of NO_3^- initial concentration on its percentage removal

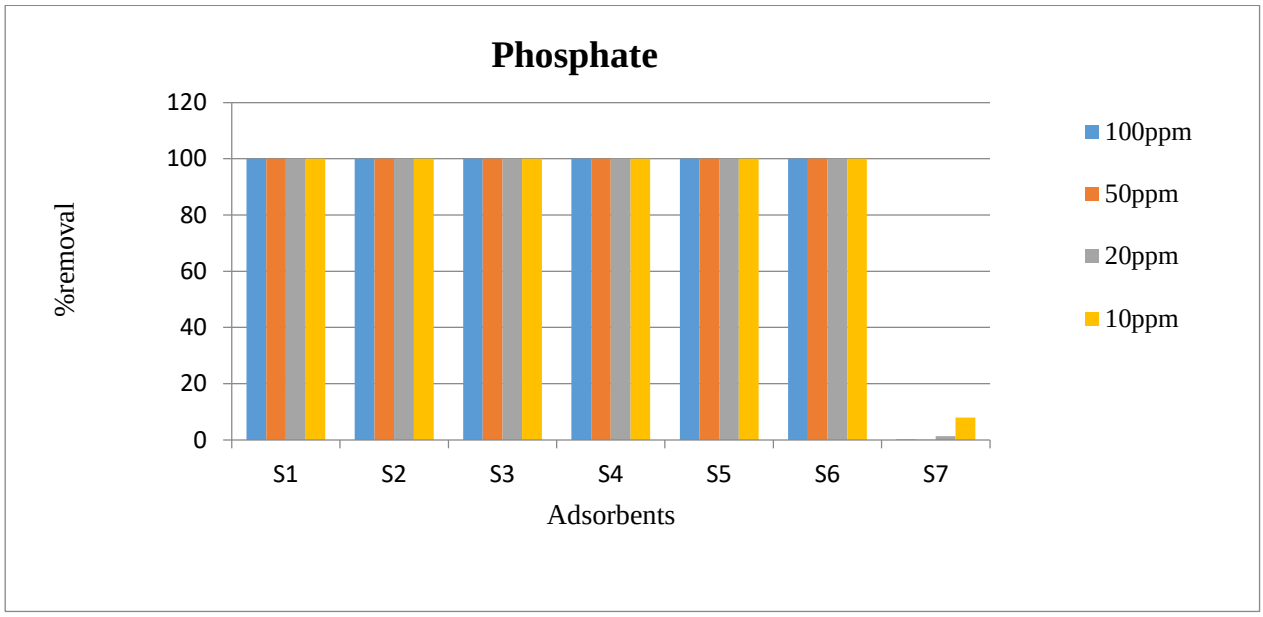

Figure 4. 24: Effect of PO_4^{3-} initial concentration on its percentage removal

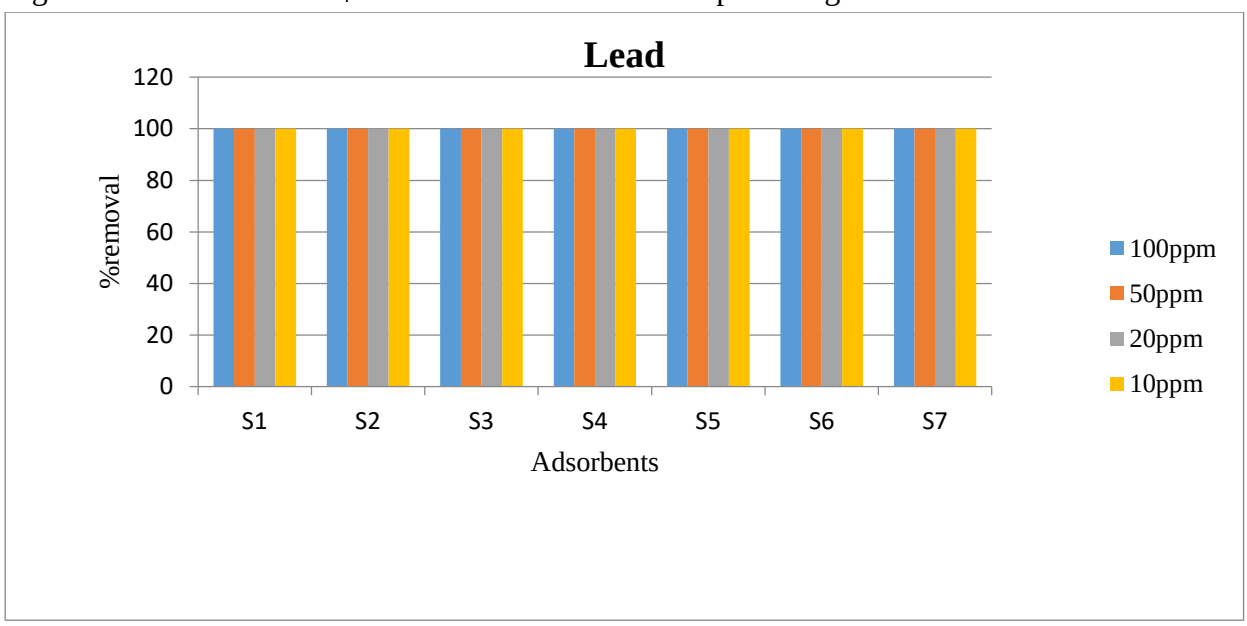

Figure 4. 25: Effect of Pb^{2+} initial concentration on its percentage removal

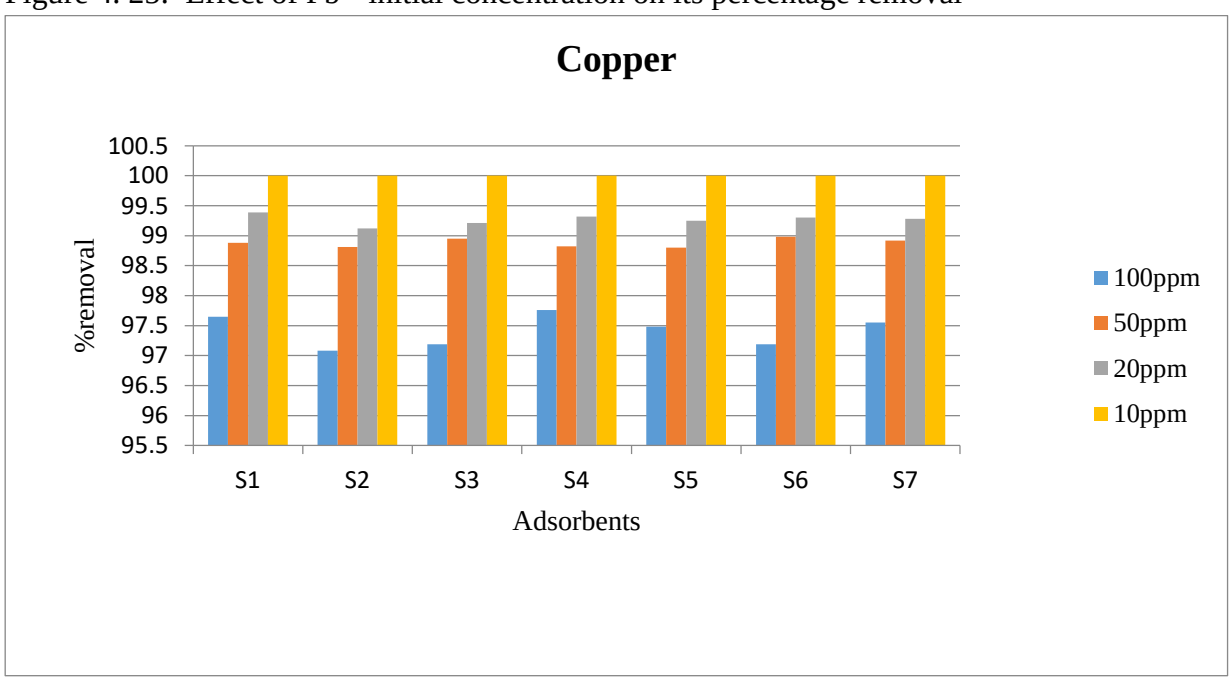

Figure 4. 26: Effect of Cu^{2+} initial concentration on its percentage removal

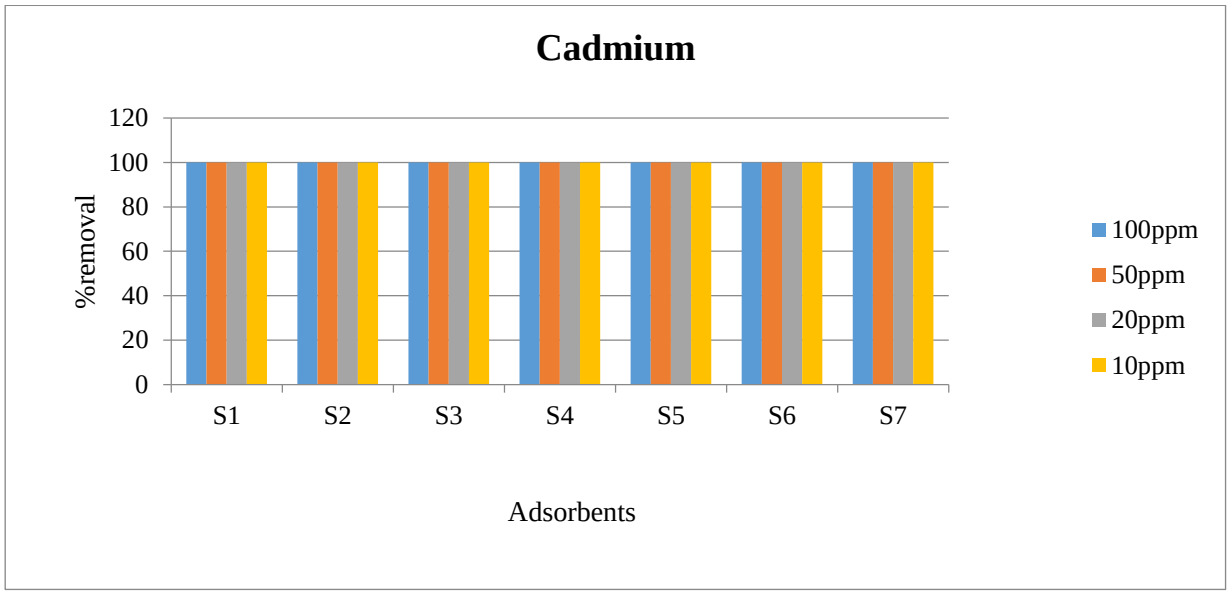

Figure 4. 27: Effect of Cd^{2+} initial concentration on its percentage removal

The impact of initial ion concentration becomes evident as the percentage removal decreases with increasing initial concentration. This phenomenon typically occurs when the adsorbent reaches saturation, indicating that the available sorption sites on the adsorbents become fewer than the ions present in the solution (Gorzin & Bahri, 2017 and Mayyahi & Al-Asadi, 2018). Figures 4.23, 4.24, 4.25, and 4.26 illustrate that, up to 100 ppm, most adsorbents maintained a 100% removal rate, except for copper, which exhibited a decrease in removal efficiency starting from 20 ppm. Furthermore, Figure 4.23 demonstrates that at concentrations of 20 ppm, 50 ppm, and 100 ppm, the percentage removal decreased to 99%, 98%, and 97%, respectively. This observation aligns with the expected behavior of adsorption processes at varying initial ion concentrations.

4.3.4 Effect of temperature

The impact of temperature on the adsorption process was systematically examined, with an initial dosage of 0.10g for nitrate and phosphate and 0.20g for cadmium, lead, and copper. The initial concentration was set at 10 ppm, the pH was maintained at 7, 50 ml of adsorbate was used, and the contact time was fixed at 30 minutes. Temperature variations were introduced, ranging from 298K to 353K.

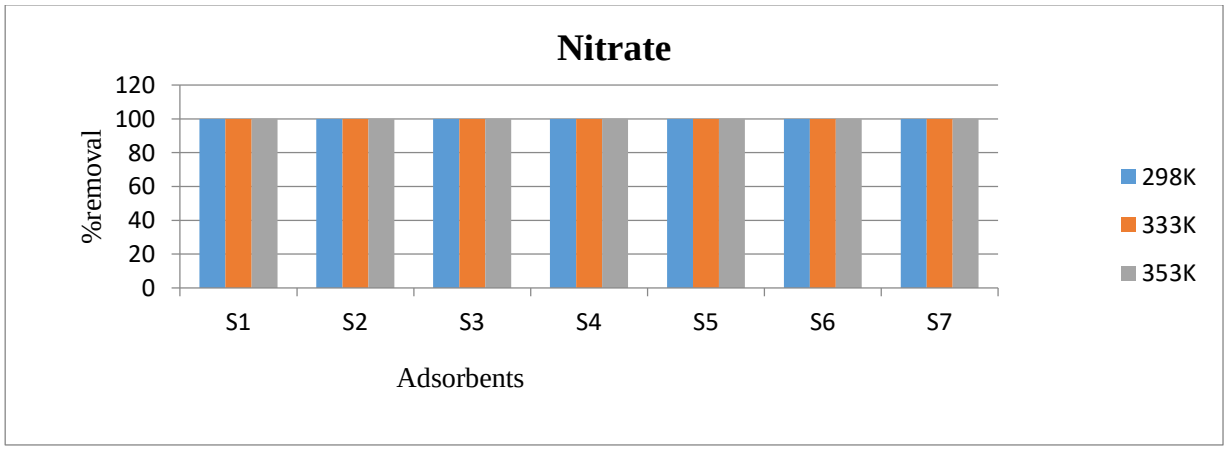

Figure 4. 28: Effect of temperature on the percentage removal of NO_3^-

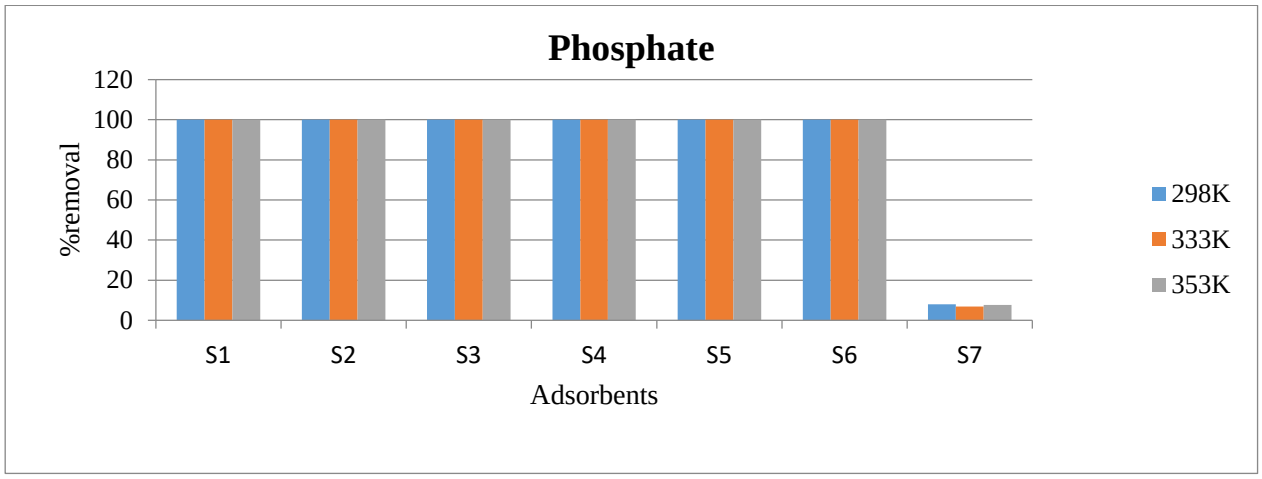

Figure 4. 29: Effect of temperature on the percentage removal of PO_4^{3-}

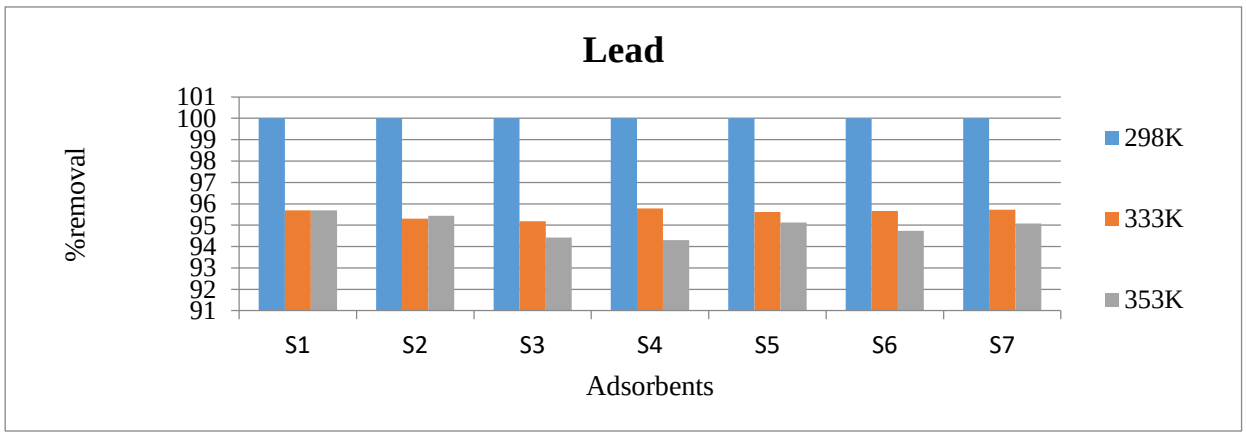

Figure 4. 30: Effect of temperature on the percentage removal of Pb^{2+}

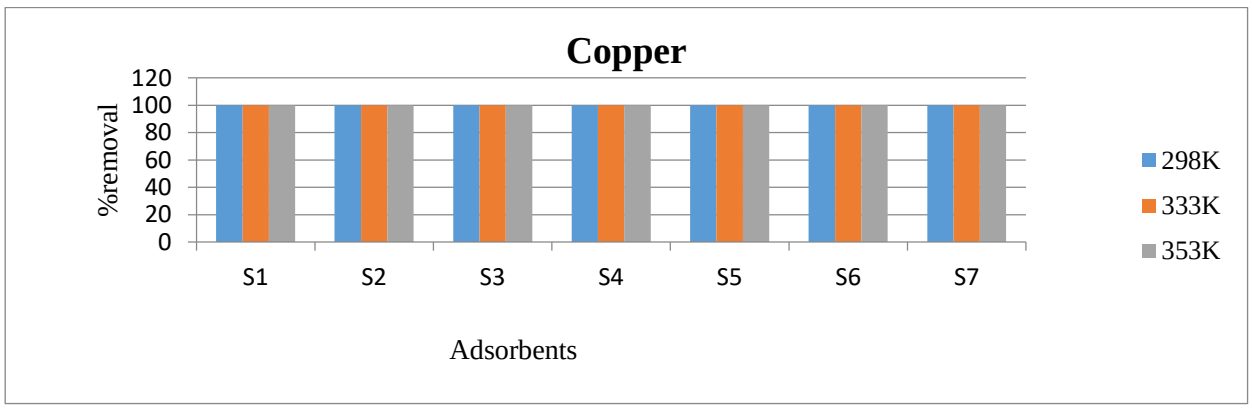

Figure 4. 31: Effect of temperature on the percentage removal of Cu^{2+}

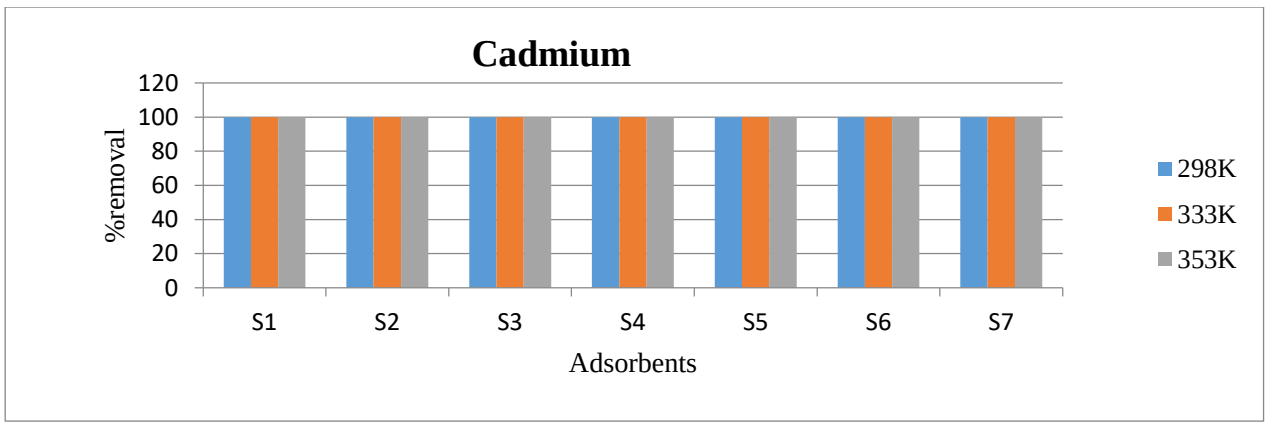

Figure 4. 32: Effect of temperature on the percentage removal of Cd^{2+}

The experimental results depicted in Figures 4.25, 4.26, 4.28, and 4.29 indicate that temperature exerted minimal influence on the adsorption process. Generally, an increase in temperature leads to reduced adsorption due to decreased attractive forces between the adsorbent and the adsorbate ions (Wei *et al*., 2019). However, it's important to note that the impact of temperature can vary for different ions. In the case of lead, as illustrated in Figure 4.27, an increase in temperature from 298 K to 353 K corresponded to a decrease in the percentage removal, suggesting a distinctive temperature sensitivity for this particular ion.

4.3.5 Effect of pH

The influence of pH on the adsorption process was systematically examined under controlled conditions: 298 K temperature, 50 ml of a 10 ppm concentration, and adsorbent dosages of 0.10 g for nitrate and phosphate and 0.20 g for lead, copper, and cadmium

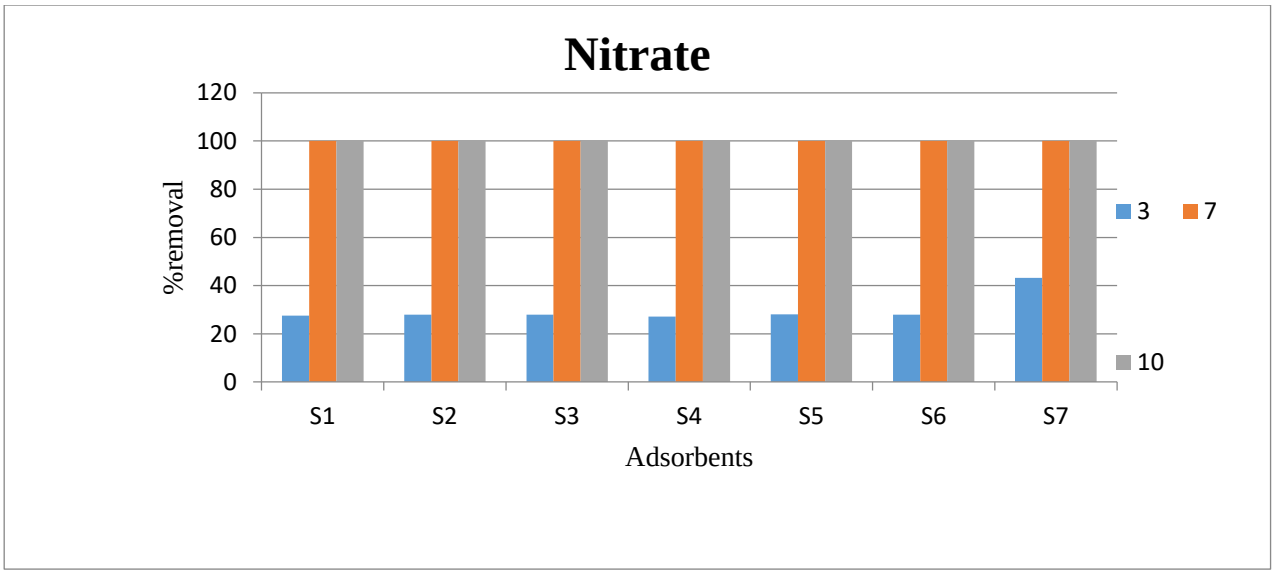

Figure 4. 33: Effect of pH on the percentage removal of NO_3^-

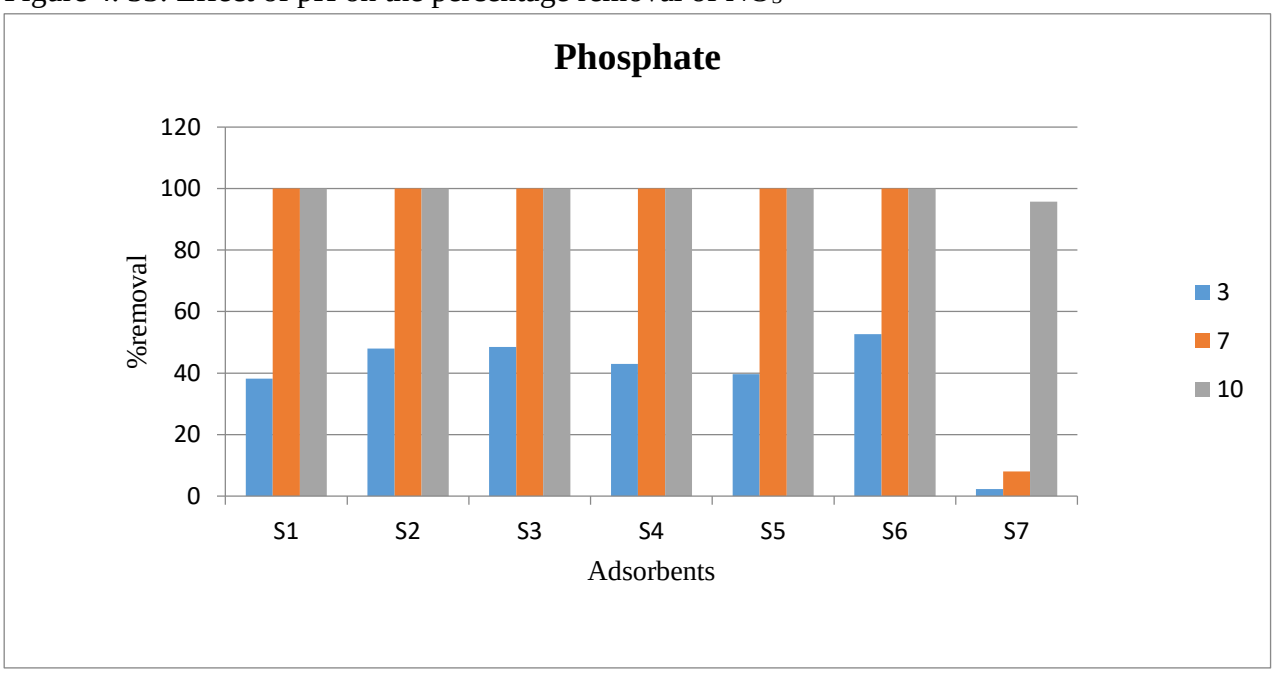

Figure 4. 34: Effect of pH on the percentage removal of PO_4^{3-}

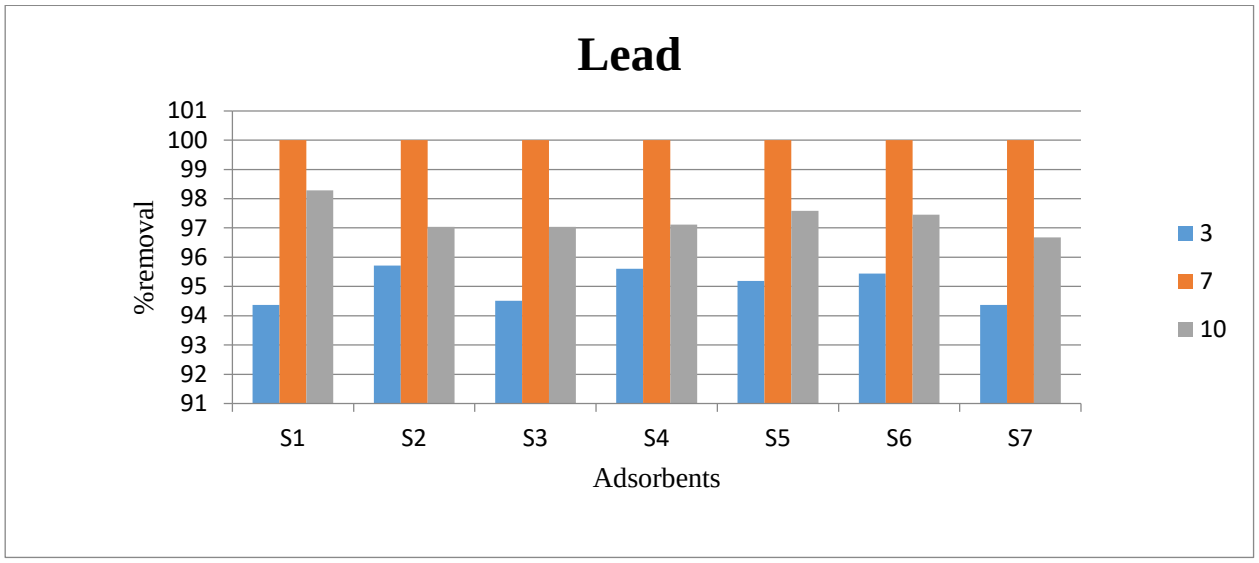

Figure 4. 35: Effect of pH on the percentage removal of Pb^{2+}

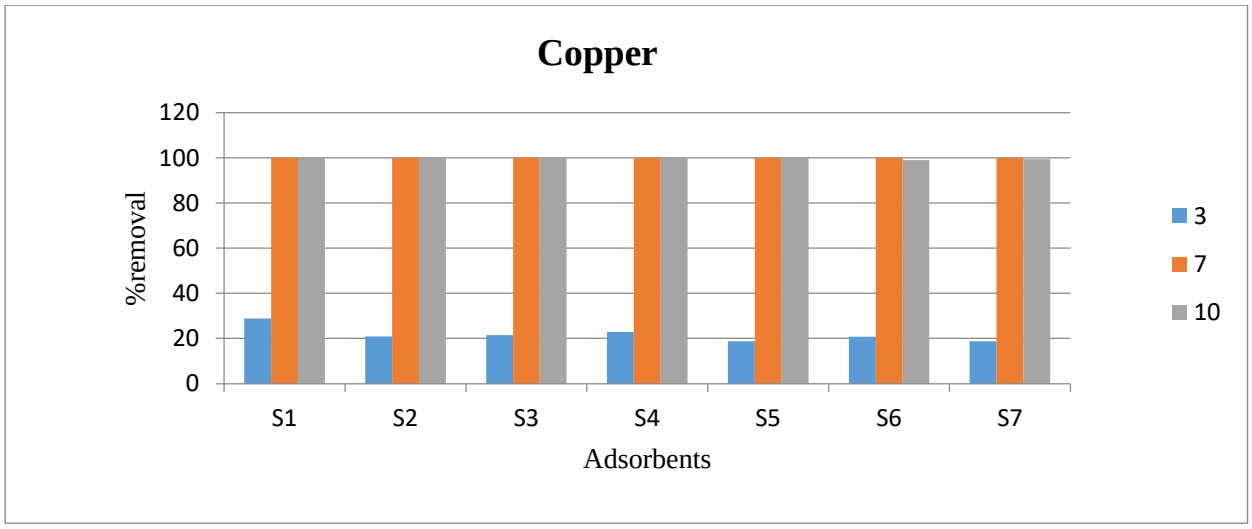

Figure 4. 36: Effect of pH on the percentage removal of Cu^{2+}

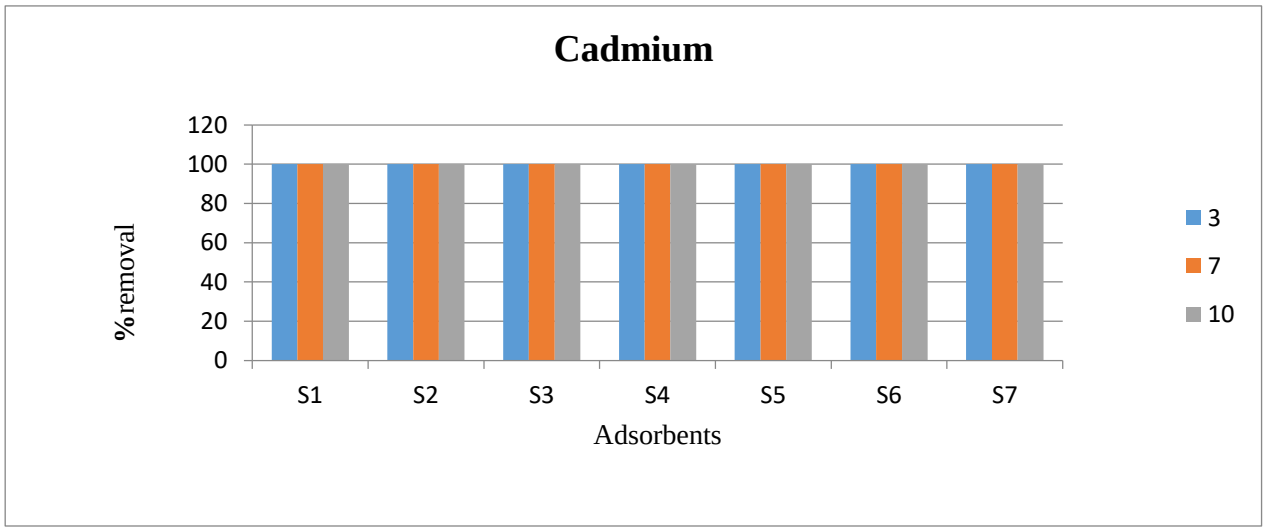

Figure 4. 37: Effect of pH on the percentage removal of Cd^{2+}

The pH environment is a critical parameter in adsorption studies, as different adsorbates and adsorbents exhibit varying behaviors at different pH levels. Alkali-treated clay minerals, in particular, play a significant role as adsorbents in this study. In an acidic environment, both the

medium and the adsorbate compete for the active sites on the adsorbent surface. Conversely, in a basic medium, the likelihood of hydroxyl group formation is higher (Emam *et al*., 2016).

In Figure 4.30, where nitrate was employed as the adsorbate in an acidic medium, the percentage removal was notably low at 27%. This contrasted with the near-complete removal observed for the same adsorbate in alkaline and neutral media, where it reached 100%. The decrease in nitrate removal in the acidic medium can be attributed to the saturation of active sites on the adsorbent. Similar trends were observed for phosphate (Figure 4.31), lead (Figure 4.32), and copper (Figure 4.33) adsorbates in acidic conditions. However, in the case of cadmium (Figure 4.34) as the adsorbate, pH had no discernible effect on the percentage removal.

4.4 Adsorption isotherms

The concept of adsorption isotherms, as defined by Bleam (2017), pertains to equations that describe the relationships among adsorbents, adsorbates, and external factors. These isotherms also manifest as curves that elucidate the adsorption capacity of adsorbents at equilibrium, as noted by Sahu & Singh, (2019). In this investigation, the focus was on three distinct adsorption isotherms: Langmuir, Freundlich, and Temkin adsorption isotherms. These isotherms were systematically examined under standardized conditions, including room temperature, a pH of 7, and a contact time of 30 minutes, where Ce represents the equilibrium concentration, and qe signifies the equilibrium adsorption capacity.

Throughout the adsorption isotherm analysis, adsorbents S1, S2, S3, S4, S5, and S6 exhibited similar behaviours. Therefore, for the sake of brevity and clarity, adsorbent S1 was selected as a representative of the entire group of adsorbents.

4.4.1 Langmuir adsorption isotherm model

Using the Langmuir linear equation

$$\frac{C_e}{q_e} = \left(\frac{1}{b}\right)\left(\frac{1}{K_l}\right) + \left(\frac{1}{b}\right)C_e \qquad \text{Equation 4:1}$$

Ce/qe vs. Ce were plotted and from the slope and intercept, the Langmuir constant K_L and the maximum monolayer capacity q_{max} were calculated**.** The maximum monolayer capacity q_{max} was calculated using the following equation:

$$q_{max} = \frac{1}{\text{slope}}. \qquad \text{Equation 4 :2}$$

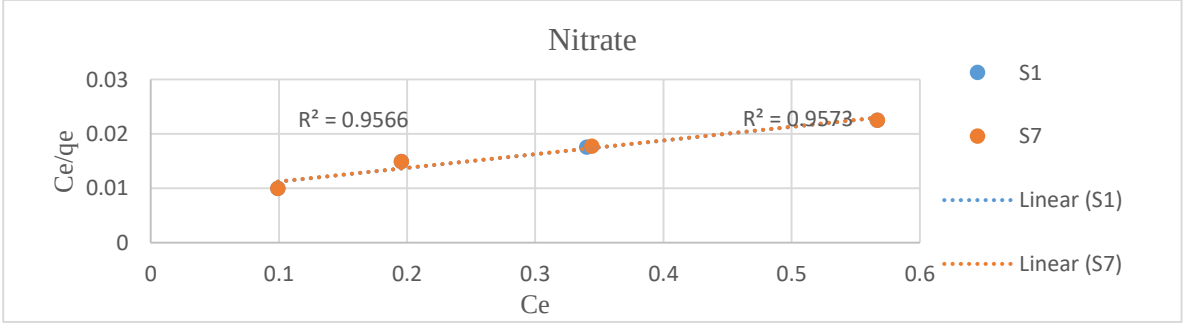

Figure 4. 38: Langmuir adsorption isotherm of NO_3^-

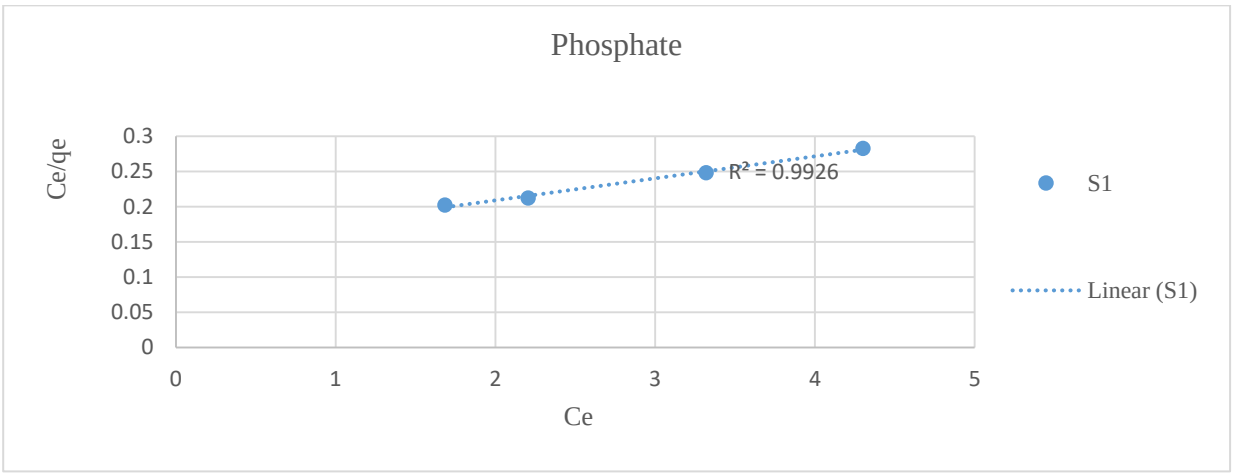

Figure 4. 39: Langmuir adsorption isotherm of PO_4^{3-}

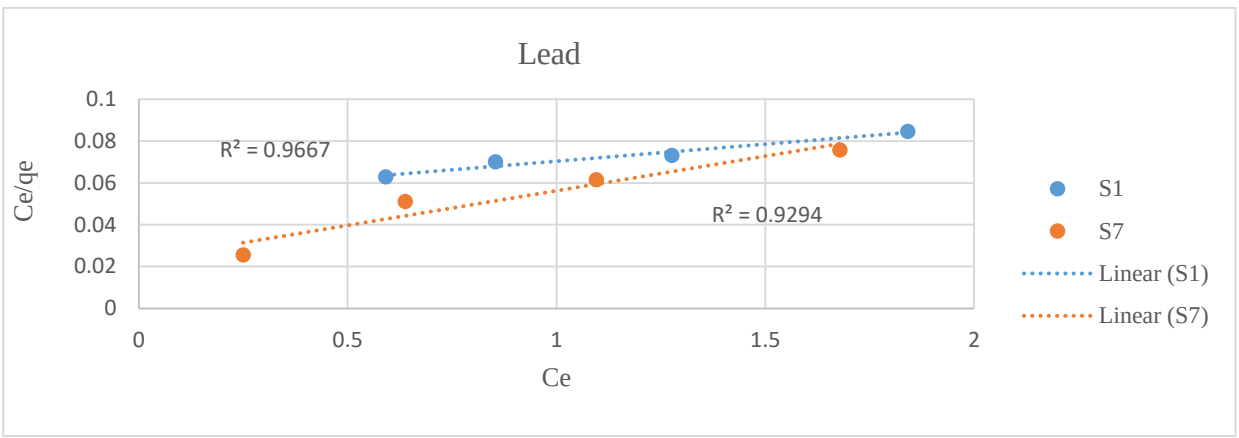

Figure 4. 40: Langmuir adsorption isotherm of Pb^{2+}

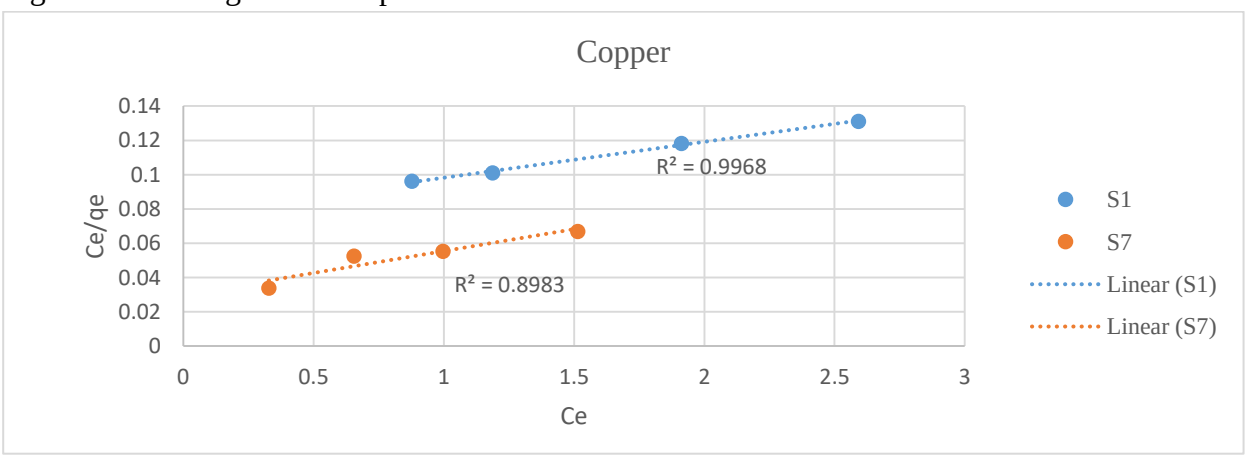

Figure 4. 41: Langmuir adsorption isotherm of Cu^{2+}

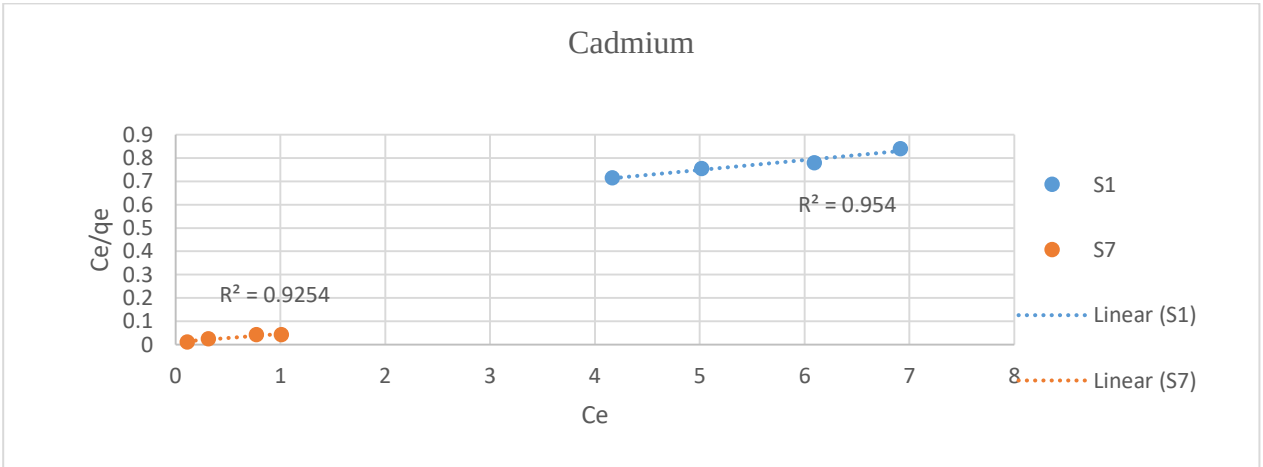

Figure 4. 42: Langmuir adsorption isotherm Cd^{2+}

Figure 4.38 to 4.42 illustrate the Langmuir adsorption isotherms for NO^{-}_{3}, PO_4^{3-}, Cu^{2+}, Pb^{2+} and Cd^{2+}, respectively. The Langmuir isotherm model posits a monolayer adsorption process where each adsorption site on the adsorbent surface can accommodate only one molecule (Luo & Deng, 2018). The Langmuir parameters, as outlined in Table 4:5, offer insights into several crucial aspects of the adsorption process.

Firstly, the dimensionless equilibrium parameter R_L is employed to assess the favorability of adsorption. When RL falls between 0 and 1, it signifies favorable adsorption (Emam *et al*., 2016). In this study, the RL values were determined as 0.0335, 0.3189, 0.2485, 0.2695, and 0.5577 for nitrate, phosphate, lead, copper, and cadmium, respectively.

Secondly, the maximum adsorption capacity (qmax) is a pivotal indicator of adsorbent performance. Lead exhibited the highest qmax in this study at 61.208 g/g, followed by copper at 47.7502 g/g, nitrate at 39.7702 g/g, phosphate at 31.9686 g/g, and cadmium with the lowest maximum adsorption capacity of 23.5164 g/g.

Lastly, the Langmuir equilibrium constant (K_L) characterizes the adsorption/desorption equilibrium for each adsorbate in contact with the adsorbents under specific temperature and pressure conditions (Luo & Deng, 2018). In this study, the highest K_L was observed when nitrate served as the adsorbate at 2.882 L/g, followed by 0.302 L/g, 0.271 L/g, 0.213 L/g, and 0.079 L/g for lead, copper, phosphate, and cadmium, respectively.

The adsorption process represented in Figures 4:35 to 4:39 illustrates a linear progression of adsorbate per unit mass of adsorbent, aligning with the Langmuir adsorption isotherm model, as indicated by correlation coefficients (R^2) exceeding 0.95 (Table 4:5). Therefore, it can be concluded that the adsorption process adheres to a monolayer adsorption mechanism.

Table 4. 6: Langmuir adsorption isotherms constants

ADSORPTION ISOTHERMS CONSTANTS						
	LANGMUIR					
	CONSTANTS	**NITRATE**	**PHOSPHATE**	**LEAD**	**COPPER**	**CADMIUM**
S1	**K_L(L/g)**	2.882317	0.213562	0.302365	0.271048	0.079307
	q_{max}(g/g)	39.77028	31.96866	61.20896	47.75029	23.5164
	R_L	0.0335	0.3189	0.24853	0.2695	0.5577
	R^2	0.957323	0.992624	0.966697	0.996844	0.953959
S2	**K_L(L/g)**	2.882317	0.213562	0.302365	0.271048	0.079307
	q_{max}(g/g)	39.77028	31.96866	61.20896	47.75029	23.5164
	R_L	0.0335	0.3189	0.24853	0.2695	0.5577
	R^2	0.957323	0.992624	0.966697	0.996844	0.953959
S3	**K_L(L/g)**	2.882317	0.213562	0.302365	0.271048	0.079307
	q_{max}(g/g)	39.77028	31.96866	61.20896	47.75029	23.5164
	R_L	0.0335	0.3189	0.24853	0.2695	0.5577
	R^2	0.957323	0.992624	0.966697	0.996844	0.953959
S4	**K_L(L/g)**	2.882317	0.213562	0.302365	0.271048	0.079307
	q_{max}(g/g)	39.77028	31.96866	61.20896	47.75029	23.5164

	R_L	0.0335	0.3189	0.24853	0.2695	0.5577
	R^2	0.957323	0.992624	0.966697	0.996844	0.953959
S5	**K_L(L/g)**	2.882317	0.213562	0.302365	0.271048	0.079307
	q_{max}(g/g)	39.77028	31.96866	61.20896	47.75029	23.5164
	R_L	0.0335	0.3189	0.24853	0.2695	0.5577
	R^2	0.957323	0.992624	0.966697	0.996844	0.953959
S6	**K_L(L/g)**	2.882317	0.213562	0.302365	0.271048	0.079307
	q_{max}(g/g)	39.77028	31.96866	61.20896	47.75029	23.5164
	R_L	0.0335	0.3189	0.24853	0.2695	0.5577
	R^2	0.957323	0.992624	0.966697	0.996844	0.953959
S7	**K_L(L/g)**	2.883494	-1.00757	1.429442	0.856043	3.301867
	qmax(g/g)	39.6923	0.000323	30.20675	39.12857	28.6401
	R_L	0.0335	-0.10249	0.24853	0.2695	0.5577
	R^2	0.956622	0.149531	0.929424	0.898283	0.925385

4.4.2 Freundlich adsorption isotherm model

From the Freundlich linear equation,

$$\ln q_e = \ln K_f + \frac{1}{n}\ln C_e \qquad \text{Equation 4:3}$$

The Freundlich constant K_f and n, which is the index, representing the free energy associated with the multilayer adsorbents were determined after plotting lnqe vs. lnCe.

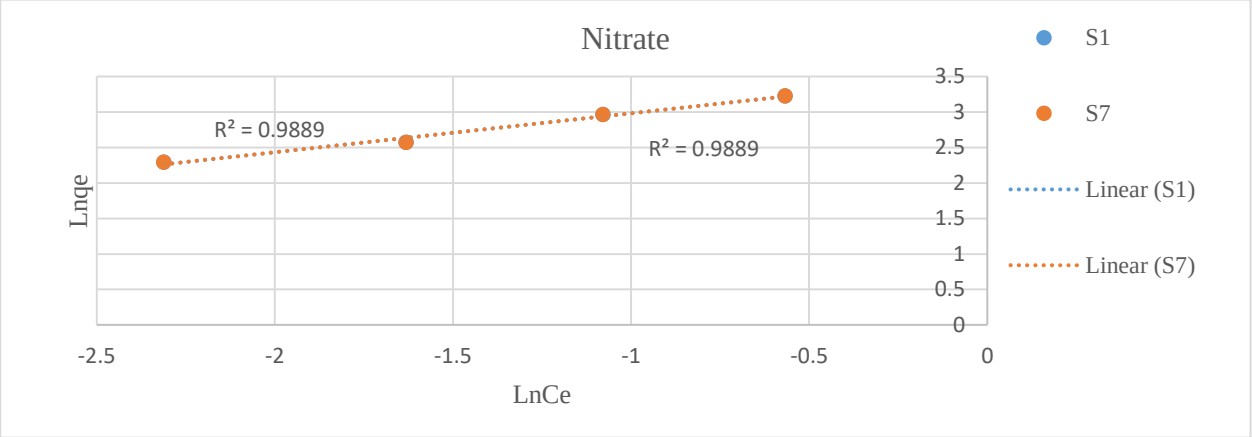

Figure 4. 43: Freundlich adsorption isotherm of NO_3^-

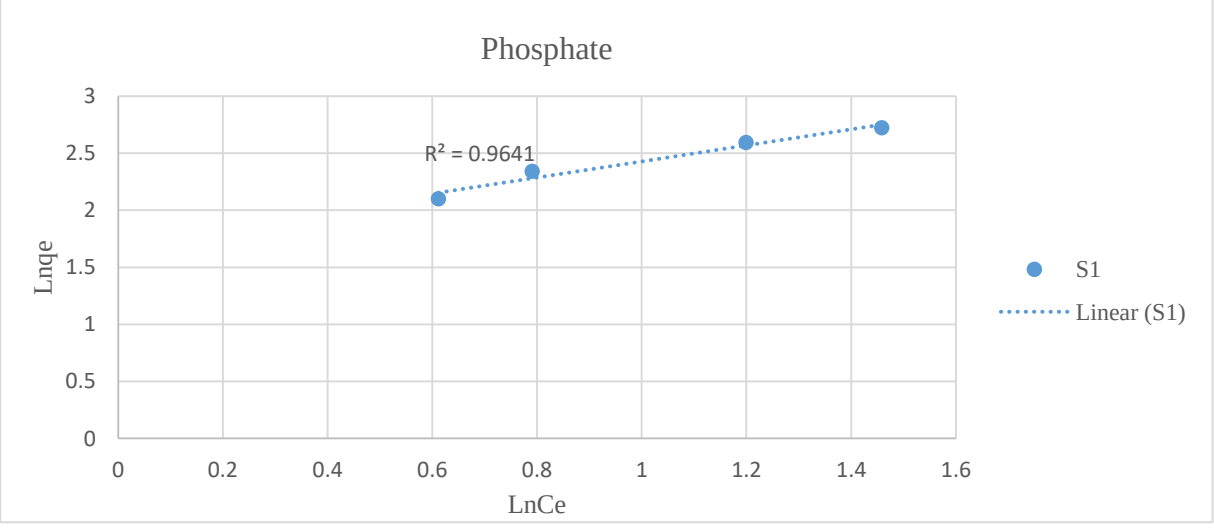

Figure 4. 44: Freundlich adsorption isotherm of PO_4^{3-}

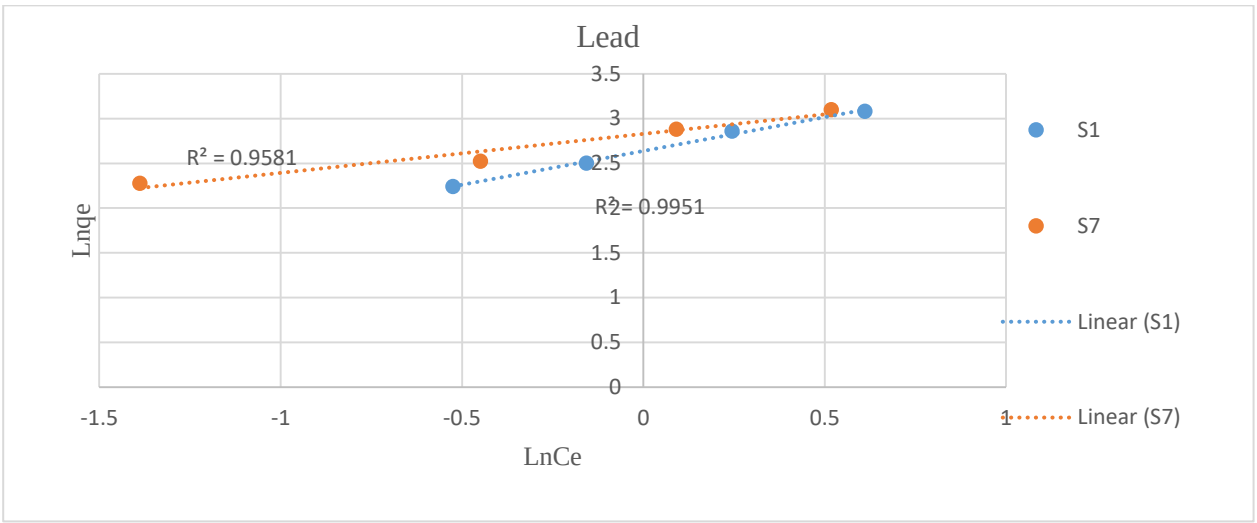

Figure 4. 45: Freundlich adsorption isotherm of Pb^{2+}

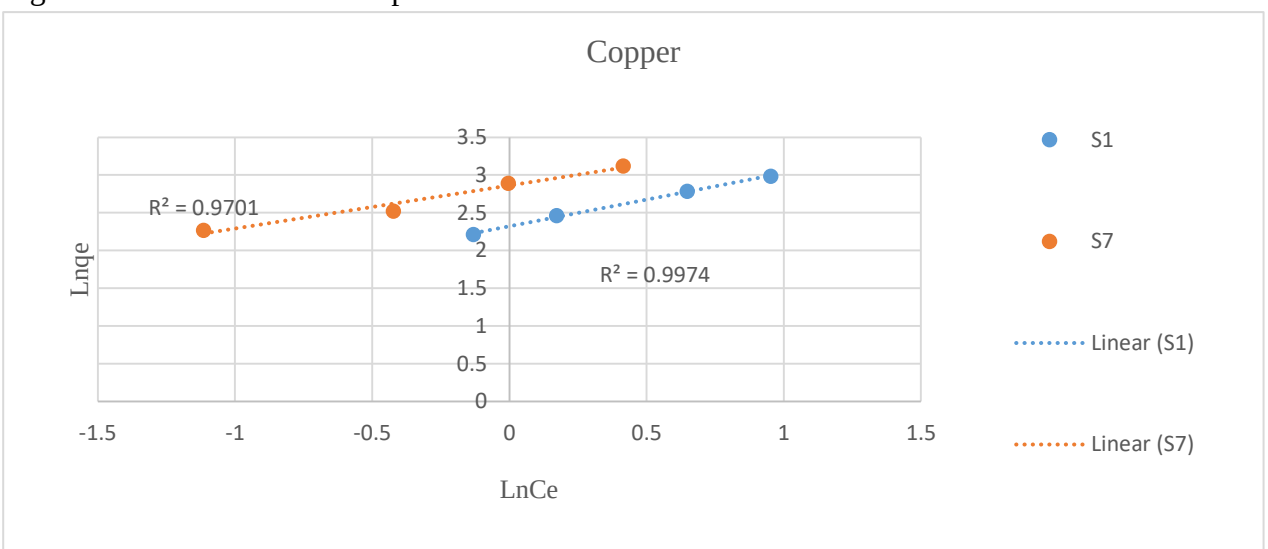

Figure 4. 46: Freundlich adsorption isotherm of Cu^{2+}

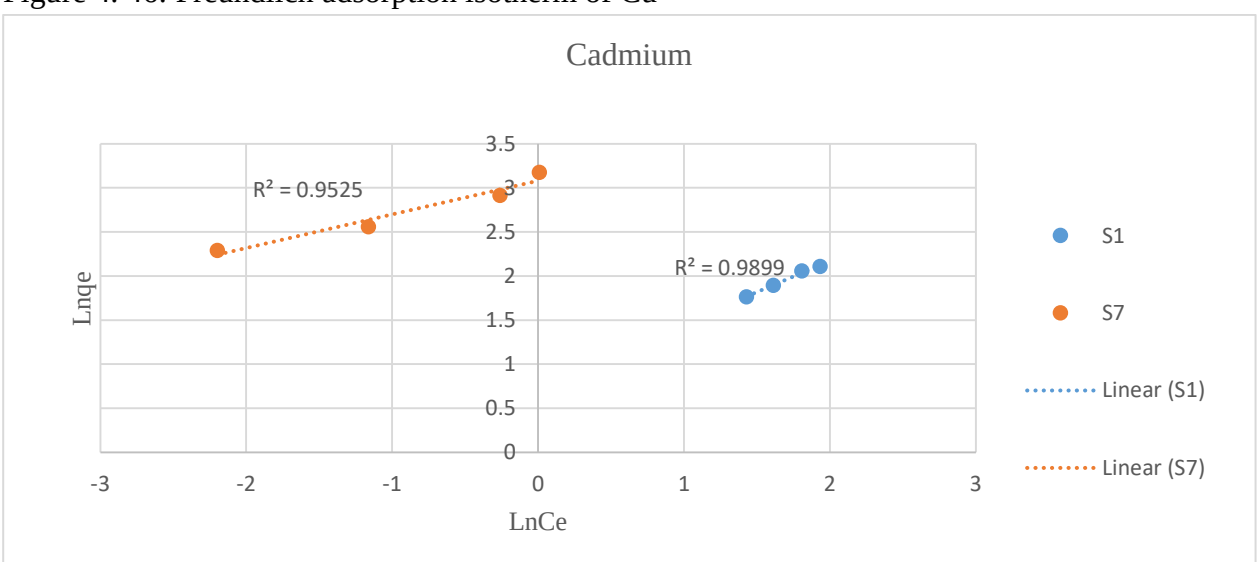

Figure 4. 47: Freundlich adsorption isotherm of Cd^{2+}

In the context of our investigation, the Freundlich adsorption isotherm figures, specifically Figure 4.43 for NO^{-}_{3} Figure 4.44 for PO_4^{3-}, Figure 4.45 for Pb^{2+}, Figure 4.46 for Cu^{2+}, and Figure 4.47 for Cd^{2+}, have been employed to gain deeper insights into multilayer coverage phenomena.

K_F represents the adsorption capacity and n is the index representing the free energy associated with the multilayer adsorbents. If 1/n=0, the adsorption isotherm is linear. If 1/n<1, the adsorption is non-linear. For this model to be applicable, 1\n has to be between 1 and 0 (n >0) (Khayyun & Mseer, 2019) .K_F represents the adsorption capacity but not at saturation like the qmax in Langmuir adsorption isotherm. In table 4:6, the values of n are between 1 and 3. This means that, 1/n is less than 1. Implying that, the Freundlich model is applicable for this study. The adsorption capacity ranking K_F was similar to the Langmuir adsorption isotherm. However, their values differed. The highest adsorption capacity in (mg/g) $(L/mg)^{(1/n)}$ was nitrate with a value equals to 34.0732, followed by 13.9861, 10.1812, 5.602 and 2.1407 respectively for lead, copper, phosphate and cadmium.
The coefficient of correlation (R^2) for our study's data sets was found to be 0.9889, 0.9664, 0.995, 0.997, and 0.9889 for nitrate, phosphate, lead, copper, and cadmium, respectively. These high R^2 values further affirm the suitability of the Freundlich adsorption isotherm for describing the adsorption process in our study, reinforcing the notion of a multilayer adsorption phenomenon.

Table 4. 7: Adsorption isotherms constants

ADSORPTION ISOTHERMS CONSTANTS						
FREUNDLICH						
		NITRATE	**PHOSPHATE**	**LEAD**	**COPPER**	**CADMIUM**
S1	**n(L/mg)**	1.823821	1.419142	1.324247	1.415708	1.419274
	K_F((mg/g)(L/mg)$^{(1/n)}$)	34.07326	5.602627	13.9861	10.18126	2.140731
	R^2	0.988942	0.96408	0.995076	0.997383	0.989909
S2	**n(L/mg)**	1.823821	1.419142	1.324247	1.415708	1.419274
	K_F((mg/g)(L/mg)$^{(1/n)}$)	34.07326	5.602627	13.9861	10.18126	2.140731
	R^2	0.988942	0.96408	0.995076	0.997383	0.989909
S3	**n(L/mg)**	1.823821	1.419142	1.324247	1.415708	1.419274
	K_F((mg/g)(L/mg)$^{(1/n)}$)	34.07326	5.602627	13.9861	10.18126	2.140731
	R^2	0.988942	0.96408	0.995076	0.997383	0.989909
S4	**n(L/mg)**	1.823821	1.419142	1.324247	1.415708	1.419274
	K_F((mg/g)(L/mg)$^{(1/n)}$)	34.07326	5.602627	13.9861	10.18126	2.140731
	R^2	0.988942	0.96408	0.995076	0.997383	0.989909
S5	**n(L/mg)**	1.823821	1.419142	1.324247	1.415708	1.419274
	K_F((mg/g)(L/mg)$^{(1/n)}$)	34.07326	5.602627	13.9861	10.18126	2.140731
	R^2	0.988942	0.96408	0.995076	0.997383	0.989909
S6	**n(L/mg)**	1.823821	1.419142	1.324247	1.415708	1.419274
	K_F((mg/g)(L/mg)$^{(1/n)}$)	34.07326	5.602627	13.9861	10.18126	2.140731
	R^2	0.988942	0.96408	0.995076	0.997383	0.989909
S7	**n(L/mg)**	1.823821	-0.25072	2.295767	1.750613	2.621857
	K_F((mg/g)(L/mg)$^{(1/n)}$)	34.07326	8.690597	16.92915	17.48657	21.7668
	R^2	0.988942	0.921083	0.958092	0.970116	0.952525

4.4.3 Temkin adsorption isotherm model

Using this equation,

$$q_e = \left(\frac{RT}{b}\right) \times \ln A + \left(\frac{RT}{b}\right) \times \ln C_e \qquad \text{Equation 4:4}$$

The Temkin constants were determined after plotting qe vs. lnCe.

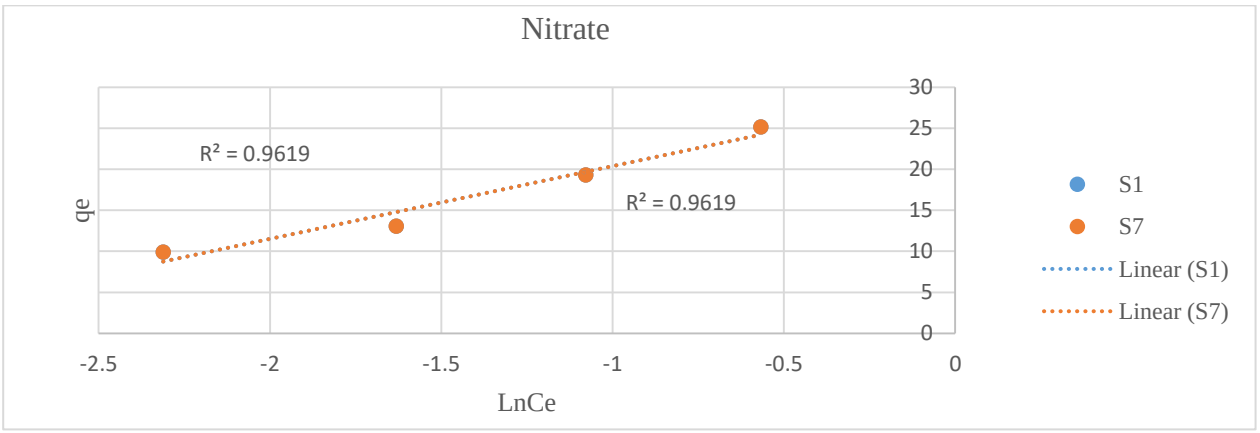

Figure 4. 48: Temkin adsorption isotherm of NO_3^-

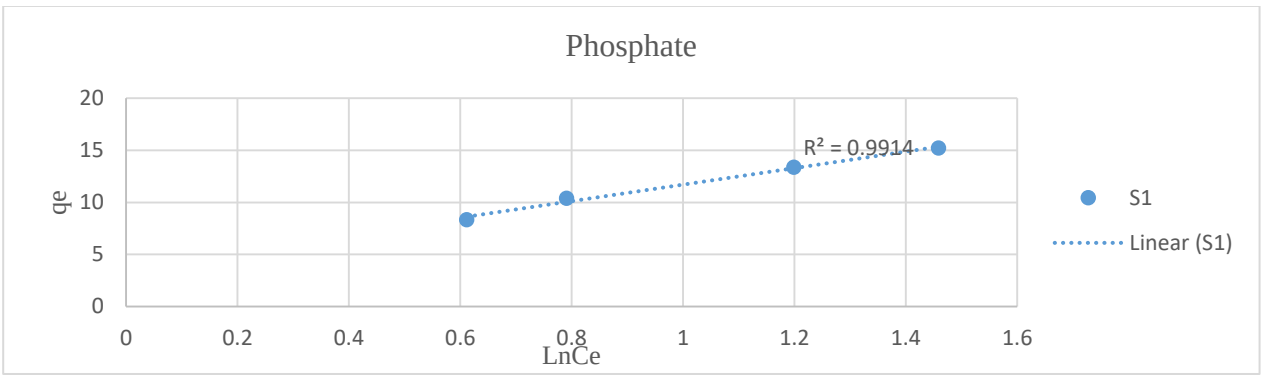

Figure 4. 49: Temkin adsorption isotherm of PO_4^{3-}

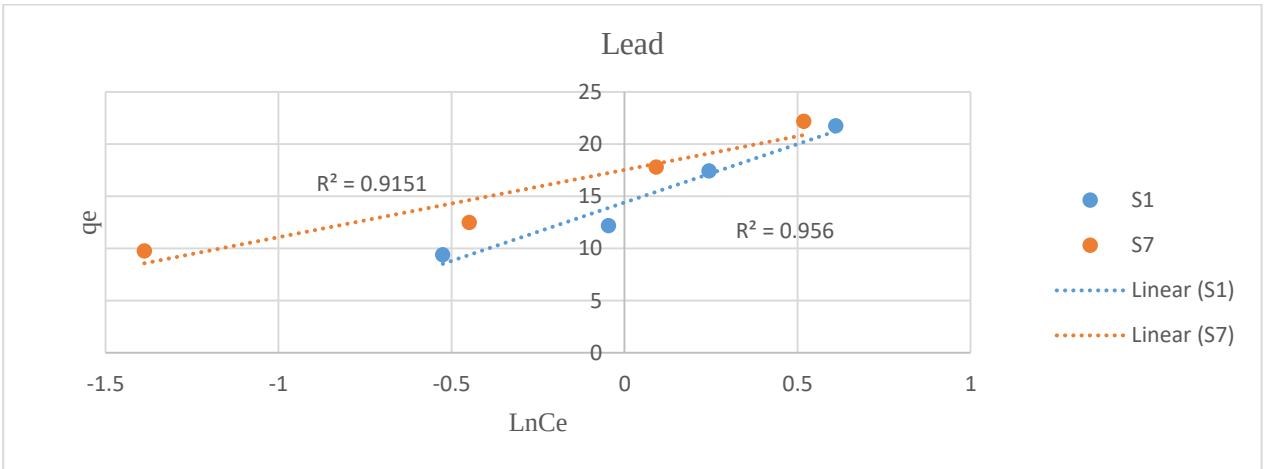

Figure 4. 50: Temkin adsorption isotherm of Pb^{2+}

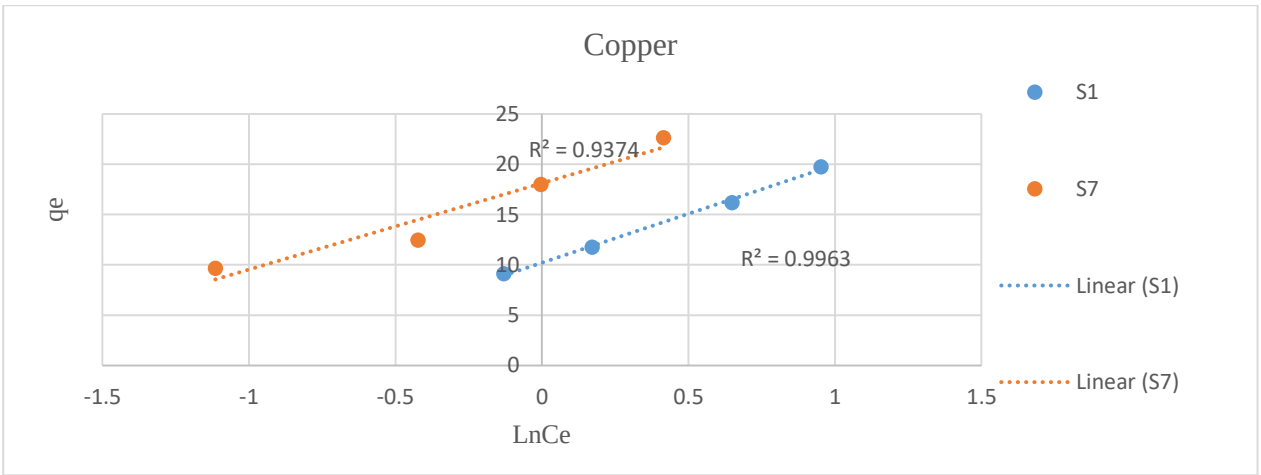

Figure 4. 51: Temkin adsorption isotherm of Cu^{2+}

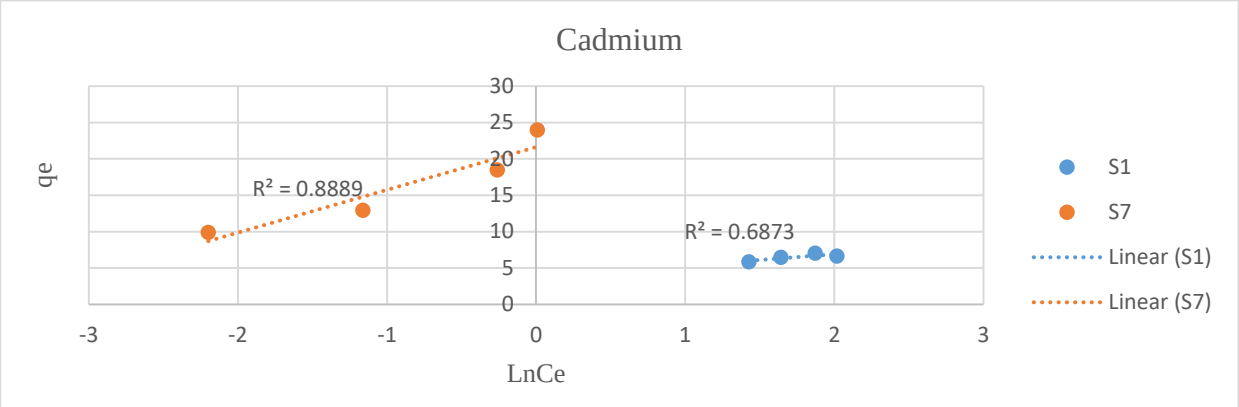

Figure 4. 52: Temkin adsorption isotherm of Cd^{2+}

In the investigation, the Temkin adsorption isotherm model was used, as illustrated in Figure 4.48 for NO_3^-, Figure 4.49 for PO_4^{3-}, Figure 4.50 for Pb^{2+}, Figure 4.51 for $Cu^{2+,}$ and Figure 4.52 for Cd^{2+}. The Temkin model places significant importance on achieving a uniform distribution of binding energy, extending up to the maximum binding energy. This emphasis on uniformity is crucial because it plays a pivotal role in governing the interaction between the adsorbent and adsorbate, as highlighted in the research by Piccin *et al*. (2011).

The Temkin isotherm is primarily defined by two key factors: the equilibrium binding constant (K_T), representing the maximum binding energy, and the heat of adsorption (B). In our study, we plotted Lnqe and LnCe to ascertain these vital parameters. It's noteworthy that the heat of adsorption, represented by B, consistently exhibited positive values throughout the adsorption phase. This discovery, coupled with adsorption energies below 20 J/mol, implies that the physical adsorption process is exothermic.

A detailed examination of the K_T values provided in Table 4.7 indicates that nitrate had the highest equilibrium binding constant at 27.04 L/mg. This suggests a substantial interaction between the adsorbent and the nitrate adsorbate. Lead exhibited the second-highest equilibrium binding constant, followed in decreasing order by copper, phosphate, and cadmium.

In all the cases we examined, the coefficient of correlation obtained from our analysis consistently exceeded 0.92. This robust correlation underscores the suitability of the Temkin adsorption isotherm model in explaining the observed adsorption phenomena. Consequently, we can conclude that energy is evenly distributed during the adsorption process between the adsorbent and the adsorbate.

Table 4. 8: Temkin adsorption isotherm constants

ADSORPTION ISOTHERMS CONSTANTS						
TEMKIN						
		NITRATE	**PHOSPHATE**	**LEAD**	**COPPER**	**CADMIUM**
S1	**K_T(L/mg)**	27.04686	1.609475	4.142331	2.855076	0.782683
	B(J/mol)	8.873852	7.926844	8.118019	9.730484	4.918514
	R^2	0.961867	0.991406	0.929582	0.9963	0.99149
S2	**K_T(L/mg)**	27.04686	1.609475	4.142331	2.855076	0.782683
	B(J/mol)	8.873852	7.926844	8.118019	9.730484	4.918514
	R^2	0.961867	0.991406	0.929582	0.9963	0.99149
S3	K_T(L/mg)	27.04686	1.609475	4.142331	2.855076	0.782683
	B(J/mol)	8.873852	7.926844	8.118019	9.730484	4.918514
	R^2	0.961867	0.991406	0.929582	0.9963	0.99149
S4	**K_T(L/mg)**	27.04686	1.609475	4.142331	2.855076	0.782683
	B(J/mol)	8.873852	7.926844	8.118019	9.730484	4.918514
	R^2	0.961867	0.991406	0.929582	0.9963	0.99149
S5	**K_T(L/mg)**	27.04686	1.609475	4.142331	2.855076	0.782683
	B(J/mol)	8.873852	7.926844	8.118019	9.730484	4.918514
	R^2	0.961867	0.991406	0.929582	0.9963	0.99149
S6	**K_T(L/mg)**	27.04686	1.609475	4.142331	2.855076	0.782683
	B(J/mol)	8.873852	7.926844	8.118019	9.730484	4.918514
	R^2	0.961867	0.991406	0.929582	0.9963	0.99149
S7	**K_T(L/mg)**	27.04686	0.099966	15.15285	8.257104	39.53823
	B(J/mol)	8.873852	-3.89668	6.452853	8.578505	5.881098
	R^2	0.961867	1	0.915121	0.937422	0.888923

The three adsorption isotherm models under consideration exhibit coefficients of correlation (R^2) exceeding 0.91, signifying that all these models effectively depict the adsorption phenomena. Nonetheless, it is notable that among these models, the Langmuir model provides the most accurate description of the interactions between phosphate-adsorbents and copper-adsorbents, yielding R^2 values of 0.9926 and 0.9968, respectively.

Conversely, the Freundlich model emerges as the optimal choice for characterizing the interactions involving nitrate-adsorbents, lead-adsorbents, and copper-adsorbents, with R^2 values of 0.9889, 0.995, and 0.9973, respectively.

From the results of these experiments, we can confidently conclude that the predominant mode of adsorption observed is predominantly multilayer, primarily owing to the higher R^2 values associated with the Freundlich model.

4.5 Adsorption kinetics

The adsorption kinetics was determined at room temperature, pH7, with an initial dosage and concentration 0.050 g and 10 ppm respectively, where Ce is the concentration at equilibrium, Ct the concentration at time t, q_e the adsorption capacity at equilibrium and q_t the adsorption capacity at time t.

For the pseudo first model using this linear equation;

$$\ln(q_e - q_t) = \ln q_e - K_1 t \qquad \text{Equation 4:5}$$

Ln (qe-qt) vs t was plotted and for the pseudo second model t/qt vs t was plotted from its linear equation;

$$\frac{t}{q_t} = \frac{1}{K_2\ q_e{}^2} + \frac{1}{q_e}t$$

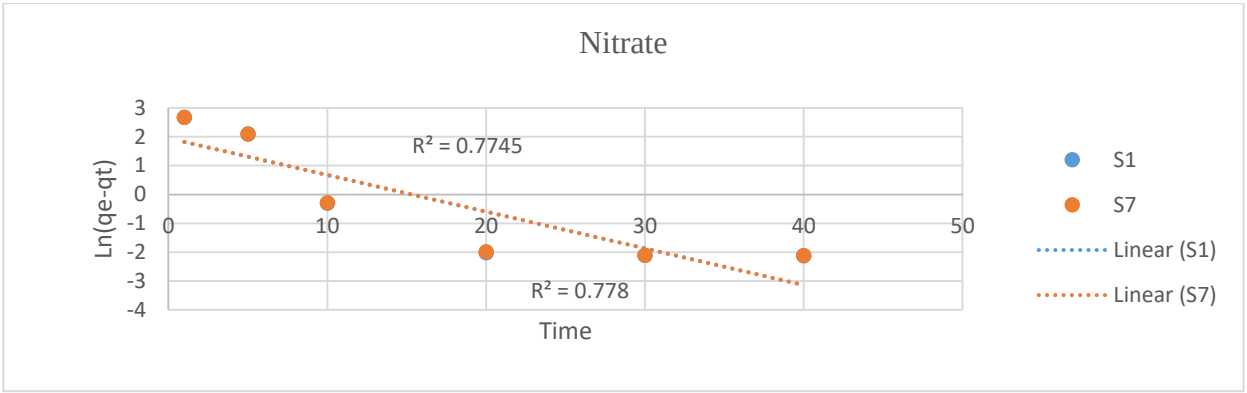

Figure 4. 53: Pseudo first order reaction of NO_3^-

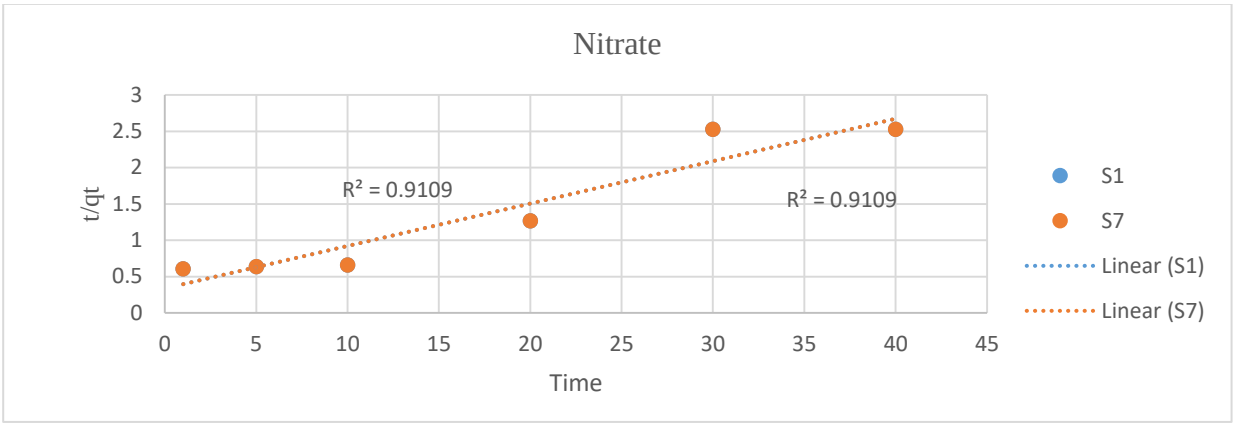

Figure 4. 54: Pseudo second order reaction of NO_3^-

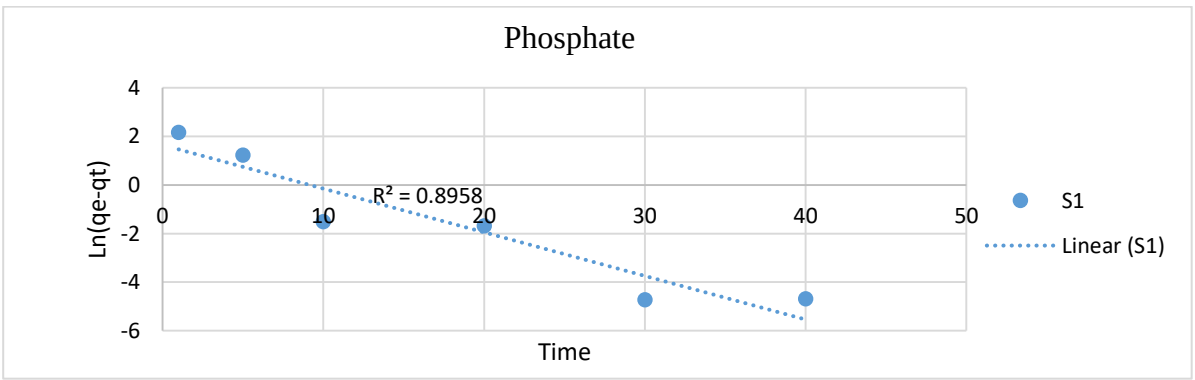

Figure 4. 55: Pseudo first order reaction of PO_4^{3-}

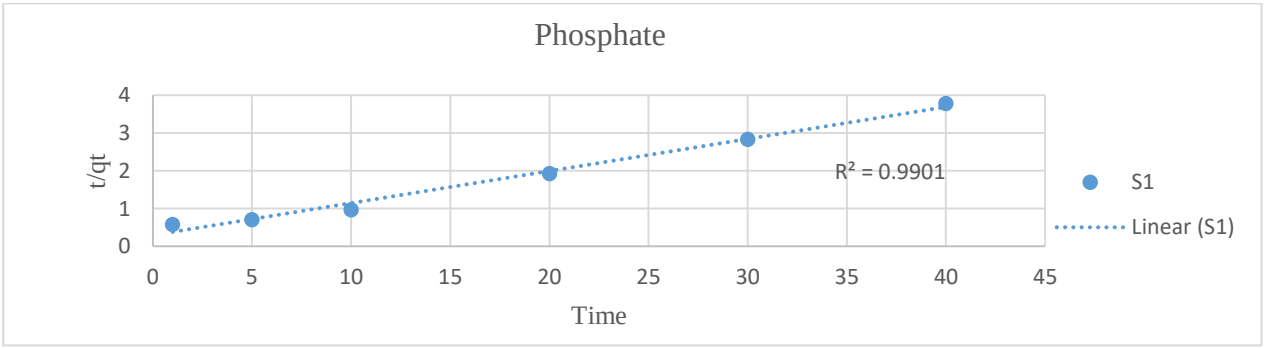

Figure 4. 56: Pseudo second order reaction of PO_4^{3-}

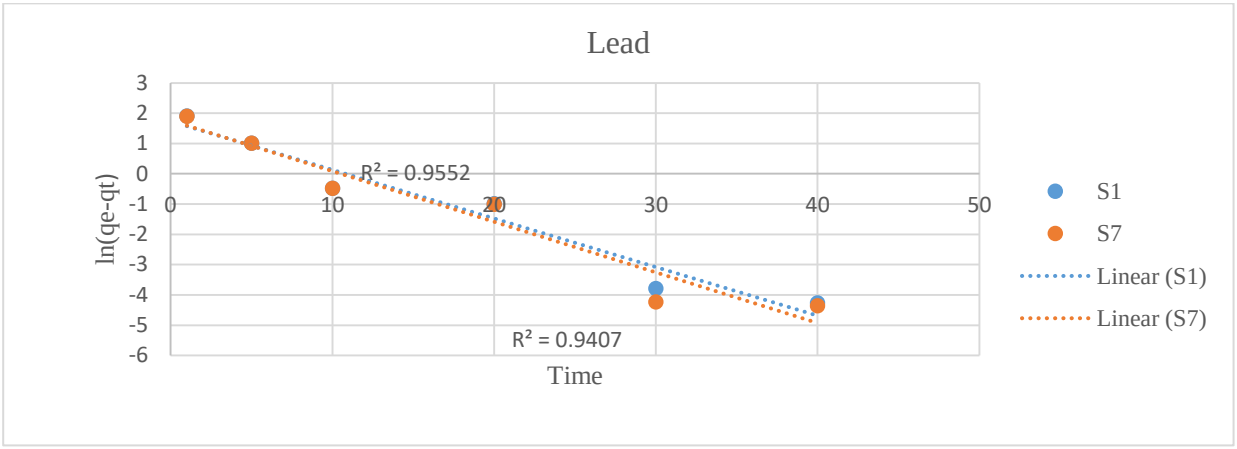

Figure 4. 57: Pseudo first order reaction of Pb^{2+}

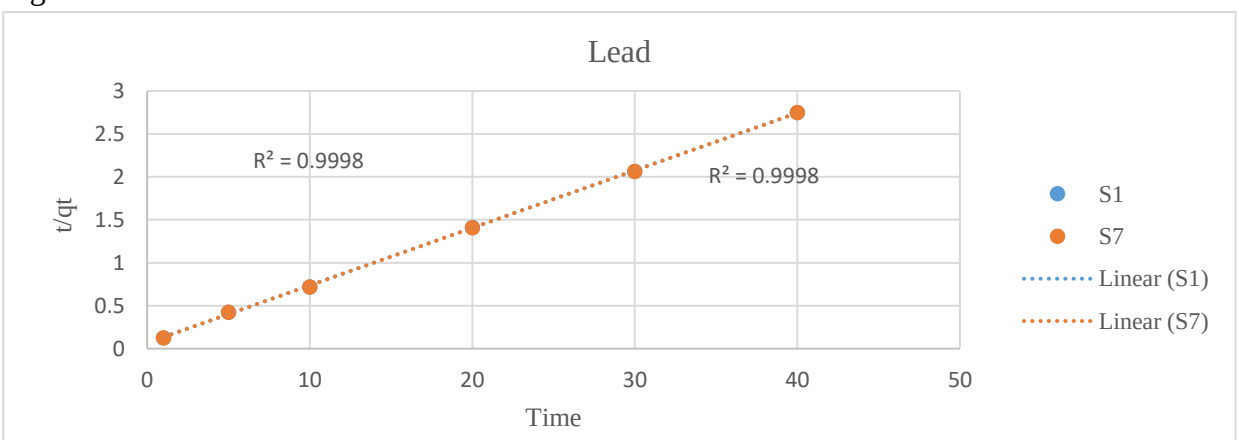

Figure 4. 58: Pseudo second order reaction of Pb^{2+}

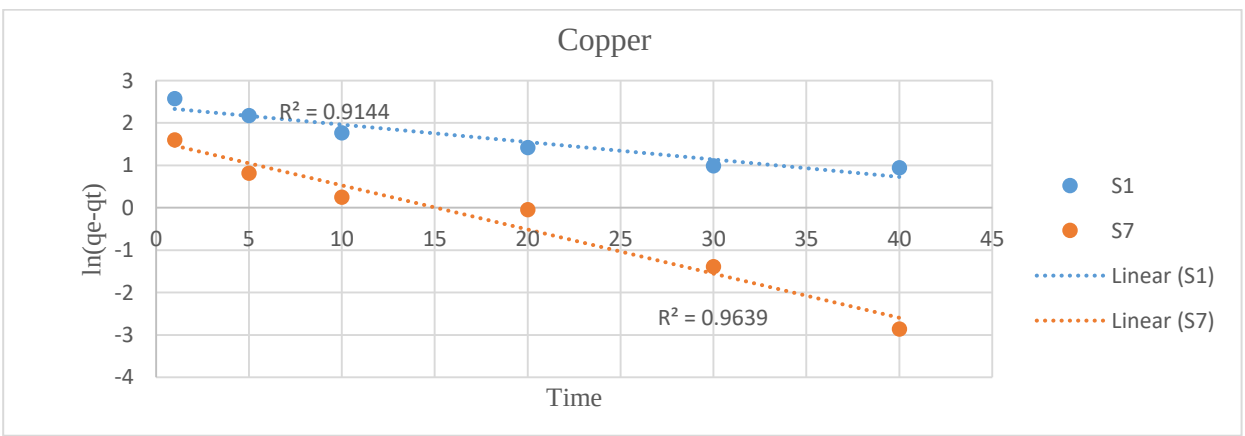

Figure 4. 59: Pseudo first order reaction of Cu^{2+}

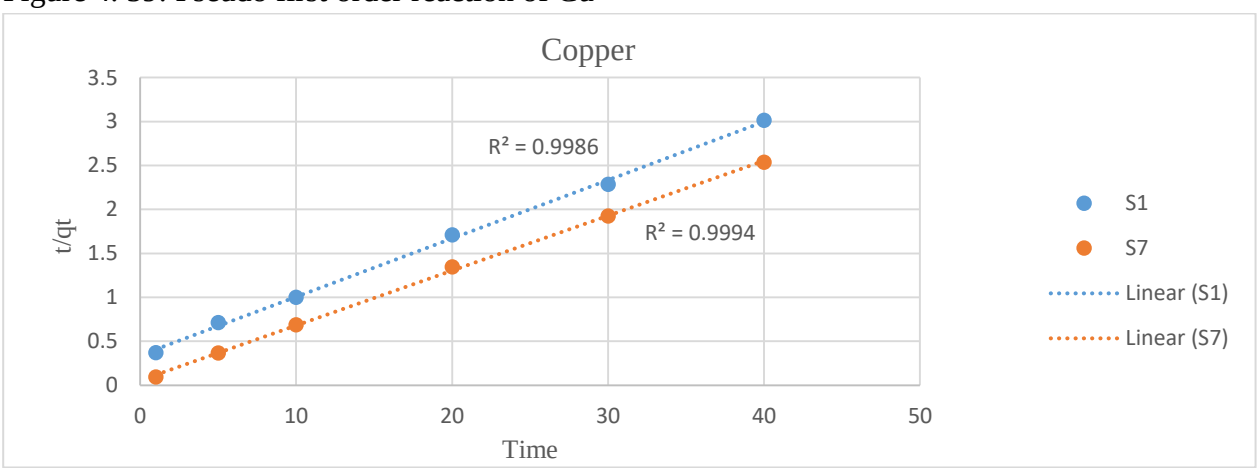

Figure 4. 60: Pseudo second order reaction of Cu^{2+}

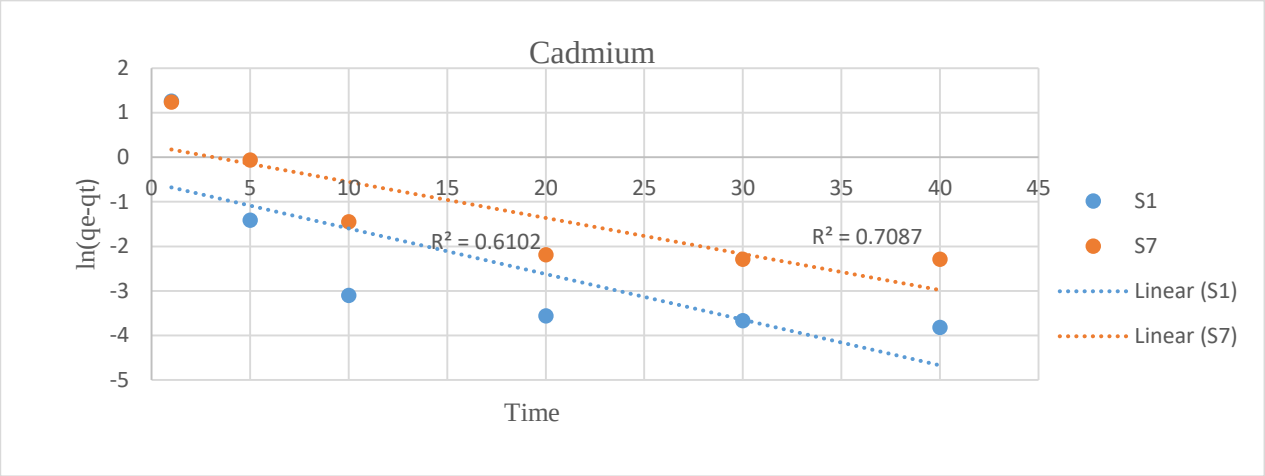

Figure 4. 61: Pseudo first order reaction of Cd^{2+}

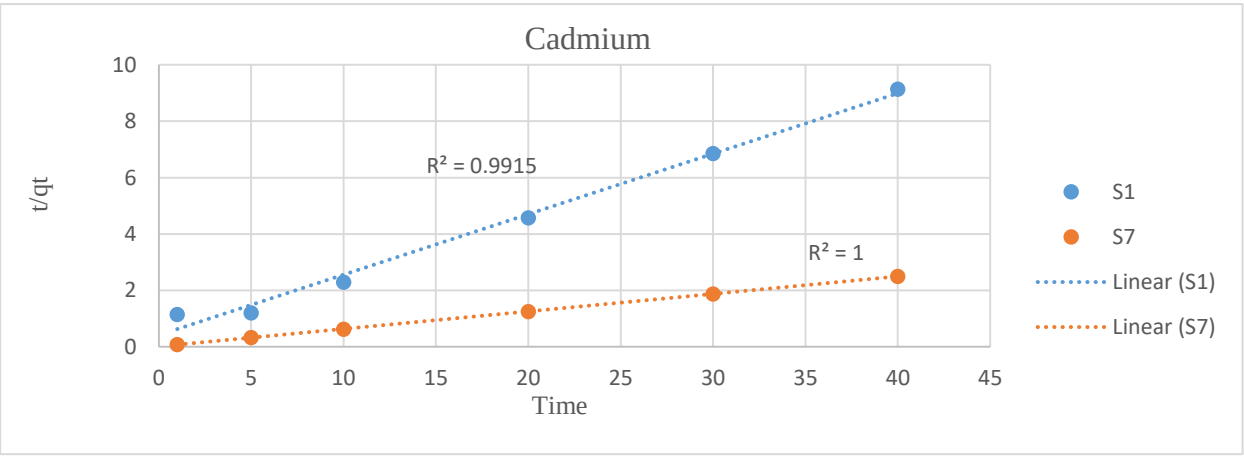

Figure 4. 62: Pseudo second order reaction of Cd^{2+}

Figures 4.53 to 4.62 employ the pseudo-first-order and pseudo-second-order reaction models to illustrate adsorption kinetics. We have analyzed the statistics from these figures along with the data from Table 4.8 to provide further insights into the observed trends.

The coefficient of correlation (R^2) for the adsorption of nitrate as an adsorbate was found to be 0.77 for the pseudo-first-order reaction and 0.91 for the pseudo-second-order reaction. These results suggest that the pseudo-second-order reaction model provides a better fit to the data for nitrate adsorption. Conversely, the pseudo-second-order reaction model yielded an impressive R^2 of 0.99 for the adsorption of phosphate, while the pseudo-first-order model resulted in an R^2 of 0.89. Therefore, it is concluded that the pseudo-second-order reaction model is the more suitable choice for describing the kinetics of both phosphate and nitrate adsorption.

The pseudo-second-order reaction model consistently provided a better fit for heavy metals such as lead, copper, and cadmium, yielding R^2 values of 0.99 for each metal. In contrast, the R^2 values obtained from the first-order reaction model for lead, copper, and cadmium were 0.95, 0.91, and 0.65, respectively. It's noteworthy that the preference for the pseudo-second-order reaction model is further supported by the experimental qe values closely aligning with the predicted qe values, in addition to the higher R^2 values.

Table 4.9 provides the kinetic parameters for the pseudo-first-order reaction model, while Table 4.10 outlines the parameters for the pseudo-second-order reaction model. These tables enable a comprehensive understanding of the observed adsorption behaviours, offering detailed insights into the kinetics of adsorption for each adsorbate.

Table 4. 9: Pseudo first order reaction parameters

PSEUDO FIRST ORDER REACTION						
		NITRATE	**PHOSPHATE**	**LEAD**	**COPPER**	**CADMIUM**
Qe		15.96	10.6	14.555	15.84	4.4
S1	**K_1**	0.127072	0.179682	0.160535	0.041113	0.102411
	Qe	6.978864	5.194721	5.672493	10.71605	0.563398
	R^2	0.774508	0.895827	0.955193	0.914379	0.610233
S2	**K_1**	0.127114	0.174732	0.15996	0.041185	0.102468
	Qe	6.920808	5.155216	5.647248	10.72998	0.611788
	R^2	0.769582	0.913515	0.958211	0.914619	0.632592
S3	**K_1**	0.126762	0.17087	0.162533	0.041311	0.101591
	Qe	6.890812331	5.141563375	5.674843593	10.73207726	0.57379997
	R^2	0.770635	0.911887	0.947041	0.913591	0.608845
S4	**K_1**	0.126876	0.180012	0.163487	0.041258	0.102398
	Qe	6.923078	5.31329	5.795355	10.72169	0.564987
	R^2	0.772493	0.904417	0.954124	0.913355	0.607254
S5	**K_1**	0.127016	0.172188	0.1611	0.04142	0.106544
	Qe	6.991629	5.007803	5.698515	10.73104	0.654938
	R^2	0.775496	0.902764	0.955708	0.912184	0.634011
S6	**K_1**	0.126751	0.171707	0.161054	0.041648	0.102167
	Qe	6.884793174	5.214297842	5.673688243	10.7383316	0.598375147
	R^2	0.770371	0.91713	0.954986	0.910278	0.625525
S7	**K_1**	0.127094	-4.6E-05	0.167182	0.104121	0.080879
	Qe	7.02694	10.58053238	5.807350417	4.804314108	1.290551384
	R^2	0.77798	0.120631	0.940709	0.963888	0.708665

Table 4. 10: Pseudo second order reaction parameters

PSEUDO SECOND ORDER REACTION						
		NITRATE	**PHOSPHATE**	**LEAD**	**COPPER**	**CADMIUM**
S1	**H**	2.965056	3.402777	15.02452	2.929116	2.417588
	K_2	0.010104	0.024549	0.067307	0.012917	0.111201
	Qe	17.13041811	11.77328566	14.94064787	15.05873983	4.662691709
	R^2	0.910921	0.990128	0.999797	0.998596	0.991493
S2	**H**	2.967272	3.405985	15.055	2.919399	2.41343
	K_2	0.010113	0.024585	0.067445	0.012856	0.1111
	Qe	17.12906689	11.77031495	14.94045927	15.06961028	4.660804657
	R^2	0.910867	0.990101	0.999799	0.99851	0.991727
S3	**H**	2.982175	3.401603	15.05218	2.920403	2.257227
	K_2	0.010184	0.024564	0.067421	0.01284	0.102909
	Qe	17.1121339	11.76774656	14.94173119	15.08135041	4.683389897
	R^2	0.911255	0.990193	0.999797	0.998397	0.990067

S4	**H**	2.976973	3.398703	14.97942	2.927416	2.404947
	K_2	0.01016	0.024519	0.067086	0.012885	0.110557
	Qe	17.117800	11.77355014	14.94279134	15.07305846	4.664020309
	R^2	0.911155	0.990168	0.999793	0.998414	0.991417
S5	**H**	2.974326	3.424855	15.027	2.92004	2.360553
	K_2	0.010149	0.024761	0.067318	0.012818	0.108304
	Qe	17.11944113	11.76082949	14.94070292	15.09346989	4.668584964
	R^2	0.911261	0.99025	0.999798	0.998289	0.992005
S6	**H**	2.971666	3.416574	15.01791	2.918251	2.408782
	K_2	0.010134	0.024697	0.067264	0.012772	0.110837
	Qe	17.1242	11.76189968	14.94216625	15.1157393	4.661833526
	R^2	0.910876	0.99037	0.999795	0.998049	0.991613
S7	**H**	2.962753	6.08E-06	15.0468	18.06875	67.4791
	K_2	0.010094	45.16615	0.067375	0.070427	0.259744
	Qe	17.13234522	0.00036692	14.94419057	16.01744793	16.11803117
	R^2	0.910927	0.006633	0.999795	0.99941	0.99998

4.6 Adsorption thermodynamics

At pH=7, 10 ppm adsorbate concentration, 0.030g adsorbent dosage, and a contact time of 30 minutes, the thermodynamic parameters were investigated.

The following equation was used to calculate the Gibb's free energy:

$$\Delta G^{\circ} = -RT\ln K \qquad \text{Equation 4:7}$$

The entropy and enthalpy were determined using this equation;

$$\ln k = \frac{\Delta S^{\circ}}{R} - \frac{\Delta H^{\circ}}{RT} \qquad \text{Equation 4:8}$$

Where:

ΔS° is the change in entropy,

ΔH° is the change in enthalpy,

R is the universal gas constant,

T is the absolute temperature and

K is the equilibrium constant (K=Qe/Ce).

Lnk vs 1\T was plotted and ΔS° and ΔH° were calculated from the slope and intercept.

Determining adsorption thermodynamics parameters is a valuable technique for gaining a comprehensive understanding of how temperature impacts adsorption processes. These parameters provide insights into the nature of interactions between adsorbents and adsorbates, as well as the feasibility and spontaneity of adsorption reactions.

Table 4.11 displays the Gibbs' free energy change (ΔG°) values for various adsorption processes at different temperatures, including 298 K, 333 K, and 353 K. Remarkably, all measured ΔG°

values were found to be negative, indicating the feasibility and spontaneity of all the examined adsorption processes, except for adsorbent S7 with phosphate as the adsorbate. In this case, the ΔG° values were 22.1076 kJ/mol, 28.0378 kJ/mol, and 30.9128 kJ/mol at 298 K, 333 K, and 353 K, respectively. This anomaly can be attributed to the absence of adsorption under these conditions. Table 4.11 also includes coefficients of correlation (R2), enthalpy change (ΔH°), and entropy change (ΔS°) to further assess the thermodynamic parameters. The coefficients of correlation represent the degree of linear correlation between the experimental and computed values and range from 0.77 to 0.98 for nitrate, 0.89 to 0.99 for phosphate, 0.94 to 0.999 for lead, 0.87 to 0.999 for copper, and 0.94 to 0.999 for cadmium.

The negative values of ΔH° indicate that these processes are exothermic adsorption processes.

Furthermore, it's worth noting that for all five adsorbates and across all seven adsorbents, a positive entropy change (ΔS°) is observed. This suggests that the degree of unpredictability or disorder at the solid-liquid interface increases during the adsorption reactions. These thermodynamic parameters provide a comprehensive understanding of the studied phenomena by offering valuable insights into the energy changes and behaviour of adsorption processes under different conditions.

Table 4. 11: Thermodynamics parameters

THERNODYNAMICS PARAMETERS						
GIBB'S FREE ENERGY (ΔG°)						
	TEMPERATURE	**NITRATE**	**PHOSPHATE**	**LEAD**	**COPPER**	**CADMIUM**
S1	**298 K**	-10.4562	-3.79466	-6.6226	-5.68843	-0.76228
	333 K	-11.6319	-4.21728	-7.37698	-6.33299	-0.71987
	353 K	-12.332	-4.43069	-7.79206	-6.70163	-0.6449
S2	**298 K**	-10.4483	-3.79951	-6.64644	-5.67918	-0.76252
	333 K	-11.642	-4.21871	-7.37926	-6.32825	-0.71976
	353 K	-12.3412	-4.43336	-7.79019	-6.70275	-0.6451
S3	**298 K**	-10.4575	-3.79694	-6.65617	-5.69627	-0.7624
	333 K	-11.6347	-4.22014	-7.37694	-6.33537	-0.71998
	353 K	-12.3289	-4.44038	-7.78197	-6.6969	-0.6449
S4	**298 K**	-10.4549	-3.80408	-6.6526	-5.68629	-0.76228
	333 K	-11.6376	-4.21903	-7.37798	-6.33774	-0.71965
	353 K	-12.3289	-4.4352	-7.79132	-6.70414	-0.6451
S5	**298 K**	-10.4562	-3.8018	-6.64386	-5.68084	-0.76252
	333 K	-11.6362	-4.21966	-7.3768	-6.33194	-0.71987
	353 K	-12.3397	-4.43804	-7.79094	-6.69829	-0.6449
S6	**298 K**	-10.4536	-3.79766	-6.64709	-5.69152	-0.76228
	333 K	-11.642	-4.21712	-7.37705	-6.33326	-0.71976
	353 K	-12.3305	-4.42802	-7.78982	-6.69913	-0.6452
S7	**298 K**	-10.4106	22.10761	-6.76189	-7.28274	-8.92068
	333 K	-11.6667	28.03781	-7.5557	-8.1345	-8.64068
	353 K	-12.3689	30.91184	-7.98449	-8.61639	-8.38337
R^2, ΔH^o and ΔS^o						

		NITRATE	PHOSPHATE	LEAD	COPPER	CADMIUM
S1	**R^2**	0.883164	0.890912	0.946662	0.999958	0.960947
	$-\Delta H^o$	0.315814	0.325572	0.273159	0.198961	0.008559
	ΔS^o	0.034017	0.011652	0.021313	0.018421	0.002136
S2	**R^2**	0.77699	0.92108	0.994905	0.988648	0.998097
	$-\Delta H^o$	0.2156	0.344857	0.443023	0.136252	0.008986
	ΔS^o	0.034327	0.011603	0.02082	0.018599	0.002135
S3	**R^2**	0.984381	0.918077	0.997463	0.99702	0.94196
	$-\Delta H^o$	0.325941	0.293032	0.550779	0.271709	0.007877
	ΔS^o	0.033994	0.011767	0.020491	0.018205	0.002138
S4	**R^2**	0.961617	0.949305	0.999904	0.98008	0.999796
	$-\Delta H^o$	0.313415	0.367474	0.481871	0.16661	0.010209
	ΔS^o	0.034026	0.011541	0.020708	0.018525	0.00213
S5	**R^2**	0.843794	0.943412	0.998006	0.980354	0.989429
	$-\Delta H^o$	0.27502	0.337843	0.424924	0.163432	0.007479
	ΔS^o	0.034153	0.011632	0.020871	0.018517	0.002139
S6	**R^2**	0.983216	0.904133	0.998479	0.999784	0.999056
	$-\Delta H^o$	0.291765	0.358695	0.452039	0.23142	0.010749
	ΔS^o	0.034096	0.011552	0.020791	0.018323	0.002129
S7	**R^2**	0.402346	0.993604	0.576261	0.879377	0.990749
	$-\Delta H^o$	0.03387	26.01607	0.117379	0.052811	5.580872
	ΔS^o	0.886315	-0.16169	0.022307	0.024263	0.009351

CHAPTER FIVE: CONCLUSIONS AND RECOMMENDATIONS

5.1 Conclusions

In the pursuit of a comprehensive understanding of the unknown clay mineral from Mukurweini and its alkali thermal-treated counterpart, this study has yielded significant insights.

First and foremost, the unidentified clay mineral was unequivocally identified as kaolinite 1A, while the alkali thermal-treated clay mineral revealed itself as hydrosodalite sodium hexakis (alumino silicate) upon thorough characterization.

In the realm of adsorption phenomena, the findings unveil a compelling trend where the percentage removal increased proportionally with the dosage of adsorbents. Remarkably, equilibrium was attained within a relatively short contact time of 30 minutes. At an adsorbate concentration of 100 ppm, the percentage removal consistently held steady at an impressive 99.2%. Surprisingly, the impact of temperature variations on the adsorption process proved negligible, whereas alterations in pH levels exerted a pronounced influence.

The analysis of adsorption isotherms unveiled consistently high coefficients of correlation (R^2) exceeding the threshold of 0.91, indicative of effective modelling. Notably, the Freundlich isotherm model emerged as the frontrunner, boasting the highest coefficient of correlation. Consequently, it is deduced that the adsorption processes predominantly involve multilayer coverage, interspersed with some monolayer interactions and a judiciously distributed binding energy.

Delving deeper into the Langmuir isotherm model, it was found that lead exhibited the highest adsorption capacity at an impressive 47750.2 $mg.g^{-1}$, while cadmium displayed the lowest at 23.5164 $mg.g^{-1}$.

The study also unravelled that the pseudo-second order reaction model was the most fitting representation for this adsorption investigation. This conclusion was substantiated by two key factors: the remarkably high R^2 values and the closer alignment of calculated qe values with those predicted by the pseudo-second order reaction model, in contrast to the pseudo-first order reaction.

Furthermore, the investigation ascertained the spontaneous and feasible nature of the adsorption processes. This conclusion is underscored by the consistently negative values of Gibbs' free energy, with nitrate registering the highest at -12.36 $KJ.mol^{-1}$ and cadmium the lowest at -0.064 $KJ.mol^{-1}$.

Lastly, the exothermic nature of all the reactions was elucidated through negative enthalpy values. As these adsorption reactions unfolded, the degree of randomness at the solid-liquid interface perceptibly increased, adding an additional layer of understanding to the dynamics of the adsorption process.

5.2 Recommendations

i) Further research should be conducted in this domain to ascertain the adsorbent's effectiveness in capturing other heavy metals.

ii) Investigation into appropriate methods for the disposal of used adsorbents, such as kaolinite and alkali-modified kaolinite, is warranted.

iii) Government bodies should actively promote the adoption of organic manure as an agricultural practice to curtail the absorption of heavy metals, nitrate, and phosphate into water sources.

REFERENCES

Acevedo, N.I.A., Rocha, M. C. G., & Bertolino, L. C. (2017, April). Mineralogical characterization of natural clays from Brazilian Southeast region for industrial applications. *Cerâmica*, *63*(366), 253–262. https://doi.org/10.1590/0366-69132017633662045

Adejumoke, I.A., Babatunde, A. B., Abimbola, O. A., Tabitha, A. A. T., Adewumi, D. A., & Toyin, O. T. (2018, March 21). Water Pollution: Effects, Prevention, and Climatic Impact. *Water Challenges of an Urbanizing World*. https://doi.org/10.5772/intechopen.72018

Adeyi, A.A., Abayomi, T. G., Purkait, M. K., & Mondal, P. (2019). Adsorptive Removal of Phosphate from Aqueous Solution by Magnetic-Supported Kaolinite: Characteristics, Isotherm and Kinetic Studies. *Open Journal of Applied Sciences*, *09*(07), 544–563. https://doi.org/10.4236/ojapps.2019.97043

Ahmaruzzaman, M., & Laxmi Gayatri, S. (2010, June 30). Adsorptive Removal of p-Nitrophenol (p-NP) On Charred Jute Stick. *International Journal of Chemical Reactor Engineering*, *8*(1). https://doi.org/10.2202/1542-6580.2147

Ajala, O. A., AKINNAWO, S. O., BAMISAYE, A., ADEDIPE, D. T., ADESINA, M. O., OKON-AKAN, O. A., ADEBUSUYI, T. A., OJEDOKUN, A. T., ADEGOKE, K. A., & BELLO, O. S. (2023). Adsorptive removal of antibiotic pollutants from wastewater using biomass/biochar-based adsorbents. *RSC Advances*, *13*(7), 4678–4712. https://doi.org/10.1039/d2ra06436g

Alengebawy, A., Abdelkhalek, S. T., Qureshi, S. R., & Wang, M. Q. (2021, February 25). Heavy Metals and Pesticides Toxicity in Agricultural Soil and Plants: Ecological Risks and Human Health Implications. *Toxics*, *9*(3), 42. https://doi.org/10.3390/toxics9030042

Ani, & Sarapää. (2008). *Clay and clay mineralogy*.

Ansari, A. A., & Gill, S. S. (2013, November 19). *Eutrophication: Causes, Consequences and Control*. Springer Science & Business Media.

Ansari, A. A., Singh Gill, S., Lanza, G. R., & Rast, W. (Eds.). (2011). *Eutrophication: causes, consequences and control*. https://doi.org/10.1007/978-90-481-9625-8

Assi, M. A., Hezmee, M. N. M., Haron, A. W., Sabri, M. Y., & Rajion, M. A. (2016, June). The detrimental effects of lead on human and animal health. *Veterinary World*, *9*(6), 660–671. https://doi.org/10.14202/vetworld.2016.660-671

Astuti, T. R. P., Aditiyo, R., Oktavioni, A., & Supriyanto. (2020, July 1). SEM-EDX study on authigenic clay minerals in sandstone of Jatiluhur formation. *IOP Conference Series: Earth and Environmental Science*, *538*(1), 012041. https://doi.org/10.1088/1755-1315/538/1/012041

Bain, Allen, & keppy. (2009). Analysis of Nitrate Nitrogen (NO3 -) in Water by the EPA Approved Brucine Method . *Thermo Fisher Scientific*. http://www.epa.gov/waterscience/methods/method/files/352_1.pdf

Battas, A., Gaidoumi, A. E., Ksakas, A., & Kherbeche, A. (2019, February 3). Adsorption Study for the Removal of Nitrate from Water Using Local Clay. *The Scientific World Journal*, *2019*, 1–10. https://doi.org/10.1155/2019/9529618

Bener, S., Bulca, Z., Palas, B., Tekin, G., Atalay, S., & Ersöz, G. (2019, September). Electrocoagulation process for the treatment of real textile wastewater: Effect of operative conditions on the organic carbon removal and kinetic study. *Process Safety and Environmental Protection*, *129*, 47–54. https://doi.org/10.1016/j.psep.2019.06.010

Bergaya, F., Theng, B., & Lagaly, G. (2006). Structures and Mineralogy of Clay Minerals. In *Handbook of Clay Science* (pp. 19–86). Elsevier.

Bernhoft, R. A. (2013). Cadmium Toxicity and Treatment. *The Scientific World Journal, 2013*, 1–7. https://doi.org/10.1155/2013/394652

Bleam. (2017). Soil and Environmental Chemistry. In *Surface Chemistry and Adsorption* (2nd ed., pp. 385–443). https://doi.org/10.1016/C2015-0-01022-X

Bryan, N. S., & van Grinsven, H. (2013). The Role of Nitrate in Human Health. *Advances in Agronomy*, 153–182. https://doi.org/10.1016/b978-0-12-407247-3.00003-2

Bushra, & Ahmad. (2016). Mechanism of Adsorption on Nanomaterials. In *Advanced Environmental Analysis: Applications of Nanomaterials.* (Vol. 1, pp. 90–11). Royal Society of Chemistry. https://doi.org/10.1039/9781782623625-00090

Cannata, M. G., Carvalho, R., Bertoli, A. C., Augusto, A. S., Bastos, A. R. R., Carvalho, J. G., & Freitas, M. P. (2013, March 9). Effects of Cadmium and Lead on Plant Growth and Content of Heavy Metals in Arugula Cultivated in Nutritive Solution. *Communications in Soil Science and Plant Analysis*, *44*(5), 952–961. https://doi.org/10.1080/00103624.2012.747604

Caponi, N., Collazzo, G. C., Jahn, S. L., Dotto, G. L., Mazutti, M. A., & Foletto, E. L. (2017, May 11). Use of Brazilian Kaolin as a Potential Low-cost Adsorbent for the Removal of Malachite Green from Colored Effluents. *Materials Research*, *20*(suppl 2), 14–22. https://doi.org/10.1590/1980-5373-mr-2016-0673

Carbinatti, C., da Conceição, F. T., Moruzzi, R. B., & Menegário, A. A. (2021). Functionalization of kaolinite for removal of phosphate from urban sewage. *MethodsX*, *8*, 101423. https://doi.org/10.1016/j.mex.2021.101423

Cho, D. W., Chon, C. M., Jeon, B. H., Kim, Y., Khan, M. A., & Song, H. (2010, October). The role of clay minerals in the reduction of nitrate in groundwater by zero-valent iron. *Chemosphere*, *81*(5), 611–616. https://doi.org/10.1016/j.chemosphere.2010.08.005

Connor, R. (2015, March 23). *The United Nations world water development report 2015: water for a sustainable world*. UNESCO Publishing.

Council, N. R., Sciences, C. O. L., Toxicology, B. O. E. S. A., & Water, C. O. C. I. D. (2000, April 12). *Copper in Drinking Water*. National Academies Press.

Cundy, C. S., & Cox, P. A. (2003, May 13). The Hydrothermal Synthesis of Zeolites: History and Development from the Earliest Days to the Present Time. *ChemInform*, *34*(19). https://doi.org/10.1002/chin.200319217.

Dali Youcef, L., Belaroui, L. S., & López-Galindo, A. (2019, October). Adsorption of a cationic methylene blue dye on an Algerian palygorskite. *Applied Clay Science*, *179*, 105145. https://doi.org/10.1016/j.clay.2019.105145

Das, & Chowdhury, S. C. (2011, January 14). Insight into Adsorption Thermodynamics. In *Thermodynamics* (pp. 349–364). Intech Open. https://doi.org/10.5772/13474

Dewi, R., Agusnar, H., Alfian, Z., & Tamrin. (2018, December). Characterization of technical kaolin using XRF, SEM, XRD, FTIR and its potentials as industrial raw materials. *Journal of Physics: Conference Series, 1116*, 042010. https://doi.org/10.1088/1742-6596/1116/4/042010

El Ouardi, M., Qourzal, S., Alahiane, S., Assabbane, A., & Douch, J. (2015). Effective Removal of Nitrates Ions from Aqueous Solution Using New Clay as Potential Low-Cost Adsorbent. *Journal of Encapsulation and Adsorption Sciences*, *05*(04), 178–190. https://doi.org/10.4236/jeas.2015.54015

El-Shater, A., Mansour, A., Osman, M., El Ghany, A. A. A., & El-Samee, A. A. (2021, June). Evolution and significance of clay minerals in the Esna Shale Formation at Dababiya

area, Luxor, Egypt. *Egyptian Journal of Petroleum*, *30*(2), 9–16. https://doi.org/10.1016/j.ejpe.2021.03.001

Emam, Ismail, & Abdelkhalek. (2016). Adsorption Study of Some Heavy Metal Ions on Modified Kaolinite Clay. *International Journal of Advancement in Engineering Technology, Management and Applied*, *3*(7), 152–163.

Erhayem, M., Al-Tohami, F., Mohamed, R., & Ahmida, K. (2015). Isotherm, Kinetic and Thermodynamic Studies for the Sorption of Mercury (II) onto Activated Carbon from <i>Rosmarinus officinalis</i> Leaves. *American Journal of Analytical Chemistry*, *06*(01), 1–10. https://doi.org/10.4236/ajac.2015.61001

Fernandes, F. M., Lourenço, P. B., & Castro, F. (2010). Ancient Clay Bricks: Manufacture and Properties. In *Materials, Technologies and Practice in Historic Heritage Structures* (pp. 29–48). Springer Netherlands. https://doi.org/10.1007/978-90-481-2684-2_3

Filipič, M. (2013, August 15). Metal Ions in Life Sciences Vol. 11: Cadmium: From Toxicity to Essentiality. Edited by Astrid Siegel, Helmut Siegel and Roland K. O. Siegel. *ChemBioChem*, *14*(13), 1662–1663. https://doi.org/10.1002/cbic.201300507

Gamoudi, S., & Srasra, E. (2019, October). Adsorption of organic dyes by HDPy+-modified clay: Effect of molecular structure on the adsorption. *Journal of Molecular Structure*, *1193*, 522–531. https://doi.org/10.1016/j.molstruc.2019.05.055

Ganesh, S., Khan, F., Ahmed, M. K., Velavendan, P., Pandey, N. K., & Kamachi Mudali, U. (2012, December 1). Spectrophotometric determination of trace amounts of phosphate in water and soil. *Water Science and Technology*, *66*(12), 2653–2658. https://doi.org/10.2166/wst.2012.468

Georgiev, Hristov, Bogdanov, & Markovska. (2011). Synthesis of naa zeolite from natural kaolinite. *Oxidation Communications*, *34*(4), 812–819.

Gibbons, E., Léveillé, R., & Berlo, K. (2020, August). Data fusion of laser-induced breakdown and Raman spectroscopies: Enhancing clay mineral identification. *Spectrochimica Acta Part B: Atomic Spectroscopy*, *170*, 105905. https://doi.org/10.1016/j.sab.2020.105905

Gorzin, F., & Bahri, M. (2017, January 21). Adsorption of Cr (VI) from aqueous solution by adsorbent prepared from paper mill sludge: Kinetics and thermodynamics studies. *Adsorption Science & Technology*, *36*(1–2), 149–169. https://doi.org/10.1177/0263617416686976

Gupta, & Babu. (2006). Adsorption of Cr (VI) by a Low-Cost Adsorbent Prepared from Neem Leaves. *National Conference on Environmental Conservation, 1–3*, 175–180.

Gupta, D., Chatterjee, S., Datta, S., Veer, V., & Walther, C. (2014, August). Role of phosphate fertilizers in heavy metal uptake and detoxification of toxic metals. *Chemosphere*, *108*, 134–144. https://doi.org/10.1016/j.chemosphere.2014.01.030

Hamdi, N., & Srasra, E. (2012, April). Removal of phosphate ions from aqueous solution using Tunisian clays minerals and synthetic zeolite. *Journal of Environmental Sciences*, *24*(4), 617–623. https://doi.org/10.1016/s1001-0742(11)60791-2

Haseena, M., Faheem Malik, M., Javed, A., Arshad, S., Asif, N., Zulfiqar, S., & Hanif, J. (2017). Water pollution and human health. *Environmental Risk Assessment and Remediation*, *01*(03). https://doi.org/10.4066/2529-8046.100020

Heller-Kallai, L., & Lapides, I. (2007, January). Reactions of kaolinites and metakaolinites with NaOH—comparison of different samples (Part 1). *Applied Clay Science*, *35*(1–2), 99–107. https://doi.org/10.1016/j.clay.2006.06.006

Hillier. (1978, January 1). Clay mineralogy. In *Sedimentology* (pp. 223–228). Springer, Berlin, Heidelberg. https://doi.org/10.1007/3-540-31079-7_47

Hofbauer, W. K. (2021, June 30). Toxic or Otherwise Harmful Algae and the Built Environment. *Toxins*, *13*(7), 465. https://doi.org/10.3390/toxins13070465

Hu, & Xu. (2020). Physicochemical technologies for HRPs and risk control. In *High-Risk Pollutants in Wastewater* (pp. 169–207). https://doi.org/10.1016/B978-0-12-816448-8.00008-3

Huang, G. (2013). Characterization of Nitrate Contamination in an Arid Region of China. *Journal of Environmental Protection*, *04*(07), 46–52. https://doi.org/10.4236/jep.2013.47a006

Huggett. (2020, December 16). Encyclopedia of Geology. In *Clay Mineral* (2nd ed., pp. 341–349). Petroclays Ltd, Heathfield, United Kingdom.

Ibrahim, Yusoff, Rahman, & Saidin. (2014). Thermal transformation of kaolinite to metakaolinite: An in situ high-temperature X-ray powder diffraction study. *Powder Diffraction*, *29*(3), 244–251.

Ismadji, S., Soetaredjo, F. E., & Ayucitra, A. (2015, March 24). *Clay Materials for Environmental Remediation*. Springer.

Jaishankar, M., Tseten, T., Anbalagan, N., Mathew, B. B., & Beeregowda, K. N. (2014, June 1). Toxicity, mechanism and health effects of some heavy metals. *Interdisciplinary Toxicology*, *7*(2), 60–72. https://doi.org/10.2478/intox-2014-0009

Jaiswal, A., Verma, A., & Jaiswal, P. (2018). Detrimental Effects of Heavy Metals in Soil, Plants, and Aquatic Ecosystems and in Humans. *Journal of Environmental Pathology, Toxicology and Oncology*, *37*(3), 183–197. https://doi.org/10.1615/jenvironpatholtoxicoloncol.2018025348

Jarraud, M. (2008, December 5). Keynote speech: Responding to the challenges posed by climate change in the water sector. *Water International*, *33*(4), 529–537. https://doi.org/10.1080/02508060802561115

Johnson, E., Arshad, S. E., & Asik, J. (2014, November 15). Hydrothermal Synthesis of Zeolite A Using Natural Kaolin from KG. Gading Bongawan Sabah. *Journal of Applied Sciences*, *14*(23), 3282–3287. https://doi.org/10.3923/jas.2014.3282.3287

Khan, T. A. (2011). Trace Elements in the Drinking Water and Their Possible Health Effects in Aligarh City, India. *Journal of Water Resource and Protection*, *03*(07), 522–530. https://doi.org/10.4236/jwarp.2011.37062

Khayyun, T. S., & Mseer, A. H. (2019, October 14). Comparison of the experimental results with the Langmuir and Freundlich models for copper removal on limestone adsorbent. *Applied Water Science*, *9*(8). https://doi.org/10.1007/s13201-019-1061-2

Kianfar, E. (2019, May 28). Nanozeolites: synthesized, properties, applications. *Journal of Sol-Gel Science and Technology*, *91*(2), 415–429. https://doi.org/10.1007/s10971-019-05012-4

Leghari, Laghari, & Laghari. (2016). Role of Nitrogen for Plant Growth and Development: A review. *Advances in Environmental Biology*, *10*(9), 209–2018.

Lowell, S., Shields, J. E., Thomas, M. A., & Thommes, M. (2012, September 14). *Characterization of Porous Solids and Powders: Surface Area, Pore Size and Density*. Springer Science & Business Media.

Luo, X., & Deng, F. (2018, November 15). *Nanomaterials for the Removal of Pollutants and Resource Reutilization*. Elsevier.

Mahdi, M. H., Mohammed, T. J., & Al-Najar, J. A. (2021, June 1). Advanced Oxidation Processes (AOPs) for treatment of antibiotics in wastewater: A review. *IOP Conference Series: Earth and Environmental Science*, *779*(1), 012109. https://doi.org/10.1088/1755-1315/779/1/012109

Majumdar, D. (2003, October). The Blue Baby Syndrome. *Resonance*, *8*(10), 20–30. https://doi.org/10.1007/bf02840703

Manna, K., Debnath, B., & Singh, W. (2019). Sources and toxicological effects of lead on human health. *Indian Journal of Medical Specialities*, *10*(2), 66. https://doi.org/10.4103/injms.injms_30_18

Mastropietro, T. F., Drioli, E., Candamano, S., & Poerio, T. (2016, July). Crystallization and assembling of FAU nanozeolites on porous ceramic supports for zeolite membrane synthesis. *Microporous and Mesoporous Materials*, *228*, 141–146. https://doi.org/10.1016/j.micromeso.2016.03.037

Mayyahi, & Al-Asadi. (2018). Advanced Oxidation Processes (AOPs) for Wastewater Treatment and Reuse: A Brief Review. *Asian Journal of Applied Science and Technology*, *2*(3), 18–30.

Mnasri-Ghnimi, S., & Frini-Srasra, N. (2019, October). Removal of heavy metals from aqueous solutions by adsorption using single and mixed pillared clays. *Applied Clay Science*, *179*, 105151. https://doi.org/10.1016/j.clay.2019.105151

Mulinta, S., & Thiansem, S. (2019, April). Characterization and Properties of Lampang Kaolinite Clay for Standard Clay. *Key Engineering Materials*, *798*, 248–253. https://doi.org/10.4028/www.scientific.net/kem.798.248

Naddeo, V., Uyguner-Demirel, C. S., Prado, M., Cesaro, A., Belgiorno, V., & Ballesteros, F. (2015, March 18). Enhanced ozonation of selected pharmaceutical compounds by sonolysis. *Environmental Technology*, *36*(15), 1876–1883. https://doi.org/10.1080/09593330.2015.1014864

Nawaz, & Sengupta. (2019). Contaminants of Emerging Concern: Occurrence, Fate, and Remediation. In *Advances in Water Purification Techniques* (pp. 67–114). https://doi.org/10.1016/B978-0-12-814790-0.00004-1

Nghi, N. H., Cuong, L. C., Dieu, T. V., Ngu, T., & Oanh, D. T. Y. (2018, December). Ozonation process and water disinfection. *Vietnam Journal of Chemistry*, *56*(6), 717–720. https://doi.org/10.1002/vjch.201800076

Nordberg, G. F., Fowler, B. A., & Nordberg, M. (2014, August 7). *Handbook on the Toxicology of Metals*. Academic Press.

O'Connor, T. P. (2011, January 1). Total Water Management: A Research Project of the United States Environmental Protection Agency. *Proceedings of the Water Environment Federation*, *2011*(9), 6334–6346. https://doi.org/10.2175/193864711802766452

Ochieng, O. (2016, November 30). Characterization and classification of clay minerals for potential applications in Rugi Ward, Kenya. *African Journal of Environmental Science and Technology*, *10*(11), 415–431. https://doi.org/10.5897/ajest2016.2184

Olaremu, Odebunmi, Odebunmi, Nwosu, & Adela. (2018). SYNTHESIS OF ZEOLITE FROM KAOLIN CLAY FROM ERUSU AKOKO SOUTHWESTERN. *JOURNAL OF CHEMICAL SOCIETY OF NIGERIA*, *43*(3).

Padmavathy, K., Madhu, G., & Haseena, P. (2016). A study on Effects of pH, Adsorbent Dosage, Time, Initial Concentration and Adsorption Isotherm Study for the Removal of Hexavalent Chromium (Cr (VI)) from Wastewater by Magnetite Nanoparticles. *Procedia Technology*, *24*, 585–594. https://doi.org/10.1016/j.protcy.2016.05.127

Patel, R. (2010, October 20). Overview of industrial filtration technology and its applications. *Indian Journal of Science and Technology*, *3*(10), 1121–1127. https://doi.org/10.17485/ijst/2010/v3i10.12

Pathak, Kumar Sanyal, Prasad Bhatt, & Mali. (2015, January 1). *State of Indian Agriculture*.

Piccin, J. S., Dotto, G. L., & Pinto, L. A. A. (2011, June). Adsorption isotherms and thermochemical data of FD&C Red n° 40 binding by Chitosan. *Brazilian Journal of Chemical Engineering*, *28*(2), 295–304. https://doi.org/10.1590/s0104-66322011000200014

Pizent, A., Tariba, B., & Živković, T. (2012, January 1). Reproductive Toxicity of Metals in Men. *Archives of Industrial Hygiene and Toxicology*, *63*(Supplement-1). https://doi.org/10.2478/10004-1254-63-2012-2151

Pooi, C. K., & Ng, H. Y. (2018, August 6). Review of low-cost point-of-use water treatment systems for developing communities. *Npj Clean Water*, *1*(1). https://doi.org/10.1038/s41545-018-0011-0

Pranoto, Inayati, & Firmansyah, F. (2018, April). Effectiveness Study of Drinking Water Treatment Using Clays/Andisol Adsorbent in Lariat Heavy Metal Cadmium (Cd) and Bacterial Pathogens. *IOP Conference Series: Materials Science and Engineering*, *349*, 012047. https://doi.org/10.1088/1757-899x/349/1/012047

Proctor, & Toro-Vazquez, J. F. (2009). Bleaching and Purifying Fats and Oils. In *Chapter 10 - The Freundlich Isotherm in Studying Adsorption in Oil Processing* (2nd ed., pp. 209–219). Elsevier. https://doi.org/10.1016/B978-1-893997-91-2.50016-X

Rahimzadeh, Rahimzadeh, Kazemi, & Moghadamnia. (2017). Cadmium toxicity and treatment: An update. *Caspian Journal Internal Medecine*, *8*(3), 135–145. https://doi.org/10.22088/cjim.8.3.135

Rhodes, C. J. (2010, August). Properties and applications of Zeolites. *Science Progress*, *93*(3), 223–284. https://doi.org/10.3184/003685010x12800828155007

Roberts, T. L. (2014). Cadmium and Phosphorous Fertilizers: The Issues and the Science. *Procedia Engineering*, *83*, 52–59. https://doi.org/10.1016/j.proeng.2014.09.012

Romero-Guerrero, L. M., Moreno-Tovar, R., Arenas-Flores, A., Marmolejo Santillán, Y., & Pérez-Moreno, F. (2018, November 1). Chemical, Mineralogical, and Refractory Characterization of Kaolin in the Regions of Huayacocotla-Alumbres, Mexico. *Advances in Materials Science and Engineering*, *2018*, 1–11. https://doi.org/10.1155/2018/8156812

Roudouane, H. T., Mbey, J. A., Bayiga, E. C., & Ndjigui, P. D. (2020, March). Characterization and application tests of kaolinite clays from Aboudeia (southeastern Chad) in fired bricks making. *Scientific African*, *7*, e00294. https://doi.org/10.1016/j.sciaf.2020.e00294

Saeijs, & Van Berkel. (1995, July 1). Global water crisis: the major issue of the 21st century, a growing and explosive problem. *PubMed*, *5*(4), 26–40. Retrieved August 22, 2023, from https://pubmed.ncbi.nlm.nih.gov/12291371/

Sagasta, & Turral. (2017). Water pollution from agriculture: a global review. In *Food and Agriculture Organization of the United Nations*. The Food and Agriculture Organization of the United Nations Rome, 2017 and the International Water Management Institute on behalf of the Water Land and Ecosystems research program Colombo, 2017. https://www.fao.org/3/i7754e/i7754e.pdf

Sahu, & Singh. (2019). the Impact and Prospects of Green Chemistry for Textile Technology. In *13 - Significance of bioadsorption process on textile industry wastewater* (pp. 367–416). Woodhead Publishing. https://doi.org/10.1016/B978-0-08-102491-1.00013-7

Saki, H., Alemayehu, E., Schomburg, J., & Lennartz, B. (2019, January 24). Halloysite Nanotubes as Adsorptive Material for Phosphate Removal from Aqueous Solution. *Water*, *11*(2), 203. https://doi.org/10.3390/w11020203

Sammel, A. J., & McMartin, D. W. (2014). Teaching and Knowing beyond the Water Cycle: What Does It Mean to Be Water Literate? *Creative Education*, *05*(10), 835–848. https://doi.org/10.4236/ce.2014.510097

Savci, S. (2012). Investigation of Effect of Chemical Fertilizers on Environment. *APCBEE Procedia*, *1*, 287–292. https://doi.org/10.1016/j.apcbee.2012.03.047

Selim, M. M. (2020, May 13). Introduction to the Integrated Nutrient Management Strategies and Their Contribution to Yield and Soil Properties. *International Journal of Agronomy*, *2020*, 1–14. https://doi.org/10.1155/2020/2821678

Shaaibu, Abdullahi, Sadiq, & Odey. (2020). Physio-Chemical and Thermal Properties of Alkaleri Kaolin, Bauchi State, Nigeria for Ceramics Applications. *FUTY Journal of the Environment*, *14*(1), 60–68.

Shahid, M., Pinelli, E., Pourrut, B., Silvestre, J., & Dumat, C. (2011, January). Lead-induced genotoxicity to Vicia faba L. roots in relation with metal cell uptake and initial speciation. *Ecotoxicology and Environmental Safety*, *74*(1), 78–84. https://doi.org/10.1016/j.ecoenv.2010.08.037

Singh. (2013, January 1). *Environmental Problems and Plant* (N. Dwivedi, Ed.; 1st ed.). LAP Lambert Academic Publishing.

Sparks, D. L. (2013, October 22). *Environmental Soil Chemistry*. Elsevier.

Sun, X., Chen, M., Wei, D., & Du, Y. (2019, July). Research progress of disinfection and disinfection by-products in China. *Journal of Environmental Sciences*, *81*, 52–67. https://doi.org/10.1016/j.jes.2019.02.003

Thompson, J., & Bannigan, J. (2008, April). Cadmium: Toxic effects on the reproductive system and the embryo. *Reproductive Toxicology*, *25*(3), 304–315. https://doi.org/10.1016/j.reprotox.2008.02.001

Thuynsma, R., Kleinert, A., Kossmann, J., Valentine, A. J., & Hills, P. N. (2016, May). The effects of limiting phosphate on photosynthesis and growth of Lotus japonicus. *South African Journal of Botany*, *104*, 244–248. https://doi.org/10.1016/j.sajb.2016.03.001

Tien, C. (2018, November 27). *Introduction to Adsorption*. Elsevier.

Tzoupanos, & Zouboulis, N. (2008, September). Coagulation–flocculation processes in water/wastewater treatment: the application of new generation of chemical reagents. *S International Conference on Heat Transfer, Thermal Engineering And Environment*, *33*(1–3), 309–317.

United Nations. (2015, September). United Nations, Department of Economic and Social Affairs, Population Division, World Fertility Report 2013: Fertility at the Extremes. *Population and Development Review*, *41*(3), 555–555. https://doi.org/10.1111/j.1728-4457.2015.00081.x

Ur Rehman. (2019). Polluted Water Borne Diseases: Symptoms, Causes, Treatment and Prevention. *Journal of Medicinal and Chemical Sciences*, *2*(1), 21–26. https://doi.org/10.26655/jmchemsci.2019.6.4

Vijayakumar, Sasikala, & Ramesh. (2012). Lead poisoning-an overview. *International Journal of Pharmacology & Toxicology*, *2*(2), 70–82.

Wang, F. Y., Wang, H., & Ma, J. W. (2010, May). Adsorption of cadmium (II) ions from aqueous solution by a new low-cost adsorbent—Bamboo charcoal. *Journal of Hazardous Materials*, *177*(1–3), 300–306. https://doi.org/10.1016/j.jhazmat.2009.12.032

Wei, C., Huang, Y., Liao, Q., Xia, A., Zhu, X., & Zhu, X. (2019, December). Adsorption thermodynamic characteristics of Chlorella vulgaris with organic polymer adsorbent cationic starch: Effect of temperature on adsorption capacity and rate. *Bioresource Technology*, *293*, 122056. https://doi.org/10.1016/j.biortech.2019.122056

Wright, P. A. W., & Lozinska, M. L. (2011). Structural Chemistry and Properties of Zeolites. In *Zeolites And Ordered Porous Solids: Fundamentals And Applications* (pp. 1–37).

Yadav, V. B., Gadi, R., & Kalra, S. (2019, February). Clay based nanocomposites for removal of heavy metals from water: A review. *Journal of Environmental Management*, *232*, 803–817. https://doi.org/10.1016/j.jenvman.2018.11.120

Yahia, M. B., & Wjihi, S. (2020, September 30). Study of the hydrogen physisorption on adsorbents based on activated carbon by means of statistical physics formalism: modeling analysis and thermodynamics investigation. *Scientific Reports*, *10*(1). https://doi.org/10.1038/s41598-020-73268-w

Yamasaki, H., Pilon, M., & Shikanai, T. (2008, April). How do plants respond to copper deficiency? *Plant Signaling & Behavior*, *3*(4), 231–232. https://doi.org/10.4161/psb.3.4.5094

Zamparas, M., Gianni, A., Stathi, P., Deligiannakis, Y., & Zacharias, I. (2012, July). Removal of phosphate from natural waters using innovative modified bentonites. *Applied Clay Science*, *62–63*, 101–106. https://doi.org/10.1016/j.clay.2012.04.020

Zhang, Z., Wang, H., Provis, J. L., Bullen, F., Reid, A., & Zhu, Y. (2012, July). Quantitative kinetic and structural analysis of geopolymers. Part 1. The activation of metakaolin with sodium hydroxide. *Thermochimica Acta*, *539*, 23–33. https://doi.org/10.1016/j.tca.2012.03.021

APPENDIX

Appendix 1 Effect of adsorbents dosage on Nitrate percentage removal

NITRATE								
	0.1g		0.075g		0.050g		0.020g	
	Ce	% removal	Ce	% removal	Ce	% removal	Ce	% removal
S1	0	100	0	100	0.0059	99.94	0.393	96.07
S2	0	100	0	100	0.0056	99.94	0.399	96.01
S3	0	100	0	100	0.0067	99.93	0.396	96.04
S4	0	100	0	100	0.0054	99.95	0.396	96.04
S5	0	100	0	100	0.0058	99.94	0.389	96.11
S6	0	100	0	100	0.0064	99.94	0.398	96.02
S7	0	100	0	100	0.0052	99.95	0.098	99.02

Appendix 2 Effect of adsorbents dosage on Phosphate percentage removal

PHOSPHATE								
	0.1g		0.075g		0.050g		0.020g	
	Ce	% removal	Ce	% removal	Ce	% removal	Ce	% removal
S1	0	100	1.165	88.35	1.806	81.94	3.361	66.39
S2	0	100	1.129	88.71	1.86	81.4	3.34	66.6
S3	0	100	1.174	88.26	1.871	81.29	3.333	66.67
S4	0	100	1.029	89.71	1.813	81.87	3.391	66.09
S5	0	100	1.196	88.04	1.855	81.45	3.358	66.42
S6	0	100	1.264	87.36	1.878	81.22	3.335	66.65
S7	9.2	8	9.915	0.85	9.998	0.02	9.999	0.001

Appendix 3 Effect of adsorbents dosage on Lead percentage removal

LEAD								
	0.5g		0.2g		0.1g		0.05g	
	Ce	% removal	Ce	% removal	Ce	% removal	Ce	% removal
S1	0	100	0	100	0.0073	99.92	0.4173	95.83
S2	0	100	0	100	0.0887	99.11	0.4282	95.72
S3	0	100	0	100	0.0996	99.004	0.4747	95.25
S4	0	100	0	100	0.0174	99.82	0.4459	95.54
S5	0	100	0	100	0.0156	99.84	0.4172	95.82
S6	0	100	0	100	0.0356	99.64	0.4969	95.03
S7	0	100	0	100	0.0461	99.54	0.2422	97.57

Appendix 4 Effect of adsorbents dosage on Copper percentage removal

COPPER								
	0.50g		0.20g		0.10g		0.05g	
	Ce	% removal	Ce	% removal	Ce	% removal	Ce	% removal
S1	0	100	0	100	0.7557	92.45	1.0893	89.11
S2	0	100	0	100	0.7381	92.62	1.0807	89.2
S3	0	100	0	100	0.7773	92.23	1.0606	89.4
S4	0	100	0	100	0.7752	92.25	1.0644	89.36
S5	0	100	0	100	0.7483	92.52	1.0421	89.58
S6	0	100	0	100	0.7506	92.15	1.0083	89.92
S7	0	100	0	100	0.1127	98.88	0.2563	97.44

Appendix 5 Effect of adsorbents dosage on Cadmium percentage removal

CADMIUM								
	0.50g		0.20g		0.10g		0.05g	
	Ce	% removal	Ce	% removal	Ce	% removal	Ce	% removal
S1	0	100	0	100	0.0592	99.41	3.601	63.4
S2	0	100	0	100	0.0606	99.4	3.6978	63.03
S3	0	100	0	100	0.0465	99.54	3.686	63.14

S4	0	100	0	100	0.0598	99.41	3.675	63.21
S5	0	100	0	100	0.0632	99.37	3.67265	63.28
S6	0	100	0	100	0.0507	99.5	3.6892	63.11
S7	0	100	0	100	0.0528	99.48	0.0794	99.21

Appendix 6 Effect contact time on Nitrate percentage removal

NITRATE										
	60min		**30min**		**20min**		**10min**		**1min**	
	Ce	**% removal**	**Ce**	**% removal**	**Ce**	**% removal**	**Ce**	**% removal**	**Ce**	**% removal**
S1	0	100	0	100	0	100	0.0121	99.88	8.565	14.35
S2	0	100	0	100	0	100	0.0276	99.72	8.549	14.51
S3	0	100	0	100	0	100	0.0214	99.79	8.563	14.37
S4	0	100	0	100	0	100	0.0276	99.72	8.56	14.4
S5	0	100	0	100	0	100	0.0134	99.87	8.554	14.46
S6	0	100	0	100	0	100	0.0217	99.78	8.565	14.35
S7	0	100	0	100	0	100	0.1018	98.98	8.59	14.1

Appendix 7 Effect contact time on Phosphate percentage removal

PHOSPHATE										
	60min		**30min**		**20min**		**10min**		**1min**	
	Ce	**% removal**	**Ce**	**% removal**	**Ce**	**% removal**	**Ce**	**% removal**	**Ce**	**% removal**
S1	0	100	0	100	0	100	0.309	96.91	8.345	16.55
S2	0	100	0	100	0	100	0.313	96.87	8.352	16.48
S3	0	100	0	100	0	100	0.394	96.06	8.358	16.42
S4	0	100	0	100	0	100	0.398	96.02	8.359	16.41
S5	0	100	0	100	0	100	0.394	96.06	8.357	16.43
S6	0	100	0	100	0	100	0.399	96.01	8.357	16.43
S7	9.841	1.59	9.987	0.13	9.2	8	10	0	10	0

Appendix 8 Effect contact time on Lead percentage removal

LEAD										
	60min		**30min**		**20min**		**10min**		**1min**	
	Ce	**% removal**	**Ce**	**% removal**	**Ce**	**% removal**	**Ce**	**% removal**	**Ce**	**% removal**
S1	0	100	0	100	0.26	97.4	0.367	96.33	7.899	21.01
S2	0	100	0	100	0.242	97.58	0.338	96.61	7.894	21.06
S3	0	100	0	100	0.291	97.09	0.367	96.33	7.899	21.01
S4	0	100	0	100	0.271	97.29	0.328	96.72	7.891	21.09
S5	0	100	0	100	0.2422	97.57	0.3561	96.44	7.898	21.02
S6	0	100	0	100	0.2778	97.22	0.3709	96.29	7.897	21.03
S7	0	100	0	100	0.1887	98.11	0.3135	96.86	7.897	21.03

Appendix 9 Effect contact time on Copper percentage removal

COPPER										
	60min		**30min**		**20min**		**10min**		**1min**	
	Ce	**% removal**	**Ce**	**% removal**	**Ce**	**% removal**	**Ce**	**% removal**	**Ce**	**% removal**
S1	0	100	0	100	0.3845	96.16	2.4282	75.72	7.967	20.33
S2	0	100	0	100	0.4413	95.59	2.41835	75.82	7.956	20.44
S3	0	100	0	100	0.5417	94.59	2.4339	75.61	7.959	20.41
S4	0	100	0	100	0.5686	94.32	2.437	75.63	7.962	20.38
S5	0	100	0	100	0.3797	96.21	2.49585	75.05	7.958	20.39
S6	0	100	0	100	0.5993	94.01	2.44745	75.53	7.961	20.89
S7	0	100	0	100	0.5941	94.06	0.62405	93.76	7.057	29.43

Appendix 10 Effect contact time on Cadmium percentage removal

CADMIUM										
	60min		30min		20min		10min		1min	
	Ce	% removal	Ce	% removal	Ce	% removal	Ce	% removal	Ce	% removal
S1	0	100	0	100	0	100	0	100	7.943	20.57
S2	0	100	0	100	0	100	0	100	7.956	20.44
S3	0	100	0	100	0	100	0	100	7.902	20.98
S4	0	100	0	100	0	100	0	100	7.924	20.76
S5	0	100	0	100	0	100	0	100	7.94	20.6
S6	0	100	0	100	0	100	0	100	7.943	20.57
S7	0	100	0	100	0	100	0	100	7.711	22.89

Appendix 11 Effect of adsorbate concentration on Nitrate percentage removal

NITRATE								
	100ppm		50ppm		20ppm		10ppm	
	Ce	% removal	Ce	% removal	Ce	% removal	Ce	% removal
S1	0	100	0	100	0	100	0	100
S2	0	100	0	100	0	100	0	100
S3	0	100	0	100	0	100	0	100
S4	0	100	0	100	0	100	0	100
S5	0	100	0	100	0	100	0	100
S6	0	100	0	100	0	100	0	100
S7	0	100	0	100	0	100	0	100

Appendix 12 Effect of adsorbate concentration on Phosphate percentage removal

PHOSPHATE								
	100ppm		50ppm		20ppm		10ppm	
	Ce	% removal	Ce	% removal	Ce	% removal	Ce	% removal
S1	0	100	0	100	0	100	0	100
S2	0	100	0	100	0	100	0	100
S3	0	100	0	100	0	100	0	100
S4	0	100	0	100	0	100	0	100
S5	0	100	0	100	0	100	0	100
S6	0	100	0	100	0	100	0	100
S7	99.8	0.2	49.95	0.1	19.74	1.3	9.2	8

Appendix 13 Effect of adsorbate concentration on Lead percentage removal

LEAD								
	100ppm		50ppm		20ppm		10ppm	
	Ce	% removal	Ce	% removal	Ce	% removal	Ce	% removal
S1	0	100	0	100	0	100	0	100
S2	0	100	0	100	0	100	0	100
S3	0	100	0	100	0	100	0	100
S4	0	100	0	100	0	100	0	100
S5	0	100	0	100	0	100	0	100
S6	0	100	0	100	0	100	0	100
S7	0	100	0	100	0	100	0	100

Appendix 14 Effect of adsorbate concentration on Copper percentage removal

COPPER								
	100ppm		50ppm		20ppm		10ppm	
	Ce	% removal	Ce	% removal	Ce	% removal	Ce	% removal
S1	2.35	97.65	0.559	98.88	0.122	99.39	0	100
S2	2.92	97.08	0.598	98.81	0.176	99.12	0	100
S3	2.81	97.19	0.5234	98.95	0.158	99.21	0	100

S4	2.24	97.76	0.5877	98.82	0.136	99.32	0	100
S5	2.52	97.48	0.604	98.8	0.15	99.25	0	100
S6	2.81	97.19	0.512	98.98	0.14	99.30	0	100
S7	2.45	97.55	0.5407	98.92	0.144	99.28	0	100

Appendix 15 Effect of adsorbate concentration on Cadmium percentage removal

CADMIUM								
	100ppm		**50ppm**		**20ppm**		**10ppm**	
	Ce	**% removal**	**Ce**	**% removal**	**Ce**	**% removal**	**Ce**	**% removal**
S1	0	100	0	100	0	100	0	100
S2	0	100	0	100	0	100	0	100
S3	0	100	0	100	0	100	0	100
S4	0	100	0	100	0	100	0	100
S5	0	100	0	100	0	100	0	100
S6	0	100	0	100	0	100	0	100
S7	0	100	0	100	0	100	0	100

Appendix 16 Effect of temperature on Nitrate percentage removal

NITRATE						
	298◦K		**333◦K**		**353◦K**	
	Ce	**% removal**	**Ce**	**% removal**	**Ce**	**% removal**
S1	0	100	0	100	0	100
S2	0	100	0	100	0	100
S3	0	100	0	100	0	100
S4	0	100	0	100	0	100
S5	0	100	0	100	0	100
S6	0	100	0	100	0	100
S7	0	100	0	100	0	100

Appendix 17 Effect of temperature on Phosphate percentage removal

PHOSPHATE						
	298◦K		**333**◦K		**353**◦K	
	Ce	**% removal**	**Ce**	**% removal**	**Ce**	**% removal**
S1	0	100	0	100	0	100
S2	0	100	0	100	0	100
S3	0	100	0	100	0	100
S4	0	100	0	100	0	100
S5	0	100	0	100	0	100
S6	0	100	0	100	0	100
S7	9.2	8	9.321	6.79	9.234	7.66

Appendix 18 Effect of temperature on Lead percentage removal

LEAD						
	298◦K		**333**◦K		**353**◦K	
	Ce	**% removal**	**Ce**	**% removal**	**Ce**	**% removal**
S1	0	100	0.4313	95.69	0.4313	95.69
S2	0	100	0.4699	95.3	0.456	95.44
S3	0	100	0.4808	95.19	0.5803	94.42
S4	0	100	0.4204	95.79	0.5704	94.30
S5	0	100	0.4382	95.62	0.4882	95.12
S6	0	100	0.4328	95.67	0.5273	94.73
S7	0	100	0.4274	95.73	0.4917	95.08

Appendix 19 Effect of temperature on Copper percentage removal

COPPER						
	298◦K		**333**◦K		**353**◦C	
	Ce	**% removal**	**Ce**	**% removal**	**Ce**	**% removal**
S1	0	100	0	100	0	100
S2	0	100	0	100	0	100
S3	0	100	0	100	0	100
S4	0	100	0	100	0	100
S5	0	100	0	100	0	100
S6	0	100	0	100	0	100
S7	0	100	0	100	0	100

Appendix 20 Effect of temperature on Cadmium percentage removal

CADMIUM						
	298◦K		**333**◦K		**353**◦K	
	Ce	**% removal**	**Ce**	**% removal**	**Ce**	**% removal**
S1	0	100	0	100	0	100
S2	0	100	0	100	0	100
S3	0	100	0	100	0	100
S4	0	100	0	100	0	100
S5	0	100	0	100	0	100
S6	0	100	0	100	0	100
S7	0	100	0	100	0	100

Appendix 21 Effect of pH on Nitrate percentage removal

NITRATE						
	3		**7**		**10**	
	Ce	**% removal**	**Ce**	**% removal**	**Ce**	**% removal**
S1	7.245	27.55	0	100	0	100
S2	7.209	27.91	0	100	0	100
S3	7.211	27.89	0	100	0	100
S4	7.289	27.11	0	100	0	100
S5	7.198	28.02	0	100	0	100
S6	7.212	27.88	0	100	0	100
S7	5.678	43.22	0	100	0	100

Appendix 22 Effect of pH on Phosphate percentage removal

PHOSPHATE						
	3		**7**		**10**	
	Ce	**% removal**	**Ce**	**% removal**	**Ce**	**% removal**
S1	6.176	38.24	0	100	0	100
S2	5.206	47.94	0	100	0	100
S3	5.147	48.53	0	100	0	100
S4	5.704	42.96	0	100	0	100
S5	6.037	39.63	0	100	0	100
S6	4.733	52.67	0	100	0	100
S7	9.77	2.3	9.2	8	0.424	95.76

Appendix 23 Effect of pH on Lead percentage removal

LEAD						
	3		**7**		**10**	
	Ce	**% removal**	**Ce**	**% removal**	**Ce**	**% removal**
S1	0.563	94.37	0	100	0.1709	98.29
S2	0.4178	95.72	0	100	0.2956	97.04
S3	0.5491	94.51	0	100	0.2955	97.04
S4	0.4387	95.61	0	100	0.2891	97.11

S5	0.4812	95.19	0	100	0.2421	97.58
S6	0.456	95.44	0	100	0.2543	97.45
S7	0.563	94.37	0	100	0.2313	96.68

Appendix 24 Effect of pH on Copper percentage removal

COPPER						
	3		**7**		**10**	
	Ce	**% removal**	**Ce**	**% removal**	**Ce**	**% removal**
S1	7.108	28.92	0	100	0	100
S2	7.907	20.93	0	100	0	100
S3	7.856	21.44	0	100	0	100
S4	7.71	22.9	0	100	0	100
S5	8.124	18.76	0	100	0	100
S6	7.917	20.83	0	100	0.0897	99.11
S7	1.884	18.86	0	100	0.0556	99.45

Appendix 25 Effect of pH on Cadmium percentage removal

CADMIUM						
	2		**7**		**10**	
	Ce	**% removal**	**Ce**	**% removal**	**Ce**	**% removal**
S1	0	100	0	100	0	100
S2	0	100	0	100	0	100
S3	0	100	0	100	0	100
S4	0	100	0	100	0	100
S5	0	100	0	100	0	100
S6	0	100	0	100	0	100
S7	0	100	0	100	0	100

Appendix 26 Adsorption isotherms data of Nitrate

NITRATE										
	0.015g					**0.020g**				
	Ce	**qe**	**Ce/qe**	**lnqe**	**LnCe**	**Ce**	**qe**	**Ce/qe**	**lnqe**	**LnCe**
S1	0.567	25.15467	0.022541	3.225043	-0.5674	0.34	19.32	0.017598	2.961141	-1.07881
S2	0.567	25.15467	0.022541	3.225043	-0.5674	0.34	19.32	0.017598	2.961141	-1.07881
S3	0.567	25.15467	0.022541	3.225043	-0.5674	0.34	19.32	0.017598	2.961141	-1.07881
S4	0.567	25.15467	0.022541	3.225043	-0.5674	0.34	19.32	0.017598	2.961141	-1.07881
S5	0.567	25.15467	0.022541	3.225043	-0.5674	0.34	19.32	0.017598	2.961141	-1.07881
S6	0.567	25.15467	0.022541	3.225043	-0.5674	0.34	19.32	0.017598	2.961141	-1.07881
S7	0.567	25.15467	0.022541	3.225043	-0.5674	0.344	19.312	0.017813	2.960727	-1.06711
	0.030g`					**0.040g**				
	Ce	**qe**	**Ce/qe**	**lnqe**	**LnCe**	**Ce**	**qe**	**Ce/qe**	**lnqe**	**LnCe**
S1	0.1956	13.07253	0.014963	2.570513	-1.63168	0.0991	9.9009	0.010009	2.292626	-2.31163
S2	0.1956	13.07253	0.014963	2.570513	-1.63168	0.0991	9.9009	0.010009	2.292626	-2.31163
S3	0.1956	13.07253	0.014963	2.570513	-1.63168	0.0991	9.9009	0.010009	2.292626	-2.31163
S4	0.1956	13.07253	0.014963	2.570513	-1.63168	0.0991	9.9009	0.010009	2.292626	-2.31163
S5	0.1956	13.07253	0.014963	2.570513	-1.63168	0.0991	9.9009	0.010009	2.292626	-2.31163
S6	0.1956	13.07253	0.014963	2.570513	-1.63168	0.0991	9.9009	0.010009	2.292626	-2.31163
S7	0.1956	13.07253	0.014963	2.570513	-1.63168	0.0991	9.9009	0.010009	2.292626	-2.31163

Appendix 27 Adsorption isotherms data of Phosphate

PHOSPHATE										
	0.015g					0.020g				
	Ce	**qe**	**Ce/qe**	**lnqe**	**LnCe**	**Ce**	**qe**	**Ce/qe**	**lnqe**	**LnCe**
S1	4.2998	15.20053	0.282872	2.721331	1.458569	3.3178	13.3644	0.248257	2.592594	1.199302
S2	4.2998	15.20053	0.282872	2.721331	1.385794	3.3178	13.3644	0.248257	2.592594	1.199302
S3	4.2998	15.20053	0.282872	2.721331	1.385794	3.3178	13.3644	0.248257	2.592594	1.199302
S4	4.2998	15.20053	0.282872	2.721331	1.385794	3.3178	13.3644	0.248257	2.592594	1.199302
S5	4.2998	15.20053	0.282872	2.721331	1.385794	3.3178	13.3644	0.248257	2.592594	1.199302
S6	4.2998	15.20053	0.282872	2.721331	1.385794	3.3178	13.3644	0.248257	2.592594	1.199302
S7	9.999	0.002667	3749.625	-5.92693	2.302485	9.999	0.002	4999.5	-6.21461	2.302485
	0.030g`					**0.040g**				
	Ce	**qe**	**Ce/qe**	**lnqe**	**LnCe**	**Ce**	**qe**	**Ce/qe**	**lnqe**	**LnCe**
S1	2.2051	10.3932	0.212168	2.341152	0.790773	1.6842	8.3158	0.20253	2.098852	0.611503
S2	2.2051	10.3932	0.212168	2.341152	0.790773	1.6842	8.3158	0.20253	2.098852	0.611503
S3	2.2051	10.3932	0.212168	2.341152	0.790773	1.6842	8.3158	0.20253	2.098852	0.611503
S4	2.2051	10.3932	0.212168	2.341152	0.790773	1.6842	8.3158	0.20253	2.098852	0.611503
S5	2.2051	10.3932	0.212168	2.341152	0.790773	1.6842	8.3158	0.20253	2.098852	0.611503
S6	2.2051	10.3932	0.212168	2.341152	0.790773	1.6842	8.3158	0.20253	2.098852	0.611503
S7	9.9999	0.000133	74999.25	-8.92266	2.302575	0.991	9.009	0.110001	2.198224	-0.00904

Appendix 28 Adsorption isotherms data of Lead

LEAD										
	0.015g					0.020g				
	Ce	**qe**	**Ce/qe**	**lnqe**	**LnCe**	**Ce**	**qe**	**Ce/qe**	**lnqe**	**LnCe**
S1	1.8412	21.7568	0.084626	3.079926	0.610418	1.2764	17.4472	0.073158	2.859179	0.244044
S2	1.8412	21.7568	0.084626	3.079926	0.610418	1.2764	17.4472	0.073158	2.859179	0.244044
S3	1.8412	21.7568	0.084626	3.079926	0.610418	1.2764	17.4472	0.073158	2.859179	0.244044
S4	1.8412	21.7568	0.084626	3.079926	0.610418	1.2764	17.4472	0.073158	2.859179	0.244044
S5	1.8412	21.7568	0.084626	3.079926	0.610418	1.2764	17.4472	0.073158	2.859179	0.244044
S6	1.8412	21.7568	0.084626	3.079926	0.610418	1.2764	17.4472	0.073158	2.859179	0.244044
S7	1.6786	22.1904	0.075645	3.09966	0.51796	1.095	17.81	0.061482	2.87976	0.090754
	0.030g`					**0.040g**				
	Ce	**qe**	**Ce/qe**	**lnqe**	**LnCe**	**Ce**	**qe**	**Ce/qe**	**lnqe**	**LnCe**
S1	0.8542	12.1944	0.070049	2.500977	-0.15759	0.5913	9.4087	0.062846	2.241635	-0.52543
S2	0.8542	12.1944	0.070049	2.500977	-0.15759	0.5913	9.4087	0.062846	2.241635	-0.52543
S3	0.8542	12.1944	0.070049	2.500977	-0.15759	0.5913	9.4087	0.062846	2.241635	-0.52543
S4	0.8542	12.1944	0.070049	2.500977	-0.15759	0.5913	9.4087	0.062846	2.241635	-0.52543
S5	0.8542	12.1944	0.070049	2.500977	-0.15759	0.5913	9.4087	0.062846	2.241635	-0.52543
S6	0.8542	12.1944	0.070049	2.500977	-0.15759	0.5913	9.4087	0.062846	2.241635	-0.52543
S7	0.6381	12.48253	0.051119	2.52433	-0.44926	0.2496	9.7504	0.025599	2.277308	-1.3879

Appendix 29 Adsorption isotherms data of Copper

COPPER										
	0.015g					0.020g				
	Ce	**qe**	**Ce/qe**	**lnqe**	**LnCe**	**Ce**	**qe**	**Ce/qe**	**lnqe**	**LnCe**
S1	2.5917	19.75547	0.131189	2.98343	0.952314	1.9123	16.1754	0.118223	2.783492	0.648307
S2	2.5917	19.75547	0.131189	2.98343	0.952314	1.9123	16.1754	0.118223	2.783492	0.648307

S3	2.5917	19.75547	0.131189	2.98343	0.952314	1.9123	16.1754	0.118223	2.783492	0.648307
S4	2.5917	19.75547	0.131189	2.98343	0.952314	1.9123	16.1754	0.118223	2.783492	0.648307
S5	2.5917	19.75547	0.131189	2.98343	0.952314	1.9123	16.1754	0.118223	2.783492	0.648307
S6	2.5917	19.75547	0.131189	2.98343	0.952314	1.9123	16.1754	0.118223	2.783492	0.648307
S7	1.5137	22.63013	0.066889	3.119282	0.414557	0.9964	18.0072	0.055333	2.890772	-0.00361
	0.030g`					**0.040g**				
	Ce	**qe**	**Ce/qe**	**lnqe**	**LnCe**	**Ce**	**qe**	**Ce/qe**	**lnqe**	**LnCe**
S1	1.1871	11.75053	0.101025	2.463899	0.171513	0.8774	9.1226	0.096179	2.210755	-0.13079
S2	1.1871	11.75053	0.101025	2.463899	0.171513	0.8774	9.1226	0.096179	2.210755	-0.13079
S3	1.1871	11.75053	0.101025	2.463899	0.171513	0.8774	9.1226	0.096179	2.210755	-0.13079
S4	1.1871	11.75053	0.101025	2.463899	0.171513	0.8774	9.1226	0.096179	2.210755	-0.13079
S5	1.1871	11.75053	0.101025	2.463899	0.171513	0.8774	9.1226	0.096179	2.210755	-0.13079
S6	1.1871	11.75053	0.101025	2.463899	0.171513	0.8774	9.1226	0.096179	2.210755	-0.13079
S7	0.6548	12.46027	0.052551	2.522545	-0.42343	0.328	9.672	0.033912	2.269235	-1.11474

Appendix 30 Adsorption isotherms data of Cadmium

CADMIUM										
	0.015g					**0.020g**				
	Ce	**qe**	**Ce/qe**	**lnqe**	**LnCe**	**Ce**	**qe**	**Ce/qe**	**lnqe**	**LnCe**
S1	6.9128	8.232533	0.839693	2.108094	1.933375	6.0912	7.8176	0.779165	2.056378	1.806845
S2	6.9128	8.232533	0.839693	2.108094	1.933375	6.0912	7.8176	0.779165	2.056378	1.806845
S3	6.9128	8.232533	0.839693	2.108094	1.933375	6.0912	7.8176	0.779165	2.056378	1.806845
S4	6.9128	8.232533	0.839693	2.108094	1.933375	6.0912	7.8176	0.779165	2.056378	1.806845
S5	6.9128	8.232533	0.839693	2.108094	1.933375	6.0912	7.8176	0.779165	2.056378	1.806845
S6	6.9128	8.232533	0.839693	2.108094	1.933375	6.0912	7.8176	0.779165	2.056378	1.806845
S7	1.0075	23.98	0.042014	3.17722	0.007472	0.7702	18.4596	0.041724	2.915585	-0.26111
	0.030g`					**0.040g**				
	Ce	**qe**	**Ce/qe**	**lnqe**	**LnCe**	**Ce**	**qe**	**Ce/qe**	**lnqe**	**LnCe**
S1	5.0165	6.644667	0.754966	1.893815	1.612732	4.1671	5.8329	0.714413	1.763514	1.42722
S2	5.0165	6.644667	0.754966	1.893815	1.612732	4.1671	5.8329	0.714413	1.763514	1.42722
S3	5.0165	6.644667	0.754966	1.893815	1.612732	4.1671	5.8329	0.714413	1.763514	1.42722
S4	5.0165	6.644667	0.754966	1.893815	1.612732	4.1671	5.8329	0.714413	1.763514	1.42722
S5	5.0165	6.644667	0.754966	1.893815	1.612732	4.1671	5.8329	0.714413	1.763514	1.42722
S6	5.0165	6.644667	0.754966	1.893815	1.612732	4.1671	5.8329	0.714413	1.763514	1.42722
S7	0.3125	12.91667	0.024194	2.558518	-1.16315	0.111	9.889	0.011225	2.291423	-2.19823

Appendix 31 Adsorption kinetics data of Nitrate

NITRATE								
	1min				**5min**			
	Ct	**qt**	**ln(qe-qt)**	**t/qt**	**Ct**	**qt**	**ln(qe-qt)**	**t/qt**
S1	8.967	1.6528	2.660763	0.605034	5.081	7.8704	2.090579	0.635292
S2	8.967	1.6528	2.660763	0.605034	5.078	7.8752	2.089986	0.634905
S3	8.961	1.6624	2.660092	0.60154	5.0789	7.87376	2.090164	0.635021
S4	8.963	1.6592	2.660315	0.6027	5.0785	7.8744	2.090085	0.634969
S5	8.963	1.6592	2.660315	0.6027	5.0786	7.87424	2.090104	0.634982
S6	8.966	1.6544	2.660651	0.604449	5.0788	7.87392	2.090144	0.635008
S7	8.968	1.6512	2.660875	0.60562	5.0783	7.87472	2.090045	0.634943
	10min				**20min**			

	ct	qt	ln(qe-qt	t/qt	ct	qt	ln(qe-qt)	t/qt
S1	0.484	15.2256	-0.3087	0.656789	0.1076	15.82784	-2.02374	1.263596
S2	0.482	15.2288	-0.31307	0.656651	0.1035	15.8344	-2.07465	1.263073
S3	0.466	15.2544	-0.34871	0.655549	0.1072	15.82848	-2.0286	1.263545
S4	0.471	15.2464	-0.33743	0.655893	0.1079	15.82736	-2.02012	1.263635
S5	0.486	15.2224	-0.30435	0.656927	0.1085	15.8264	-2.01291	1.263711
S6	0.464	15.2576	-0.35325	0.655411	0.1073	15.82832	-2.02738	1.263558
S7	0.489	15.2176	-0.29787	0.657134	0.1101	15.82384	-1.99392	1.263916
	30min				**40min**			
	ct	**qt**	**ln(qe-qt)**	**t/qt**	**ct**	**qt**	**ln(qe-qt)**	**t/qt**
S1	0.1006	15.83904	-2.1123	2.525406	0.1001	15.83984	-2.11893	2.525278
S2	0.1006	15.83904	-2.1123	2.525406	0.1002	15.83968	-2.1176	2.525304
S3	0.1007	15.83888	-2.11097	2.525431	0.1002	15.83968	-2.1176	2.525304
S4	0.1005	15.8392	-2.11362	2.52538	0.1001	15.83984	-2.11893	2.525278
S5	0.1006	15.83904	-2.1123	2.525406	0.1003	15.83952	-2.11627	2.525329
S6	0.1006	15.83904	-2.1123	2.525406	0.1002	15.83968	-2.1176	2.525304
S7	0.1005	15.8392	-2.11362	2.52538	0.1001	15.83984	-2.11893	2.525278

Appendix 32 Adsorption kinetics data of Phosphate

PHOSPHATE								
	1min				**5min**			
	Ct	**qt**	**ln(qe-qt)**	**t/qt**	**CT**	**qt**	**ln(qe-qt)**	**t/qt**
S1	8.9095	1.7448	2.181005	0.573132	5.5349	7.14416	1.240066	0.699872
S2	8.9093	1.74512	2.180969	0.573026	5.5366	7.14144	1.240852	0.700139
S3	8.9093	1.74512	2.180969	0.573026	5.5323	7.14832	1.238861	0.699465
S4	8.9098	1.74432	2.181059	0.573289	5.5337	7.14608	1.23951	0.699684
S5	8.9031	1.75504	2.179848	0.569788	5.5331	7.14704	1.239232	0.69959
S6	8.9029	1.75536	2.179812	0.569684	5.5329	7.14736	1.239139	0.699559
S7	9.9996	0.00064	2.360794	1562.5	9.966	0.0544	2.355709	91.91176
	10min				**20min**			
	Ct	**qt**	**ln(qe-qt**	**t/qt**	**Ct**	**qt**	**ln(qe-qt)**	**t/qt**
S1	3.514	10.3776	-1.50328	0.963614	3.4917	10.41328	-1.67815	1.920624
S2	3.507	10.3888	-1.55495	0.962575	3.4903	10.41552	-1.69021	1.920211
S3	3.516	10.3744	-1.48899	0.963911	3.4991	10.40144	-1.61666	1.922811
S4	3.517	10.3728	-1.48192	0.96406	3.4966	10.40544	-1.63701	1.922072
S5	3.501	10.3984	-1.60147	0.961686	3.4972	10.40448	-1.63209	1.922249
S6	3.519	10.3696	-1.46794	0.964357	3.4973	10.40432	-1.63127	1.922278
S7	9.999	0.0016	2.360703	6250	9.99999	1.6E-05	2.360852	1250000
	30min				**40min**			
	Ct	**qt**	**ln(qe-qt)**	**t/qt**	**Ct**	**qt**	**ln(qe-qt)**	**t/qt**
S1	3.3806	10.59104	-4.71499	2.832583	3.38077	10.59077	-4.68508	3.776874
S2	3.386	10.5824	-4.03986	2.834896	3.38005	10.59192	-4.81836	3.776464
S3	3.3871	10.58064	-3.94455	2.835367	3.38093	10.59051	-4.65773	3.776966
S4	3.3813	10.58992	-4.5972	2.832883	3.38033	10.59147	-4.7644	3.776623
S5	3.3855	10.5832	-4.08638	2.834681	3.38077	10.59077	-4.68508	3.776874
S6	3.3878	10.57952	-3.88831	2.835667	3.38055	10.59112	-4.72395	3.776749
S7	9.998	0.0032	2.360552	9375	9.997	0.0048	2.360401	8333.333

Appendix 33 Adsorption kinetics data of Lead

LEAD								
	1min				5min			
	Ct	qt	ln(qe-qt)	t/qt	Ct	qt	ln(qe-qt)	t/qt
S1	8.155	7.845	1.902854	0.12747	2.623	11.8032	1.012255	0.423614
S2	8.151	7.849	1.902257	0.127405	2.624	11.8016	1.012837	0.423671
S3	8.152	7.848	1.902406	0.127421	2.621	11.8064	1.011092	0.423499
S4	8.157	7.843	1.903152	0.127502	2.627	11.7968	1.014578	0.423844
S5	8.157	7.843	1.903152	0.127502	2.621	11.8064	1.011092	0.423499
S6	8.156	7.844	1.903003	0.127486	2.629	11.7936	1.015738	0.423959
S7	8.151	7.849	1.902257	0.127405	2.621	11.8064	1.011092	0.423499
	10min				20min			
	ct	qt	ln(qe-qt	t/qt	ct	qt	ln(qe-qt	t/qt
S1	1.29087	13.93461	-0.4774	0.717638	1.1357	14.18288	-0.98854	1.410151
S2	1.29044	13.9353	-0.47851	0.717602	1.1302	14.19168	-1.01247	1.409276
S3	1.29076	13.93478	-0.47769	0.717629	1.1325	14.188	-1.00239	1.409642
S4	1.29016	13.93574	-0.47924	0.717579	1.1391	14.17744	-0.97403	1.410692
S5	1.29033	13.93547	-0.4788	0.717593	1.1365	14.1816	-0.98511	1.410278
S6	1.29065	13.93496	-0.47797	0.71762	1.1308	14.19072	-1.00983	1.409372
S7	1.29022	13.93565	-0.47908	0.717584	1.1317	14.18928	-1.00589	1.409515
	30min				40min			
	ct	qt	ln(qe-qt)	t/qt	ct	qt	ln(qe-qt)	t/qt
S1	0.9173	14.53232	-3.78627	2.064364	0.9119	14.54096	-4.26584	2.75085
S2	0.9182	14.53088	-3.72471	2.064569	0.91188	14.54099	-4.26813	2.750844
S3	0.9147	14.53648	-3.9889	2.063773	0.91198	14.54083	-4.25677	2.750874
S4	0.9159	14.53456	-3.89026	2.064046	0.9111	14.54224	-4.36144	2.750608
S5	0.9172	14.53248	-3.79335	2.064341	0.91167	14.54133	-4.29241	2.75078
S6	0.9169	14.53296	-3.8149	2.064273	0.91184	14.54106	-4.27271	2.750832
S7	0.9122	14.54048	-4.23223	2.063206	0.91109	14.54226	-4.36269	2.750605

Appendix 34 Adsorption kinetics data of Copper

COPPER								
	1MIN				5min			
	Ct	qt	ln(qe-qt)	t/qt	Ct	qt	ln(qe-qt)	t/qt
S1	8.312	2.7008	2.5756	0.370261	5.6109	7.02256	2.176732	0.711991
S2	8.318	2.6912	2.57633	0.371581	5.6108	7.02272	2.176713	0.711975
S3	8.315	2.696	2.575965	0.37092	5.6105	7.0232	2.176659	0.711926
S4	8.311	2.7024	2.575478	0.370041	5.6101	7.02384	2.176586	0.711861
S5	8.317	2.6928	2.576209	0.371361	5.6108	7.02272	2.176713	0.711975
S6	8.315	2.696	2.575965	0.37092	5.611	7.0224	2.17675	0.712007
S7	3.211	10.8624	1.604948	0.092061	1.511	13.5824	0.814302	0.368123
	10min				20min			
	Ct	qt	ln(qe-qt	t/qt	Ct	qt	ln(qe-qt)	t/qt
S1	3.7526	9.99584	1.765443	1.000416	2.681	11.7104	1.418181	1.707884

S2	3.7517	9.99728	1.765196	1.000272	2.6965	11.6856	1.424168	1.711508
S3	3.7568	9.98912	1.766592	1.001089	2.6922	11.69248	1.422511	1.710501
S4	3.7501	9.99984	1.764758	1.000016	2.6905	11.6952	1.421855	1.710103
S5	3.752	9.9968	1.765279	1.00032	2.6911	11.69424	1.422086	1.710244
S6	3.7563	9.98992	1.766455	1.001009	2.6907	11.69488	1.421932	1.71015
S7	0.9044	14.55296	0.252345	0.687145	0.6983	14.88272	-0.04366	1.34384
	30min				**40min**			
	Ct	**qt**	**ln(qe-qt)**	**t/qt**	**ct**	**qt**	**ln(qe-qt)**	**t/qt**
S1	1.789	13.1376	0.99414	2.283522	1.7038	13.27392	0.942379	3.013428
S2	1.78	13.152	0.988797	2.281022	1.7023	13.27632	0.941444	3.012883
S3	1.76	13.184	0.976821	2.275485	1.703	13.2752	0.941881	3.013137
S4	1.764	13.1776	0.979228	2.276591	1.7037	13.27408	0.942317	3.013392
S5	1.742	13.2128	0.965919	2.270526	1.7033	13.27472	0.942068	3.013246
S6	1.708	13.2672	0.944995	2.261216	1.7034	13.27456	0.94213	3.013283
S7	0.256	15.5904	-1.3879	1.924261	0.1358	15.78272	-2.8598	2.534417

Appendix 35 Adsorption kinetics data of Cadmium

CADMIUM								
	1MIN				**5min**			
	Ct	**qt**	**ln(qe-qt)**	**t/qt**	**Ct**	**qt**	**ln(qe-qt)**	**t/qt**
S1	9.455	0.872	1.260731	1.146789	7.402	4.1568	-1.41387	1.202848
S2	9.452	0.8768	1.25937	1.140511	7.413	4.1392	-1.344	1.207963
S3	9.4856	0.82304	1.274513	1.215008	7.404	4.1536	-1.4008	1.203775
S4	9.457	0.8688	1.261638	1.151013	7.405	4.152	-1.39433	1.204239
S5	9.451	0.8784	1.258915	1.138434	7.4805	4.0312	-0.9975	1.240325
S6	9.454	0.8736	1.260278	1.144689	7.41	4.144	-1.36258	1.206564
S7	2.092	12.6528	1.237562	0.079034	0.524	15.1616	-0.06358	0.32978
	10min				**20min**			
	Ct	**qt**	**ln(qe-qt**	**t/qt**	**Ct**	**qt**	**ln(qe-qt)**	**t/qt**
S1	7.27813	4.354992	-3.10092	2.296215	7.26776	4.371584	-3.5608	4.575001
S2	7.2839	4.34576	-2.91434	2.301093	7.26858	4.370272	-3.51567	4.576374
S3	7.27813	4.354992	-3.10092	2.296215	7.26862	4.370208	-3.51352	4.576441
S4	7.27888	4.353792	-3.0746	2.296848	7.26588	4.374592	-3.67269	4.571855
S5	7.27875	4.354	-3.07911	2.296739	7.26713	4.372592	-3.59692	4.573946
S6	7.2822	4.34848	-2.96579	2.299654	7.26855	4.37032	-3.51728	4.576324
S7	0.0845	15.8648	-1.44732	0.630326	0.0077	15.98768	-2.1864	1.250963
	30min				**40min**			
	Ct	**qt**	**ln(qe-qt)**	**t/qt**	**ct**	**qt**	**ln(qe-qt)**	**t/qt**
S1	7.266	4.3744	-3.66516	6.858083	7.26373	4.378032	-3.81817	9.136525
S2	7.2697	4.36848	-3.45713	6.867377	7.26346	4.378464	-3.83803	9.135624
S3	7.2686	4.37024	-3.51459	6.864612	7.26335	4.37864	-3.84624	9.135257
S4	7.2679	4.37136	-3.55295	6.862853	7.26334	4.378656	-3.84698	9.135223
S5	7.2672	4.37248	-3.59284	6.861095	7.26363	4.378192	-3.82548	9.136191
S6	7.2689	4.36976	-3.49859	6.865366	7.26361	4.378224	-3.82695	9.136125
S7	0.00079	15.99874	-2.29002	1.875148	0.0006	15.99904	-2.29303	2.50015

Appendix 36 Adsorption thermodynamic data of Nitrate

NITRATE K=QE/CE												
	298				333				353			
	Qe	**Ce**	**LNK**	**G(KJ/mol)**	**qe**	**Ce**	**lnk**	**G(KJ/mol)**	**qe**	**Ce**	**lnk**	**G(KJ/mol)**
S1	13.07707	0.1922	4.220079	-10.4562	13.07227	0.1958	4.201154	-11.6319	13.0724	0.1957	4.201676	-12.332
S2	13.07627	0.1928	4.216901	-10.4483	13.0732	0.1951	4.204807	-11.642	13.0732	0.1951	4.204807	-12.3412
S3	13.0772	0.1921	4.220609	-10.4575	13.07253	0.1956	4.202197	-11.6347	13.07213	0.1959	4.200634	-12.3289
S4	13.07693	0.1923	4.219548	-10.4549	13.0728	0.1954	4.20324	-11.6376	13.07213	0.1959	4.200634	-12.3289
S5	13.07707	0.1922	4.220079	-10.4562	13.07267	0.1955	4.202718	-11.6362	13.07307	0.1952	4.204285	-12.3397
S6	13.0768	0.1924	4.219018	-10.4536	13.0732	0.1951	4.204807	-11.642	13.07227	0.1958	4.201154	-12.3305
S7	13.0724	0.1967	4.201676	-10.4106	13.07547	0.1934	4.213732	-11.6667	13.0756	0.1933	4.21426	-12.3689

Appendix 37 adsorption thermodynamic data of Phosphate

PHOSPHATE												
	298				333				353			
	Qe	**Ce**	**LNK**	**G(KJ/mol)**	**qe**	**Ce**	**lnk**	**G(KJ/mol)**	**qe**	**Ce**	**lnk**	**G(KJ/mol)**
S1	10.34973	2.2377	1.531512	-3.79466	10.3304	2.2522	1.523183	-4.21728	10.29867	2.276	1.509595	-4.43069
S2	10.35427	2.2343	1.533471	-3.79951	10.3316	2.2513	1.523699	-4.21871	10.3008	2.2744	1.510505	-4.43336
S3	10.35187	2.2361	1.532434	-3.79694	10.3328	2.2504	1.524215	-4.22014	10.3064	2.2702	1.512897	-4.44038
S4	10.35853	2.2311	1.535316	-3.80408	10.33187	2.2511	1.523814	-4.21903	10.30227	2.2733	1.511131	-4.4352
S5	10.3564	2.2327	1.534393	-3.8018	10.3324	2.2507	1.524043	-4.21966	10.30453	2.2716	1.512099	-4.43804
S6	10.35253	2.2356	1.532722	-3.79766	10.33027	2.2523	1.523126	-4.21712	10.29653	2.2776	1.508685	-4.42802
S7	0.001333	9.999	-8.92256	22.10761	0.0004	9.9997	-10.1266	28.03781	0.000267	9.9998	-10.5321	30.91184

Appendix 38 Adsorption thermodynamic data of Lead

LEAD												
	298				333				353			
	Qe	**Ce**	**LNK**	**G(KJ/mol)**	**qe**	**Ce**	**lnk**	**G(KJ/mol)**	**qe**	**Ce**	**lnk**	**G(KJ/mol)**
S1	12.2092	0.8431	2.672859	-6.6226	12.20045	0.84966	2.664392	-7.37698	12.19053	0.8571	2.65486	-7.79206
S2	12.21907	0.8357	2.682483	-6.64644	12.20131	0.84902	2.665216	-7.37926	12.18987	0.8576	2.654222	-7.79019
S3	12.22307	0.8327	2.686407	-6.65617	12.20044	0.84967	2.664379	-7.37694	12.18693	0.8598	2.65142	-7.78197
S4	12.2216	0.8338	2.684967	-6.6526	12.20083	0.84938	2.664752	-7.37798	12.19027	0.8573	2.654605	-7.79132
S5	12.218	0.8365	2.681439	-6.64386	12.20039	0.84971	2.664328	-7.3768	12.19013	0.8574	2.654478	-7.79094
S6	12.21933	0.8355	2.682744	-6.64709	12.20048	0.84964	2.664418	-7.37705	12.18973	0.8577	2.654095	-7.78982
S7	12.26573	0.8007	2.729078	-6.76189	12.2656	0.8008	2.728943	-7.5557	12.2572	0.8071	2.720421	-7.98449

Appendix 39 Adsorption thermodynamic data of Copper

COPPER												
	298				333				353			
	Qe	Ce	LNK	G(KJ/mol)	qe	Ce	lnk	G(KJ/mol)	qe	Ce	lnk	G(KJ/mol)
S1	11.75533	1.1835	2.295831	-5.68843	11.74347	1.1924	2.287329	-6.33299	11.73787	1.1966	2.283336	-6.70163
S2	11.75013	1.1874	2.292099	-5.67918	11.74107	1.1942	2.285616	-6.32825	11.7384	1.1962	2.283716	-6.70275
S3	11.75973	1.1802	2.298997	-5.69627	11.74467	1.1915	2.288186	-6.33537	11.7356	1.1983	2.281723	-6.6969
S4	11.75413	1.1844	2.294969	-5.68629	11.74587	1.1906	2.289044	-6.33774	11.73907	1.1957	2.284191	-6.70414
S5	11.75107	1.1867	2.292768	-5.68084	11.74293	1.1928	2.286948	-6.33194	11.73627	1.1978	2.282197	-6.69829
S6	11.75707	1.1822	2.297077	-5.69152	11.7436	1.1923	2.287424	-6.33326	11.73667	1.1975	2.282482	-6.69913

S7	12.4548	0.6589	2.93929	-7.28274	12.45373	0.6597	2.937991	-8.1345	12.45187	0.6611	2.935721	-8.61639

Appendix 40 adsorption thermodynamic data of Cadmium

CADMIUM												
298					**333**				**353**			
	Qe	Ce	LNK	G(KJ/mol)	qe	Ce	lnk	G(KJ/mol)	qe	Ce	lnk	G(KJ/mol)
S1	6.575333	5.0685	0.26028	-0.6449	6.5744	5.0692	0.26	-0.71987	6.573467	5.0699	0.25972	-0.76228
S2	6.5756	5.0683	0.26036	-0.6451	6.574267	5.0693	0.25996	-0.71976	6.573733	5.0697	0.2598	-0.76252
S3	6.575333	5.0685	0.26028	-0.6449	6.574533	5.0691	0.26004	-0.71998	6.5736	5.0698	0.25976	-0.7624
S4	6.5756	5.0683	0.26036	-0.6451	6.574133	5.0694	0.25992	-0.71965	6.573467	5.0699	0.25972	-0.76228
S5	6.575333	5.0685	0.26028	-0.6449	6.5744	5.0692	0.26	-0.71987	6.573733	5.0697	0.2598	-0.76252
S6	6.575733	5.0682	0.2604	-0.6452	6.574267	5.0693	0.25996	-0.71976	6.573467	5.0699	0.25972	-0.76228
S7	12.75627	0.4328	3.383502	-8.38337	12.59253	0.5556	3.120811	-8.64068	12.53347	0.5999	3.039395	-8.92068